

**High Precision GPS Monitoring for Landslide Hazard and
Land Stability Evaluation in the Cerca del Cielo Urbanization,
Ponce, Puerto Rico.**

by

Félix O. Rivera Santiago

A thesis submitted in partial fulfillment of the requirements for the degree of:

MASTER OF SCIENCE
IN
GEOLOGY

UNIVERSITY OF PUERTO RICO
MAYAGÜEZ CAMPUS
2015

Approved by:

James Joyce, Ph.D.
Graduate Committee, chair

Date

Fernando Gilbes-Santaella, Ph.D.
Graduate Committee, member

Date

Alberto M. López-Venegas, Ph.D.
Graduate Committee, member

Date

Guoquan Wang, Ph.D.
Graduate Committee, member

Date

Alesandra C. Morales-Vélez, Ph.D.
Office of Graduate Students Representative

Date

Lizzette Rodríguez-Iglesias, Ph.D.
Department of Geology, Director

Date

ABSTRACT

Geodetic measurements in of the Cerca del Cielo landslide indicate that the displacement is controlled by the amount of precipitation. The decrease in creep rate over the years is considered to be the result of the lower precipitation accumulation rates. Long term changes in displacement coincide with the decrease and increase in the rate of precipitation accumulation. This study establishes a linear relation between displacement rates and precipitation accumulation rates and proposes a model to estimate future surge displacement. Precipitation equal or greater than 100mm per day on a 5-day period on the landslide should follow the estimated 0.98mm per day for the horizontal displacement and 0.49mm per day for the vertical displacement. GPS measurements outside of the landslide showed no evidence of displacements or correlation with precipitation. However we were able to establish the detection limit of the GPS to determine stable and unstable areas.

RESUMEN

Mediciones de geodésia en el deslizamiento de tierra Cerca del Cielo indican que el desplazamiento es controlado por la cantidad de precipitación. La disminución en la velocidad de movimiento durante los años es considerado el resultado de la reducción de la razón de acumulación de precipitación. Cambios a largo plazo en el desplazamiento coinciden con la disminución y aumento en la razón de acumulación de precipitación. Este estudio establece una relación lineal entre la razón de cambio de desplazamiento y la razón de cambio de acumulación de precipitación y propone un modelo para estimar futuros movimientos repentinos. Precipitación igual o superior a 100mm por día en un período de 5 días en el deslizamiento de tierra debe seguir el 0.98mm por día para el componente horizontal y 0.49mm por día para el componente vertical. Mediciones de GPS fuera del deslizamiento no mostraron evidencia de desplazamientos o correlación con la precipitación. Sin embargo fueron capaces de establecer el límite de detección del GPS para determinar las zonas estables e inestables.

ACKNOWLEDGEMENTS

This research would not have been possible without the efforts of a large number of people. First I would like to express my most sincere thanks to my graduate committee: Dr. James Joyce, Dr. Fernando Gilbes, Dr. Alberto Lopez and Dr. Guoquan Wang. Thanks for providing me support and assistance to make this project possible. Special thanks to Carlos Ponce and all the families in the Cerca del Cielo community, without them this would not have been possible.

I take this opportunity to express my gratitude to all the Geology Department faculty members. Thanks to Dr. Lysa Chyzmada for the teaching assistant experience. Many thanks to Marsha Irizarry and Catherine Pérez for their help with all the administrative paperwork related. I also extend my thanks to graduate student Francisco Hernandez, thanks for his assistance in the field and his knowledge with computers programs. Many thanks to Timmons Erickson, Marti López, Edgardo Quiñones and Elson Core for all the support and adventures during my time as a graduate student.

I wish to express my most sincere gratitude to the Puerto Rico Seismic Network for providing funding, equipment and where I learned valuable scientific knowledge. I would also like to thank UNAVCO for providing equipment loans and for their geodesy related workshops. Financial support from the Municipality of Ponce is gratefully acknowledged.

Finally, thanks to my parents for encouragement, support and attention; to Desirée and her family for understanding and supporting me during my most difficult times. I deeply appreciate everyone's support during this research.

TABLE OF CONTENTS

ABSTRACT	II
RESUMEN	III
ACKNOWLEDGEMENTS	IV
LIST OF TABLES	VII
LIST OF FIGURES	VIII
1. INTRODUCTION	12
1.1 GEOLOGIC SETTINGS	15
1.2 CLIMATIC SETTINGS	17
1.3 OBJECTIVE	19
2. PREVIOUS STUDIES.....	22
2.1 LANDSLIDE SUSCEPTIBILITY IN PUERTO RICO.....	22
2.2 LANDSLIDES IN THE MUNICIPALITY OF PONCE	23
2.3 LANDSLIDES AND RAINFALL CORRELATION IN PUERTO RICO	24
2.4 PONCE LANDSLIDE SUSCEPTIBILITY MAP.....	26
2.5 CERCA DEL CIELO LANDSLIDE	29
2.5.1 <i>Geotechnical studies and Geologic assessment</i>	29
2.5.2 <i>Geodetic monitoring of the Cerca del Cielo landslide</i>	35
3. METHODOLOGY	41
3.1 GEODETIC SURVEYS	41
3.2 EQUIPMENT.....	44
3.3 DATA.....	45
3.3.1 <i>Static GPS method</i>	47
3.4 DATA PROCESSING	49
3.4.1 <i>Data pre-processing</i>	49
3.4.2 <i>Data processing</i>	50
3.5 ACCUMULATED PRECIPITATION	55
4. RESULTS	57
4.1 MONITORING STATIONS WITHIN THE CERCA DEL CIELO LANDSLIDE	57
4.1.1 <i>Station CB: Continuous</i>	57
4.1.2 <i>Station abeg: 4-hour data coverage</i>	62
4.2 MONITORING STATIONS OUTSIDE THE CERCA DEL CIELO LANDSLIDE.....	63
4.2.1 <i>Continuous Stations:</i>	64
4.2.1.1 <i>raqg</i>	64
4.2.1.2 <i>mang</i>	67
4.2.1.3 <i>josg</i>	70
4.2.1.4 <i>carg</i>	73
4.2.1.5 <i>herg</i>	76
4.2.1.6 <i>estg</i>	79
4.2.1.7 <i>rafg</i>	82
4.2.1.8 <i>jerg</i>	85
4.2.1.9 <i>luig</i>	87
4.2.1.10 <i>refs</i>	90

4.2.1.11	<i>dang</i>	93
4.2.1.12	<i>jorg</i>	96
4.2.1.13	<i>frag</i>	99
4.2.2	<i>Stations with 4-hour data coverage:</i>	102
4.2.2.1	<i>flag</i>	102
4.2.2.2	<i>corg</i>	106
4.2.2.3	<i>tang</i>	107
4.2.2.4	<i>pisg</i>	109
4.2.2.5	<i>casg</i>	110
5.	DISCUSSIONS	113
5.1	RATE ANALYSIS.....	116
5.2	CREEP RATE AND PRECIPITATION ANALYSIS.....	129
5.3	RATES FOR 24-HOUR GPS STATIONS OUTSIDE THE LANDSLIDE.....	131
5.4	RATES FOR STATIC 4-HOUR GPS MEASUREMENTS.....	134
5.5	COMPILATION OF DATA AND INTERPRETATION.....	136
6.	CONCLUSION	138
7.	FUTURE WORK	141
	REFERENCES	142

LIST OF TABLES

Table 4-1: GPS station <i>flag</i> and inclinometer <i>Z2_23</i> displacement comparison from October 2011 to August 2012.	106
--	-----

LIST OF FIGURES

Figure 1-1: Location of the Cerca del Cielo community. The red line delineates the landslide (image from 2010 using ESRI ArcMap©).	14
Figure 1-2: Main road and houses affected by the landslide.	15
Figure 1-3: Portion of the Geologic Map of Ponce by Krushensky and Monroe H. (1978). The rectangle delineates the location of the Cerca del Cielo community and the red circle shows the location of the landslide.	16
Figure 1-4: Mean Annual precipitation in Puerto Rico from 1981-2010 in inches. Triangle shows the location of the Cerca del Cielo landslide (figure taken from the NOAA website).	18
Figure 1-5: Tropical Storm Kyle trajectory and rainfall intensity (in inches). Triangle shows the location of Cerca del Cielo (Weather Underground figure based in NOAA website).	19
Figure 2-1: Landslide Susceptibility Map in Puerto Rico by Monroe (1978) showing the location of the Cerca de Cielo community (triangle) and Mameyes (circle).....	23
Figure 2-2: Rainfall Intensity-Duration Threshold for Puerto Rico by Larsen and Simon (1993). Showing the 41 landslides triggered by storms from 1958-1991. The triangle shows rainfall event on September 2008 in Cerca del Cielo.	25
Figure 2-3: Percentage of landslide triggered by storms compared with annual rainfall from 1958-1991 (Larsen and Torres-Sanchez, 1996).	26
Figure 2-4: Ponce Landslide Susceptibility Map by Larsen et al (2004). The black square delineates the location of the Cerca del Cielo community.....	28
Figure 2-5: Map showing Geotechnical studies (Zone 1 and Zone 2) done by Suelos Inc. (2008).	30
Figure 2-6: Cerca del Cielo landslide geologic map (a) and stratigraphic column (b) done by Suelos Inc. (2008).	32
Figure 2-7: Cerca del Cielo landslide profile showing the composition. The red line shows the location of the slip surface (modified after Suelos, 2008).	34
Figure 2-8: Location of the GPS benchmarks established in March 2008 by Wang (2012).	36
Figure 2-9: GPS measurements performed by Wang (2012) from March to December 2008. At the top precipitation (a), in the middle horizontal displacement (b) and in the bottom vertical displacement (c). Right column is a 15-day window from September 19-October 4, 2008.	38
Figure 2-10: GPS measurements performed by Wang (2012) from June to December 2009. At the top local precipitation (a), N-S displacement (b), E-W displacement (c) and vertical displacement (d). Right column is a 2-week window from October 26-November 15, 2009.....	40
Figure 3-1: Image of the Cerca del Cielo community and the GPS measured points, where the blue markers are stations located outside the boundaries of the landslide	

(red line) and green markers are stations located inside the landslide (image from 2010 using ESRI ArcMap©).....	43
Figure 3-2: Equipment used to monitor the Cerca del Cielo community. The left column shows Trimble’s NetR9 receivers (a), Trimble’s NetR8 (www.trimble.com) receivers (b) and Trimble Zephyr-Geodetic Model 2 antennae (c). The right column shows the Topcon’s GB-1000 (www.topconpositioning.com) receiver (c) and Topcon’s PG-A1 (www.unavco.org) antennae (d).	44
Figure 3-3: GPS stations and the monitored periods from January 2010 to June 2012....	46
Figure 3-4: Schematic drawing of the static GPS method to determine the position of the rover station using the base station. (El-Rabbany, 2002).	48
Figure 3-5: GPS raw data pre-processing steps used to obtain the data in RINEX format from their proprietary format (either Trimble or Topcon).	50
Figure 3-6: NGS CORS GPS stations (green markers) from the CORS used as reference to monitor the Cerca del Cielo community (red marker) (Google Earth©).....	53
Figure 3-7: OPUS Solution report for the 24-hour observations from station <i>refs</i> from December 15, 2011. Red boxes show the extracted data for the Northing and Easting in UTM coordinates and the black box shows the errors used from the Latitude and Longitude. Green box shows the extracted Ellipsoid height along with the errors. .	54
Figure 3-8: Peak-to-peak errors from each baseline (OPUS website).	55
Figure 3-9: Google Earth© image showing the location of the Cerca del Cielo community (red marker), landslide boundaries (red lines) and the USGS weather station 50115230 (yellow marker).	56
Figure 4-1: GPS time series and precipitation for station <i>CB</i> . Starting at the top precipitation (a), in the middle horizontal displacement (b) and in the bottom vertical displacement (c).	61
Figure 4-2: GPS time series for station <i>abeg</i> . Beginning in the top, the time series show horizontal displacement (a) and in the bottom vertical displacement (b). Blue lines in a and b delineate the first and last observation.	63
Figure 4-3: GPS time series and precipitation for station <i>raqq</i> . Starting at the top precipitation (a), in the middle horizontal displacement (b) and in the bottom vertical displacement (c). Blue lines delineate the best-fit linear regression and green line the 2cm step in figures b and c.	66
Figure 4-4: GPS time series and precipitation for station <i>mang</i> . Starting at the top precipitation (a), in the middle horizontal displacement (b) and in the bottom vertical displacement (c). Blue lines delineate the best-fit linear regression and green line the 2cm step in figures b and c.	69
Figure 4-5: GPS time series and precipitation for station <i>josg</i> . Starting at the top precipitation (a), in the middle horizontal displacement (b) and in the bottom vertical displacement (c). Blue lines delineate the best-fit linear regression and green line the 2cm step in figures b and c.	72
Figure 4-6: GPS time series and precipitation for station <i>carg</i> . Starting at the top precipitation (a), in the middle horizontal displacement (b) and in the bottom vertical	

displacement (c). Blue lines delineate the best-fit linear regression and green line the 2cm step in figures b and c.....	75
Figure 4-7: GPS time series and precipitation for station <i>herg</i> . Starting at the top precipitation (a), in the middle horizontal displacement (b) and in the bottom vertical displacement (c). Blue lines delineate the best-fit linear regression and green line the 2cm step in figures b and c.....	78
Figure 4-8: GPS time series and precipitation for station <i>estg</i> . Starting at the top precipitation (a), in the middle horizontal displacement (b) and in the bottom vertical displacement (c). Blue lines delineate the best-fit linear regression and green line the 2cm step in figures b and c.....	81
Figure 4-9: GPS time series and precipitation for station <i>rafg</i> . Starting at the top precipitation (a), in the middle horizontal displacement (b) and in the bottom vertical displacement (c). Blue lines delineate the best-fit linear regression and green line the 2cm step in figures b and c.....	84
Figure 4-10: GPS time series and precipitation for station <i>jerg</i> . Starting at the top precipitation (a), in the middle horizontal displacement (b) and in the bottom vertical displacement (c). Blue lines delineate the best-fit linear regression and green line the 2cm step in figures b and c.....	86
Figure 4-11: GPS time series and precipitation for station <i>luig</i> . Starting at the top precipitation (a), in the middle horizontal displacement (b) and in the bottom vertical displacement (c). Blue lines delineate the best-fit linear regression and green line the 2cm step in figures b and c.....	89
Figure 4-12: GPS time series and precipitation for station <i>refs</i> . Starting at the top precipitation (a), in the middle horizontal displacement (b) and in the bottom vertical displacement (c). Blue lines delineate the best-fit linear regression and green line the 2cm step in figures b.	92
Figure 4-13: GPS time series and precipitation for station <i>dang</i> . Starting at the top precipitation (a), in the middle horizontal displacement (b) and in the bottom vertical displacement (c). Blue lines delineate the best-fit linear regression and green line the 2cm step in figures b and c.....	95
Figure 4-14: GPS time series and precipitation for station <i>jorg</i> . Starting at the top precipitation (a), in the middle horizontal displacement (b) and in the bottom vertical displacement (c). Blue lines delineate the best-fit linear regression and green line the 2cm step in figures b and c.....	98
Figure 4-15: GPS time series and precipitation for station <i>frag</i> . Starting at the top precipitation (a), in the middle horizontal displacement (b) and in the bottom vertical displacement (c). Blue lines delineate the best-fit linear regression and green line the 2cm step in figures b and c.....	101
Figure 4-16: GPS time series for station <i>flag</i> . Beginning in the top, the time series show horizontal displacement (a) and in the bottom vertical displacement (b). Blue lines in a and b delineate the first and last observation.	103
Figure 4-17 : Inclinometer Z2_23 measurements taken from April 18 to August 2012 by Suelos Inc. Each line represents cumulative displacement until April 18, 2012....	105

Figure 4-18: GPS time series for station <i>corg</i> . Beginning in the top, the time series show horizontal displacement (a) and in the bottom vertical displacement (b). Blue lines in a and b delineate the first and last observation.	107
Figure 4-19: GPS time series for station <i>tang</i> . Beginning in the top, the time series show horizontal displacement (a) and in the bottom vertical displacement (b). Blue lines in a and b delineate the first and last observation.	108
Figure 4-20 : GPS time series for station <i>pisg</i> . Beginning in the top, the time series show horizontal displacement (a) and in the bottom vertical displacement (b). Blue lines in a and b delineate the first and last observation.	110
Figure 4-21: GPS time series for station <i>casg</i> . Beginning in the top, the time series show horizontal displacement (a) and in the bottom vertical displacement (b). Blue lines in a and b delineate the first and last observation	112
Figure 5-1: Accumulated displacement and precipitation of the landslide during 2008, 2009 and 2010-11. To the left the total accumulated displacement and precipitation during 2008, 2009 and 2010-11 (a). Accumulated displacement and precipitation before, during and after the each of the surge periods (b). Yellow rectangle in (b) delineate the surge periods for each year.	115
Figure 5-2: Accumulated precipitation and landslide displacement measurements during 2008. Green lines represent the slope lines draw to estimate the rate of displacement and precipitation (modified after Wang, 2012).....	118
Figure 5-3: Average rates in each period for year 2008. Starting from period 1 (P1) to period 6 (P6).	120
Figure 5-4: Accumulated precipitation and landslide displacement during 2009. Green lines delineate the analyzed periods for this study (modified after Wang, 2012)...	122
Figure 5-5: Average rates in each period for year 2009. Starting from period 1(P1) to period 8 (P8).	124
Figure 5-6: Slope lines used to estimate rates for: accumulated precipitation (a), horizontal displacement (b) and vertical displacement (c) of the landslide during 2010 and 2011. The analyzed slope lines marked as green lines.....	126
Figure 5-7: Average rates for years 2010 and 2011. Starting from period 1(P1) to period 17 (P17).....	129
Figure 5-8: Average displacement and precipitation rates comparison.....	131
Figure 5-9: Summaries of all 24-hour static stations monitored outside the landslide from June 2011 to June 2012.....	133
Figure 5-10: Summaries of all 4-hour static stations monitored from June 2011 to June 2012.....	135

1. INTRODUCTION

The term landslide is defined as the downslope movement of a mass of rock, debris or earth (Cruden and Varnes, 1996). Movement down the slope is by falling, sliding, flowing or a combination of these. A primary factor in the development and triggering of landslides is the slope change from stable to unstable. Slope stability is related to the downward movement of soil or rock under the influence or a combination of water, steep slopes and earthquakes. On average the frequency of landslides are greater on steep slopes because hillslopes with a steep angle increase the shear stress of the overlaying material and a gentle hillslopes is expected to have a low shear stress with a low frequency of landslides. Lots of countries in Central, South America, Caribbean and Pacific Oceans, and developing countries in Asia are commonly endangered by heavy rainfall and having a high vulnerability to flooding and landslides (Harp et al., 2009).

In Puerto Rico rainfall-triggered landslides are frequent throughout the island. The most frequent triggering factors are steep slopes as well as heavy rainfall and these tend to be a recurrent problem in most of Puerto Rico. Major landslides that occur include: slip, slide, flows, avalanches and slump. Construction of highways and structures in steep mountainous areas results in frequent landsliding, but in Puerto Rico landslides takes place during heavy rainfall. Many of the landslides occur when a solid block of rock overlies clayey material and during rainfall when gentle slopes slide into deeper cuts from erosion or nearby constructions. In October 1985 a tropical storm triggered debris

flows in the south-central of the island, (Jibson, 1985). The most notable landslide disaster triggered by this storm was recorded in barrio Mameyes, Ponce where at least 129 people were killed (Jibson, 1985).

The present investigation focuses on a landslide that initiated in the summer of 2007 inside the Cerca del Cielo community (Figure 1-1), which is located near the road PR#132 in Ponce, Puerto Rico. The Cerca del Cielo landslide is about 790 ft from the headscarp to the toe and moves in a general SE direction. Its boundaries are sharply marked by its right and left flank. The community is home to around 30 families and is located about 5km NE of Barrio Mameyes. Major movements of the landslide were detected during November 2007 that resulted with the evacuation of houses inside and adjacent to the landslide mass and affected the water and power system and the only road that access the community (see Figure 1-2). Residents fear of a repeat of Mameyes landslide disaster because the same geologic unit is found in Cerca del Cielo. The Cerca del Cielo landslide has been the focus of previous investigations by:

1. Suelos Inc (2008)

- Investigated the geologic composition and structure of the landslide and slope stability affecting the community and determined damaged properties requiring evacuation.

2. Geodetic studies by Wang (2012)

- In 2008, GPS (Global Positioning System) monitoring continuous displacement of the landslide and the influence of precipitation.

During Fall 2008 a high intensity rainfall event caused major displacement.

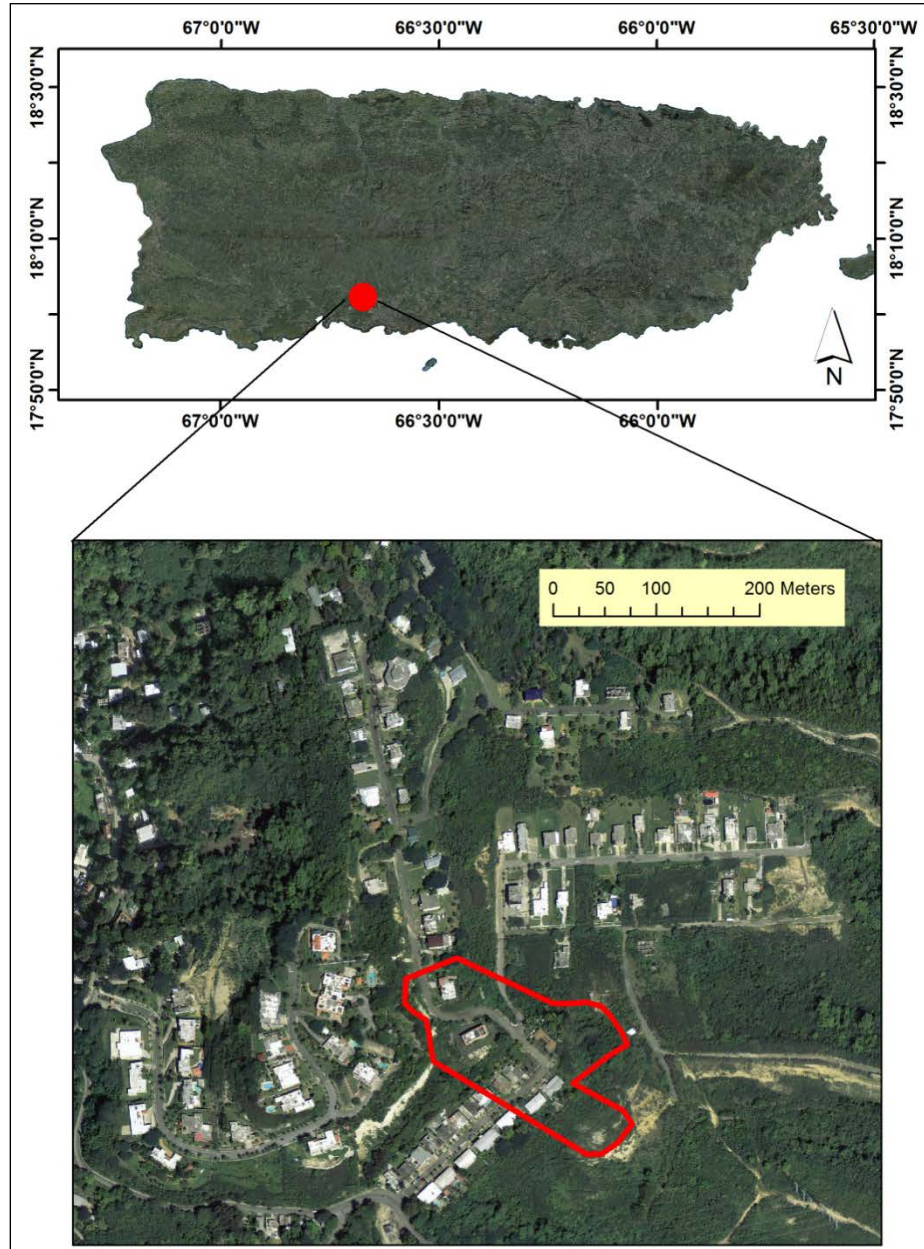


Figure 1-1: Location of the Cerca del Cielo community. The red line delineates the landslide (image from 2010 using ESRI ArcMap©).



Figure 1-2: Main road and houses affected by the landslide.

1.1 Geologic settings

The location of the Cerca del Cielo community is shown on the Geologic Map of the Peñuelas and Punta Cucharras Quadrangles (Krushensky and Monroe H., 1978) in Figure 1-3. The landslide cuts through the main road of the community and lies within faults in the Juana Diaz Formation. According to Krushensky and Monroe H. (1978), there are three Juana Diaz members found in this area: the Chalk Member (Tjc), the Mudstone and Basal Conglomerate Member (Tjd) and Limestone Member (Tjl). The chalk member is described by Krushensky and Monroe (1978) as pale orange clayey chalk and bedded

chalky limestone; the mudstone and basal conglomerate member is described as grayish-orange weathered, light blue calcareous silty to sandy mudstone, interbedded with calcareous sandstone and the limestone member is described as white to grayish limestone mostly crystalline and coralline, with lenses of cobbles and sandy mudstone.

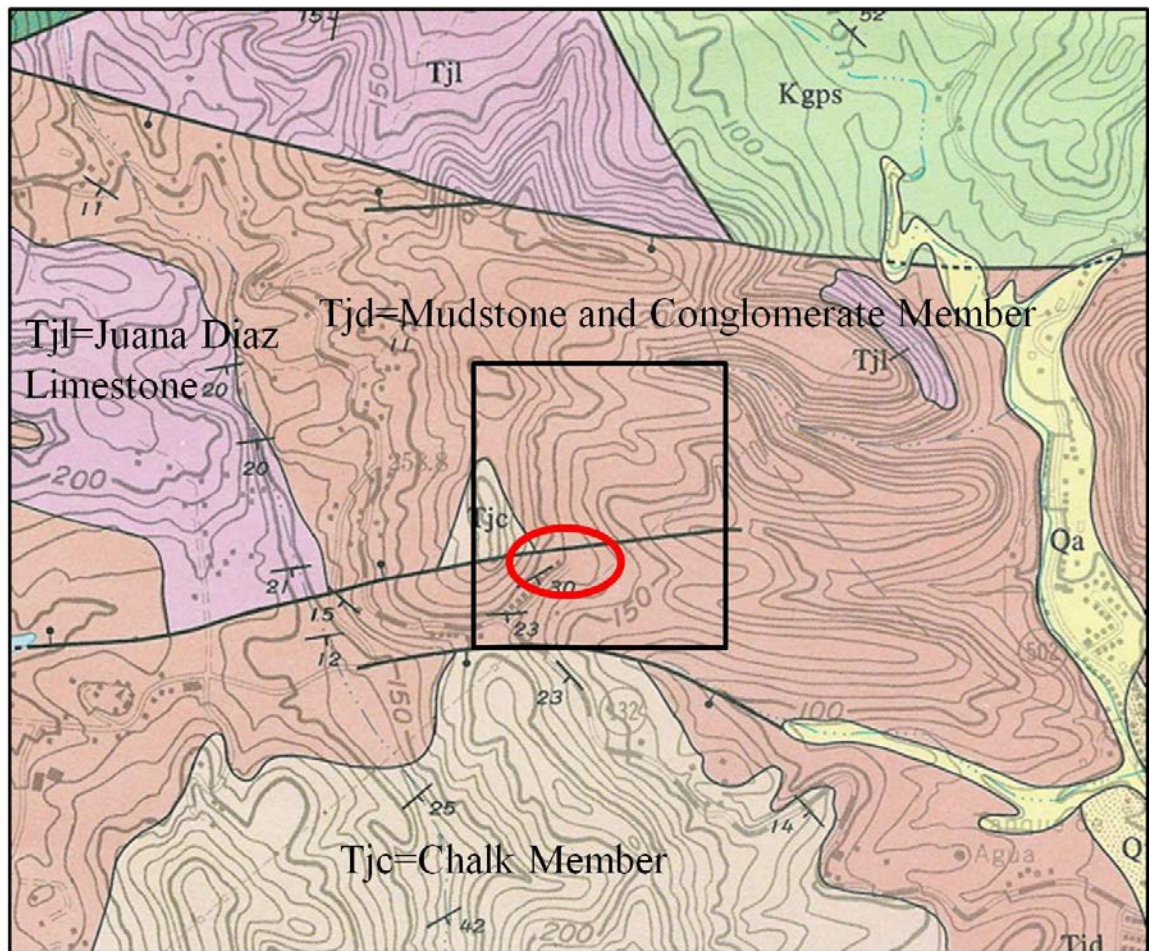


Figure 1-3: Portion of the Geologic Map of Ponce by Krushensky and Monroe H. (1978). The rectangle delineates the location of the Cerca del Cielo community and the red circle shows the location of the landslide.

1.2 Climatic settings

Puerto Rico is a tropical island located in the northeast Caribbean, between the Dominican Republic and the Virgin Islands, that is dominated by easterly winds that control the climate. The moderate to steep mountains that dominate the central region of the island are surrounded by coastal plains. Landslides in Puerto Rico take place more frequently during heavy rainfalls; the central part of the island experiences heavy rainfalls and a semiarid climate characterizes the southwestern part of the island (Figure 1-4). The climate ranges from humid tropical to dry tropical with annual rainfall ranges from 635 to 5000 mm as the result of the orographic effect of the east-west trending central mountain range (Larsen and Simon, 1993). The location of the Cerca del Cielo community is within an area with low mean annual rainfall (Figure 1-4).

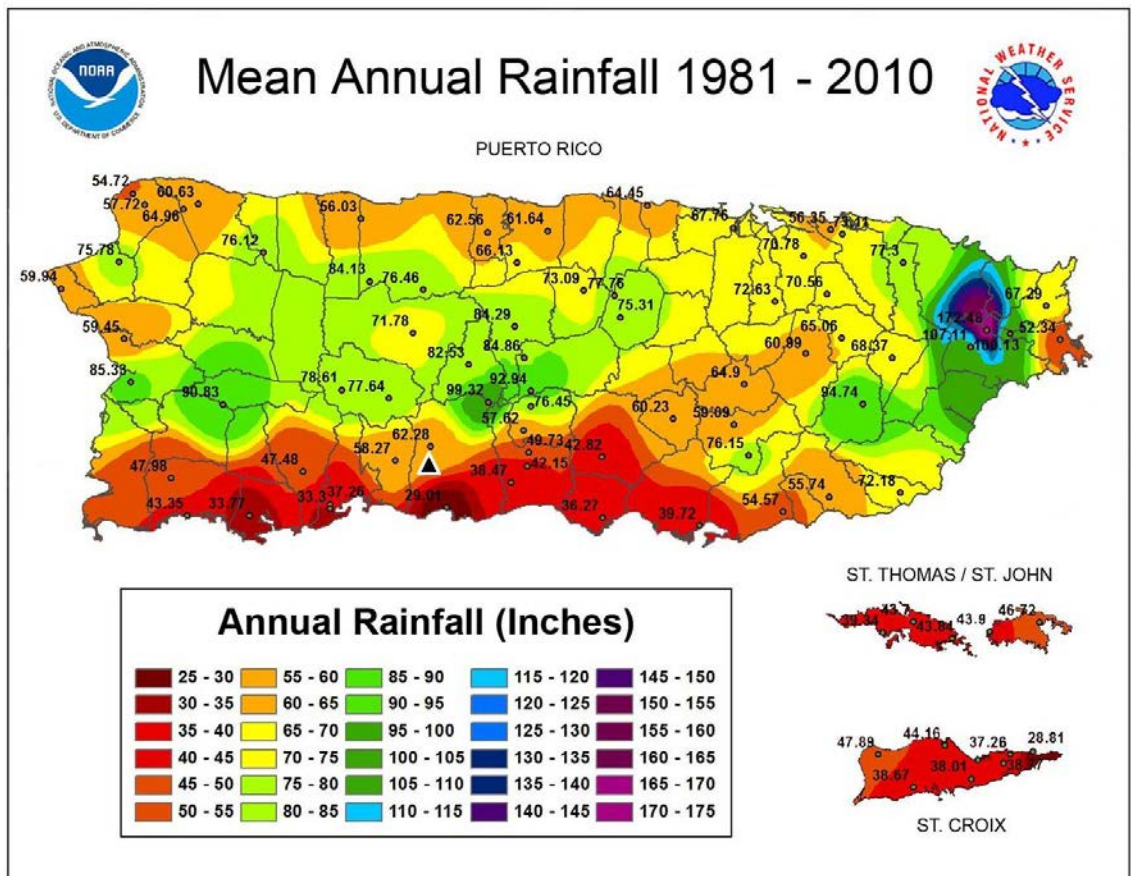


Figure 1-4: Mean Annual precipitation in Puerto Rico from 1981-2010 in inches. Triangle shows the location of the Cerca del Cielo landslide (figure taken from the NOAA website).

The southern part of the island is known to have low mean annual rainfall as seen in Figure 1-4, however it is subject to periodic heavy rainfalls. Tropical systems coming out of the south deliver much of the annual rainfall to the island during the rainy season. At least 400 landslides occurred during peak rainfall periods of hurricane Hugo in 1989 (Larsen and Torres Sanchez, 1992). A more recent example of this was the September 20-24, 2008 passing of a tropical system that later strengthen to hurricane Kyle (Figure 1-5). The storm produced heavy rainfalls in the southern part of the island and impacted the

Cerca del Cielo community with approximately 15-20in of rain. Discussions related to the Cerca del Cielo landslide and rainfall from this tropical disturbance is presented in the Previous Studies chapter of this thesis.

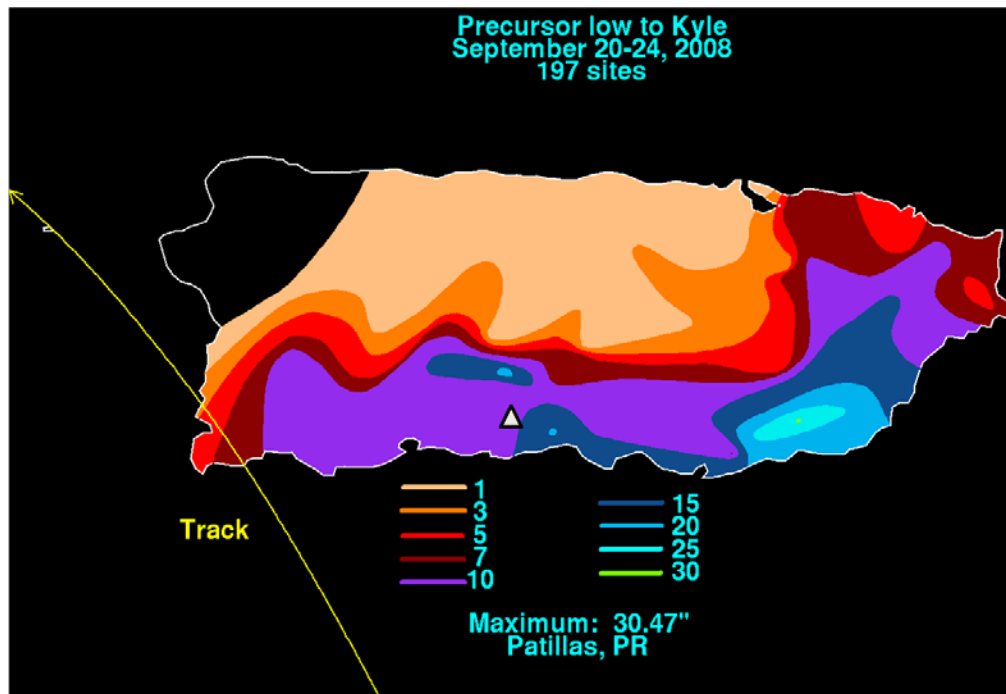


Figure 1-5: Tropical Storm Kyle trajectory and rainfall intensity (in inches). Triangle shows the location of Cerca del Cielo (Weather Underground figure based in NOAA website).

1.3 Objective

Social, political and neighborhood problems caused by the landslide's continued motion have left community and municipality uncertain about what options they have. The municipality of Ponce approved a grant for monitoring landslides and determining the stability of the residences in remaining portions of the community to determine what are the best options for the community. The objectives of this thesis under the grant were to

continuously monitor the Cerca del Cielo landslide and to evaluate of the stability of the homes in the community outside of the landslide using GPS in order to show that residences outside the landslide have not been impacted by the landslide. The aim of this thesis is to monitor the Cerca del Cielo community by:

- Generate a cumulative displacement time-series of the Cerca del Cielo landslide and stations outside the landslide mass by using differential GPS
- Determine the behavior of the landslide during dry periods and wet periods
- Compare creep and surge rates with cumulative precipitation during the monitoring period
- Establish detection limits of displacement estimated and determine stable and unstable areas in the community
- Evaluate the effectiveness and limits of the GPS methods in detecting minor displacements

The Cerca del Cielo landslide continues to move today and to impact the access road to the community. However the question remains of whether the landslide has slowed down due to less precipitation or the center of mass has been displaced enough to reduce the driving force of the slide. We propose a model that predicts that the rate of creep displacement of the landslide is controlled by cumulative precipitation. Some houses located outside the landslide mass have shown structural problems that have been attributed to soil creep. Therefore in order to help the community, we used GPS to establish stable and unstable residences in the community. This study will help the community and local agencies to overcome the fears that they might have over the

propagation and expansion of the landslide hazard and to understand the future behavior of the landslide.

2. PREVIOUS STUDIES

2.1 Landslide susceptibility in Puerto Rico

Monroe (1978) created a landside susceptibility map of the island of Puerto Rico based on the landslide deposits shown on geologic quadrangle maps of the island. He shows that the largest area of high susceptibility lies along the base of the Lares limestone escarpment at the southern margin of the northern karst plateau where it is underlain by the clastic along the base. He divided the island into areas with four levels of landslide susceptibility shown in Figure 2-1. The classifications of landslide susceptibility in the island by Monroe (1978) were: (1) areas of highest susceptibility (recent and active landslides) (2) areas of high susceptibility, (3) areas of moderate susceptibility and (4) areas of low susceptibility. He described areas of highest susceptibility as composed of colluvium material from ancient landslides of Holocene age that are no longer active, but where excavation may cause the reactivation (Monroe, 1978). He also mentioned that areas where the slopes are greater than 27° were classified as with high susceptibility. Most of the central region of the island is mapped as moderate susceptibility, these areas are composed of weathered saprolite and may be stable, but become unstable with heavy rainfall and steep cut slope excavations (Monroe, 1978). Areas with low susceptibility on the island are almost flat underlain by unweathered stable rock (Monroe, 1978). The locations of the Cerca del Cielo and Mameyes on the Landslide Susceptibility map of Puerto Rico (Figure 2-1) by Monroe (1978) are in an area that ranges from low to

moderate susceptibility. Subsequently landslide susceptibility has been mapped at the municipality level for Comerio and Ponce.

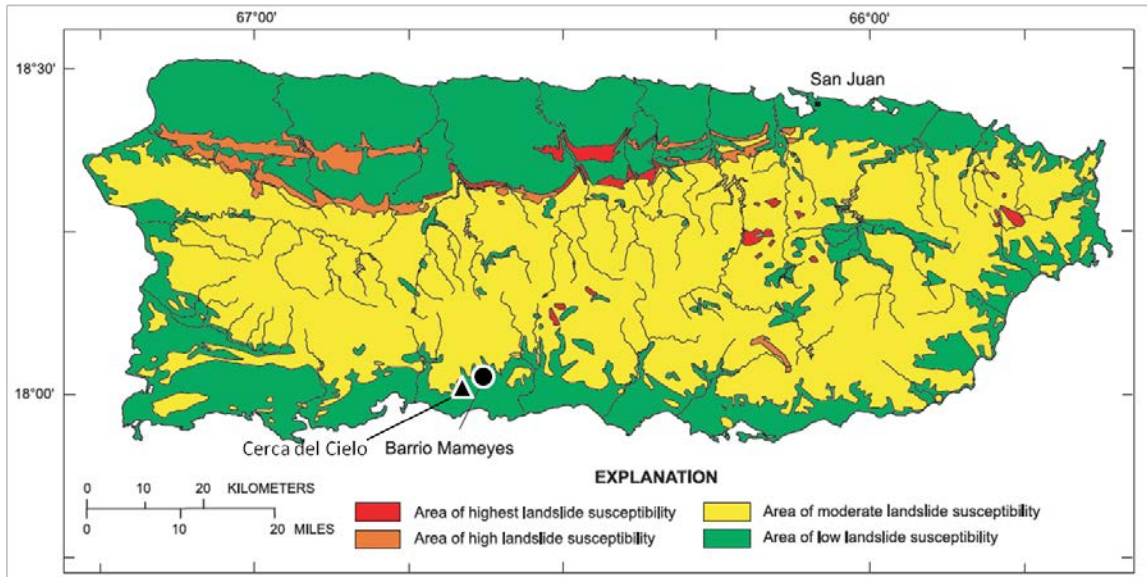


Figure 2-1: Landslide Susceptibility Map in Puerto Rico by Monroe (1978) showing the location of the Cerca de Cielo community (triangle) and Mameyes (circle).

2.2 Landslides in the municipality of Ponce

The worst landslide disasters in Puerto Rico and the United States occurred in Barrio Mameyes in Ponce (Figure 2-1) on October 7, 1985 when at least 129 people were killed during the rainfall intensity peak of a tropical wave (Jibson, 1985). The Barrio Mameyes was constructed on a steep hill and the failure was triggered by 560mm of rainfall in 24hours by (Jibson, 1989). According to Jibson (1985) the movement of this deep landslide was mainly a rock-block slide comprised of two intact blocks 20-30 feet thick that slid downslope along the chalky sandstone layers of the Juana Diaz Chalk Member that are inclined parallel to the slope surface at the landslide location. According to

Jibson (1985), debris flows were the most common type of landslide generated by this event and the majority were within the Juana Diaz Formation.

2.3 Landslides and rainfall correlation in Puerto Rico

The relationship between antecedent rainfall, rainfall duration, rainfall intensity and number of landslides has been studied in California (Wieczorek, 1987) and in Puerto Rico (Larsen and Torres-Sanchez, 1996; Larsen and Simon, 1993; Larsen and Torres Sanchez, 1992). Wieczorek (1987) determined that antecedent rainfall and duration are important to determine when a landslide will initiate; these may vary from hours to weeks. The infiltration and accumulation of rain water prior to landsliding can vary depending on soil permeability and thickness.

Larsen and Simon (1993) developed an intensity duration threshold for triggering landslide in Puerto Rico based on analysis of 256 storms from 1959 to 1991. The threshold by Larsen and Simon (1993) is shown in Figure 2-2. According to Larsen and Simon (1993) 41(1-2 per year) of the 256 storms triggered landslides. He determined on average, that durations of 10 hours or less require more than 14mm per hour to trigger landslides and that durations of 100 hours can trigger landslides with an average intensity of 2-3mm per hour. According to Larsen and Simon (1993), short duration storms like Hurricane Hugo, triggered mostly shallow landslides and long duration storms like Hurricane David triggered the largest and deepest landslides (Figure 2-2). In 2008 during September a tropical wave that strengthens to Hurricane Kyle (see Figure 1-4) accumulated 30cm in 1 day in the Cerca del Cielo area (Figure 2-2). Rainfall event during

that period falls along the Larsen and Simon (1993) intensity duration threshold (Figure 2-2).

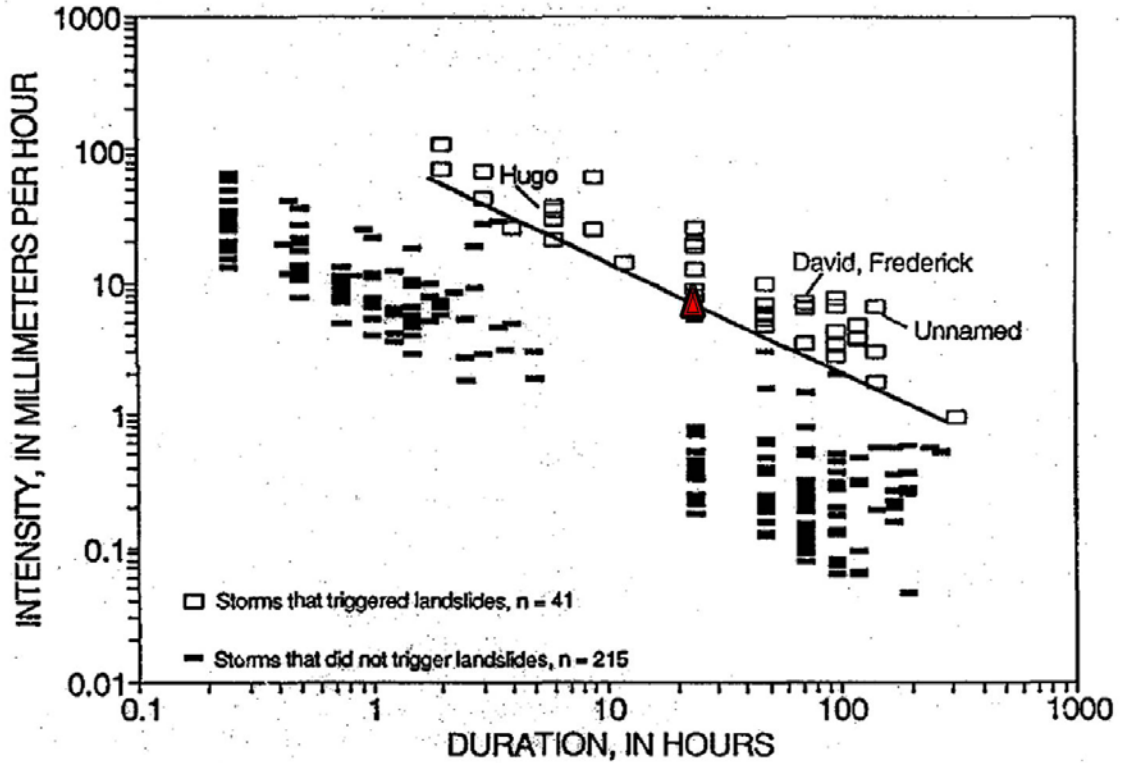


Figure 2-2: Rainfall Intensity-Duration Threshold for Puerto Rico by Larsen and Simon (1993). Showing the 41 landslides triggered by storms from 1958-1991. The triangle shows rainfall event on September 2008 in Cerca del Cielo.

Larsen and Torres-Sanchez (1996) studied the triggering of landslides in the central mountains of Puerto Rico during long-duration storms using 41 landslides triggered by storms from 1958 to 1991. More than a half (25) of the 41 landslides studied by Larsen and Torres-Sanchez (1996) occurred during hurricane season (Figure 2-3). In Figure 2-3 a large percentage of the landslide occurs in May, when the tropical waves begin to affect the island. Hurricane Hugo in September 1989 triggered more than 400 landslides and

debris flows in the northeastern area of Puerto Rico during a 24-hour period with 200mm of accumulated rainfall according to Larsen and Torres Sanchez (1992). The first major movement of the Cerca del Cielo occurred during November 2007 (Fall).

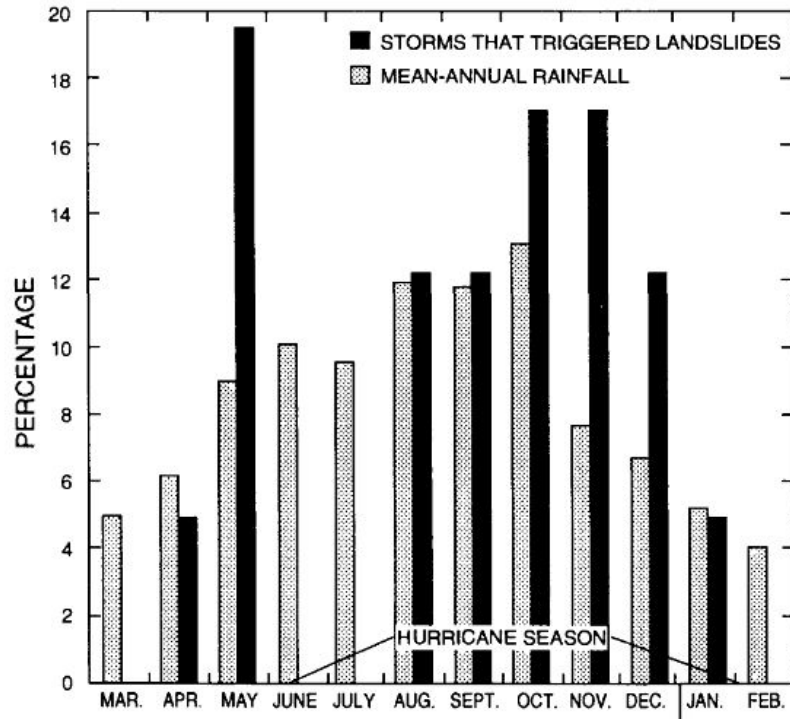


Figure 2-3: Percentage of landslide triggered by storms compared with annual rainfall from 1958-1991 (Larsen and Torres-Sanchez, 1996).

2.4 Ponce Landslide Susceptibility Map

The landslide susceptibility map of Puerto Rico by (Monroe, 1978) was too general and showed Mameyes and all of southern Puerto Rico as moderate to low susceptibility. One of the worst landslides occurred in Barrio Mameyes in Ponce, Puerto Rico (Jibson, 1985, 1989). Rainfall induced landslides and the Barrio Mameyes landslide have drawn the attention of local authorities to delineate landslide prone areas in Ponce. In 2004 Larsen

et al constructed a landslide susceptibility map for the municipality of Ponce. The study was based on hillslope angle, bedrock geology and the location of the 560 landslides recorded during the passing of the tropical storm in October 1985. In the article that accompanies the susceptibility map, shown in Figure 2-4, Larsen et al., (2004) classified the municipality of Ponce into three areas of susceptibility (low, moderate and high). According to Larsen et al (2004), areas with slopes of 30° or more had high landslide frequencies, areas with slopes of 11°-30° had moderate landslide frequencies and areas with slopes of 6°-10° had low landslide frequencies. Ponce has slopes of 10° over 56% of the municipality. The possibility of a landslide increases with heavy rainfall and construction (Larsen et al., 2004). According to Larsen et al., (2004) in Ponce 4 types of bedrocks were most prone to landsliding. Out of the 560 landslide locations in Larsen et al., (2004); 321(57%) are within the Juana Diaz Formation, 66(12%) are in the Yauco Formation, 54(10%) are in the Ponce Limestone and 43(9%) are in the Monserrate Formation. The majority of the landslides in the study fell within the Juana Diaz Formation according to Larsen et al., (2004). The location of the Cerca del Cielo community in Figure 2-4 ranges from high to moderate susceptibility to landslides and over the bedrock most prone to landslides, the Juana Diaz Formation.

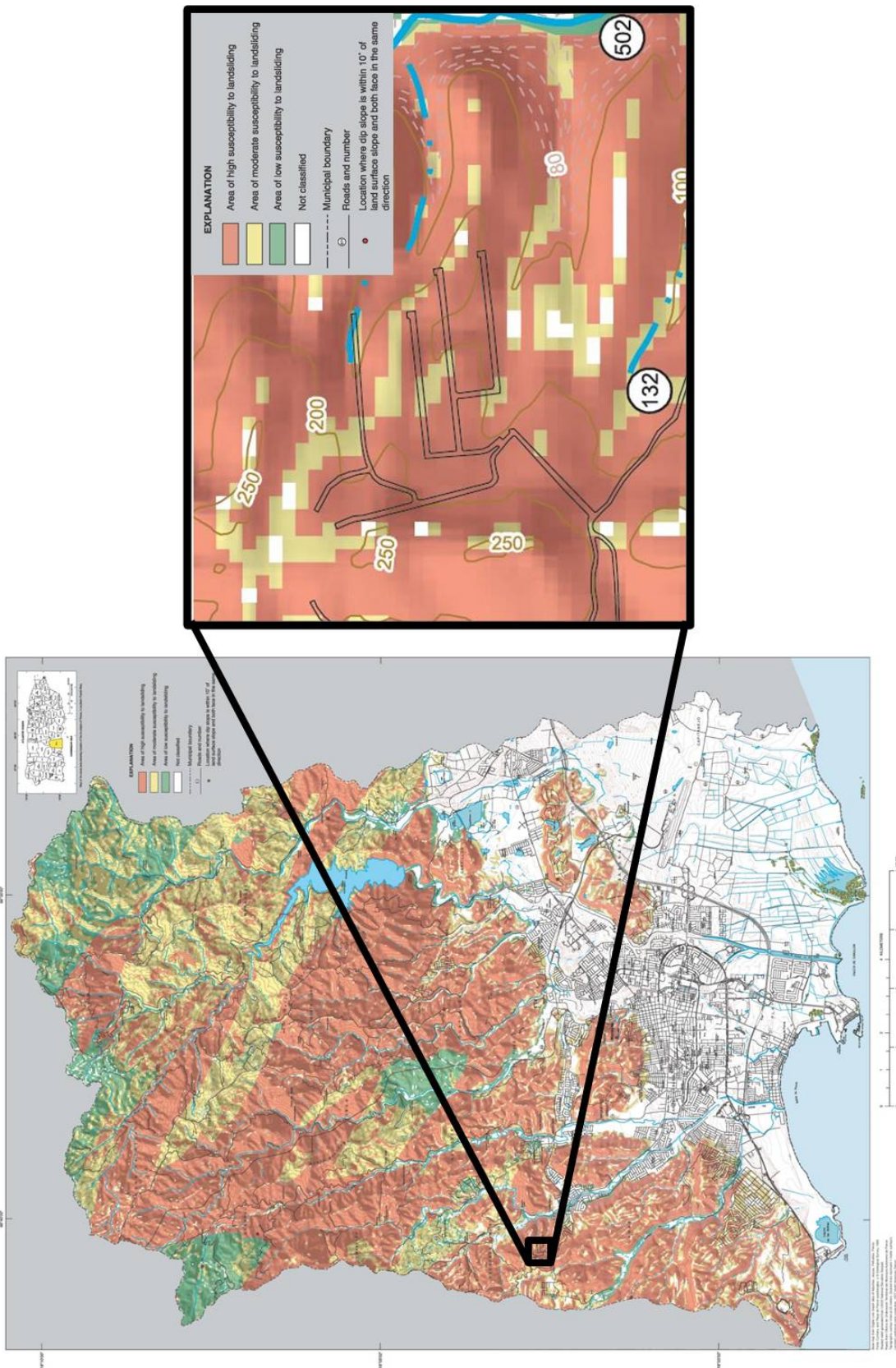


Figure 2-4: Ponce Landslide Susceptibility Map by Larsen et al (2004). The black square delineates the location of the Cerca del Cielo community.

2.5 Cerca del Cielo landslide

2.5.1 Geotechnical studies and Geologic assessment

In 2007 Geotechnical studies of the community were done by Suelos Inc. in conjunction with the geologic assessment by Dr. Joyce; both studies were reported in 2008 by Suelos Inc. Geotechnical studies by Suelos Inc. (2008) focused in two zones (Figure 2-5): Zone 1 covers slope instability and the landslide and Zone 2 covers the northern area of the community where there were residencial structural problems. In both zones SPT (standard penetration test) soil borings and inclinometers monitoring were performed.

As reported by the investigation, Zone 1 contains the landslide with features including the main scarp with crown cracks, a clear zone of depletion and a zone of accumulation and measures 790 ft from the main scarp to the toe. One of the reasons given for the reactivation of this slide was the reduction of resistance force at the base of the slope combined with the high plasticity clay of the slip surface. Volume changes of clay on hillslope create creep and tension cracks during dry periods. Displacement of the landslide recorded by inclinometers from November 2007 to February 2008 ranged from 0.5 inch per day up to 1 inch per day to the southeast during heavy rain (Suelos Inc., 2008). The soil borings and inclinometers were used to determine the location of the slip surface in the soil surface below the chalk colluviums.

According to the report by Suelos Inc. (2008), inclinometers in Zone 2 did not show deflections, but the presence of expansive soils and small creep of artificial fills were recognized in the zone. According to the Suelos Inc. (2008) report, they recommend more monitoring in this area using inclinometers and GPS to measure horizontal movement on the slopes.

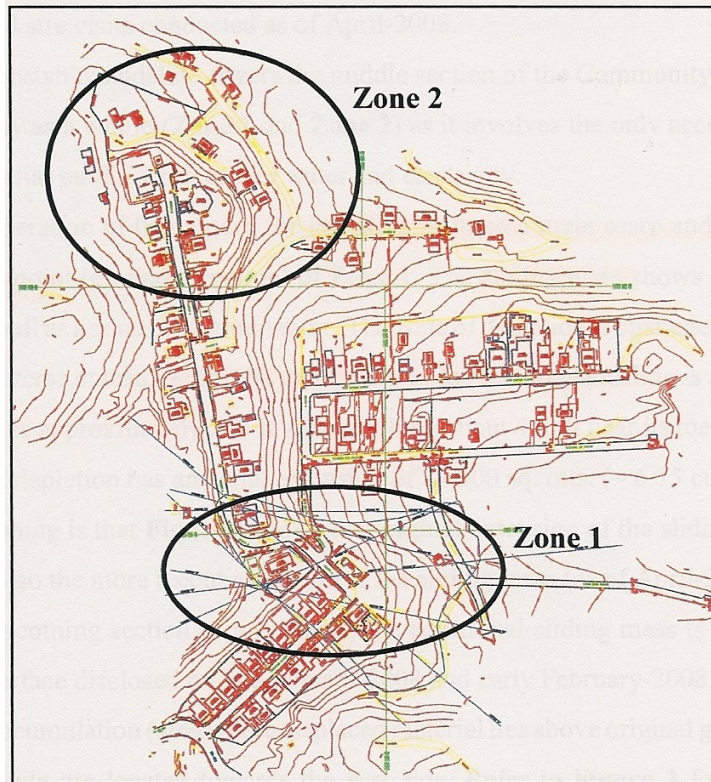


Figure 2-5: Map showing Geotechnical studies (Zone 1 and Zone 2) done by Suelos Inc. (2008).

In 2008 Suelos Inc. identified the geologic structure and composition of the Cerca del Cielo landslide based on borings and inclinometer data from Suelos Inc. (2008). Figure 2-6 shows a Geologic Map of the Cerca de Cielo Landslide (Suelos Inc., 2008). According to Suelos Inc. (2008) the landslide occurs within the mudstone of the detrital member at the base a chalk colluvial deposit. In the report, Suelos Inc. (2008) identified a geologic unit not found in the geologic map, which was described as blocks and pieces from the Chalk Member and classified as Quaternary colluvium. According to Suelos Inc. (2008) this unit was recognized within the landslide and above the headscarp and plays an important role in controlling the movement of the landslide.

The stratigraphic column descriptions done by Suelos Inc. (2008) are shown in Figure 2-6b. They described the Juana Diaz Limestone unit as recrystallized coral limestone overlain by strong cemented grainstone. The limestone is overlain by thick layers of packstones and grainstones interlayered with sandy and silty weathered weak mudstone that grades upwards into the Juana Diaz Mudstone Member (Suelos Inc., 2008). The Chalk Colluvium overlies the weathered mudstone unit with a thickness of 80 ft. The weathering of the mudstone suggests an exposure before being covered by the chalk colluviums unit (Suelos Inc., 2008). Observation and inspections of the houses located over the thick Chalk Colluvium showed limited damage, indicative of movement as a coherent sliding block.

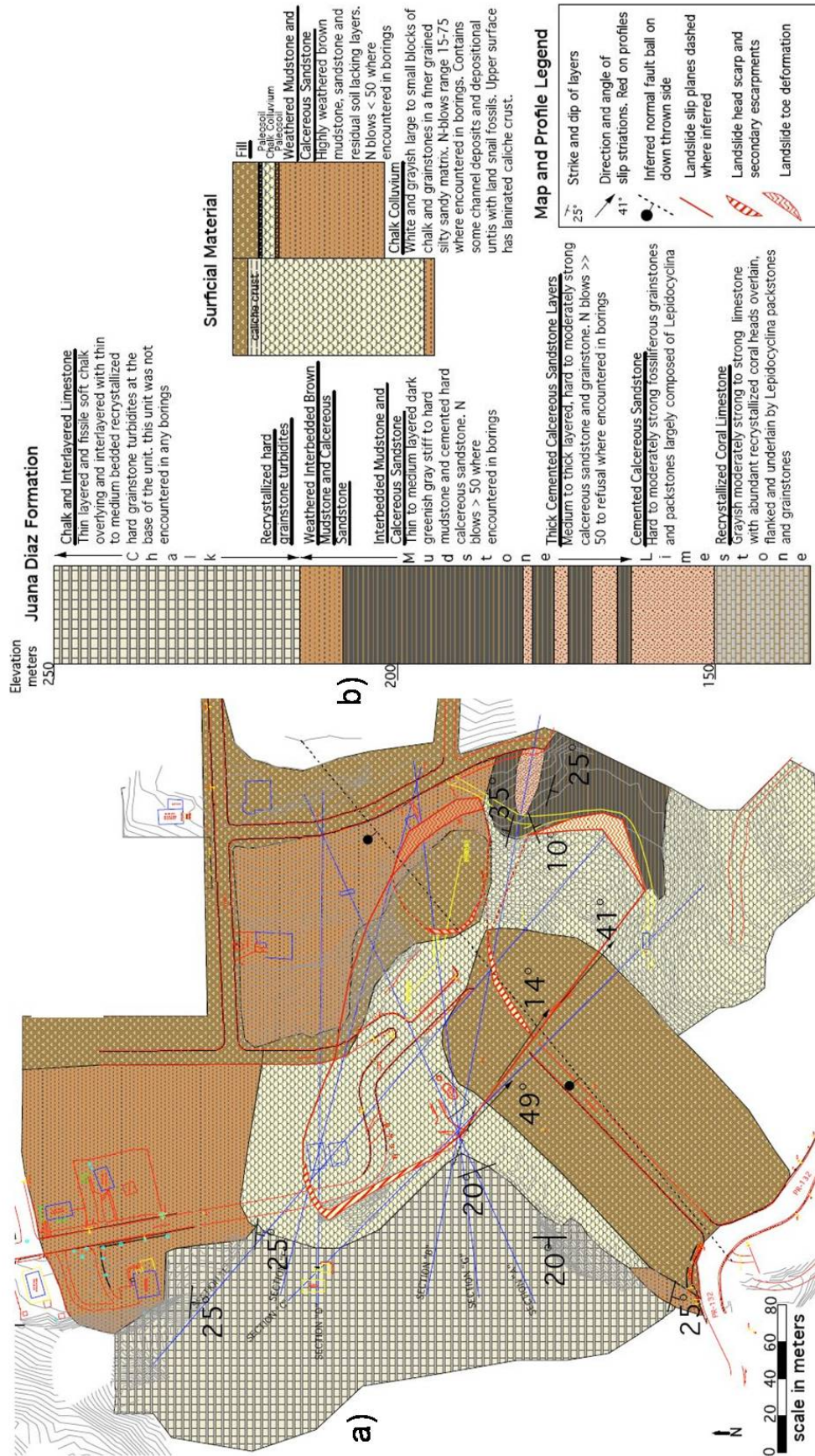


Figure 2-6: Cerca del Cielo landslide geologic map (a) and stratigraphic column (b) done by Suelos Inc. (2008).

A profile of the Cerca del Cielo landslide that cuts from the northern part of the headscarp to the left toe is shown in Figure 2-7. The landslide occurs below an 80 feet thick colluvial deposit that lies over the highly plastic weathered mudstone member. The inclinometer and boring data establish that the basal slip surface lies in the weathered mudstone directly below the thick Chalk colluvium. Straight flanks in the SE sliding direction define the limit of the thick chalk colluvium and sharp contact between the Chalk Member and the chalk colluviums in the headscarp. The 80 feet thick chalk colluviums slides over the weaker weathered brown Mudstone unit at an angle of 50° in the headscarp and 15° near the center of the mass. Inclinometer deflections, boring logs and slip striations on the right flank were used to determine that the 15° basal slip surface also lies within this contact (Suelos Inc., 2008). At the foot of the landslide according to Suelos Inc. (2008), an anticline of interlayered mudstone and calcareous sandstone divides the landslide mass into two different toes (Figure 2-7). The composition of the toe according to Suelos Inc. (2008) is somewhat the same as the headscarp but covered with reworked Chalk Colluvium indicative of man-made earthwork. In the report Suelos Inc. (2008) observed that the basal sliding plane nearing the toe is nearly horizontal, and beyond the toe, it is obstructed by the cemented sandstone of the anticline that seems capable enough to support the advance of the landslide mass.

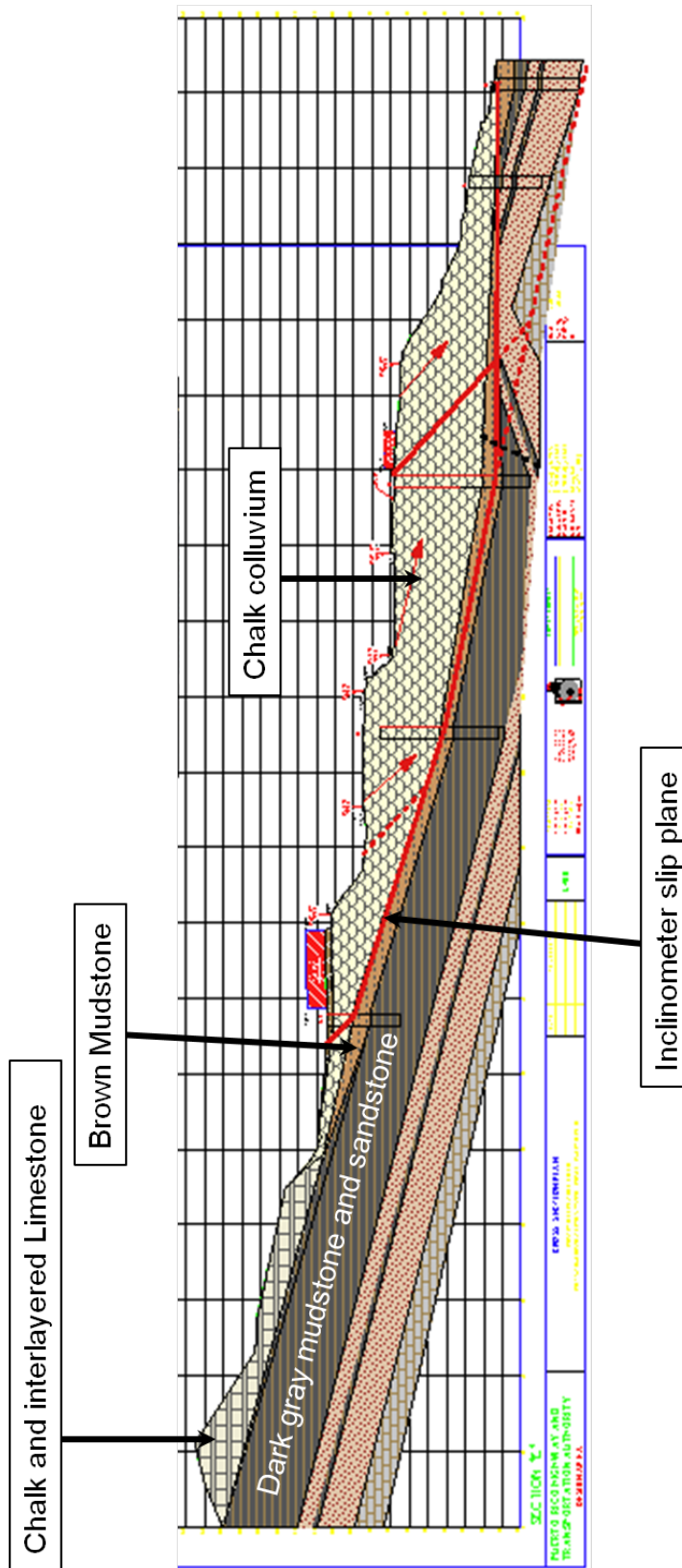


Figure 2-7: Cerca del Cielo landslide profile showing the composition. The red line shows the location of the slip surface (modified after Suelos, 2008).

According to observations by Suelos Inc. (2008) the Cerca del Cielo landslide is a reactivated ancient landslide composed of colluvium from the Chalk unit that lies within the problematic Juana Diaz Formation. This formation is known for its clay content that tends to be highly plastic and weak (Krushensky and Monroe H., 1978; Jibson, 1985, 1989 and Suelos Inc., 2008). Propagation of the landslide into the remainder of the Cerca del Cielo community is restrained due to the limited occurrence of the thick Chalk unit to within the confines of the landslide at the western entrance of the urbanization.

2.5.2 Geodetic monitoring of the Cerca del Cielo landslide

Geodetic studies of the Cerca del Cielo landslide were carried from March 2008 to December, 2009 and published by Wang in 2012. In his study Wang (2012) used continuous GPS to monitor the Cerca del Cielo community and quantified the evolution of the landslide and the influence of precipitation. The campaign network (Figure 2-8) established in March 2008 by Wang (2012) consisted of GPS benchmarks inside and outside of the sliding mass, one reference benchmark (RA) and precipitation data from a USGS weather station (station 50115230) located about 5km northeast of the landslide.

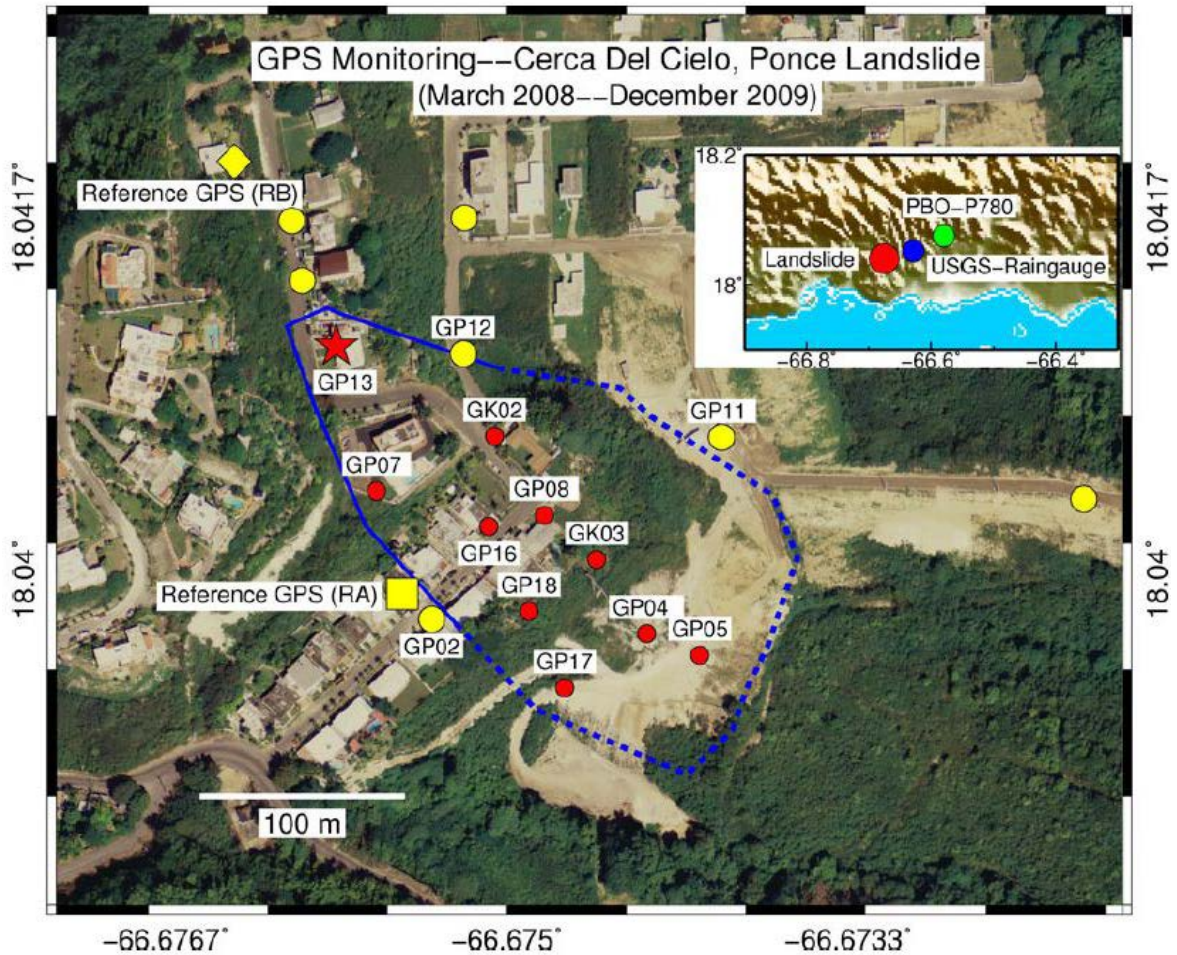


Figure 2-8: Location of the GPS benchmarks established in March 2008 by Wang (2012).

Wang (2012) was able to record landslide displacement using 4 GPS station (*GP07*, *GP13*, *GK03* and *GP18* in Figure 2-8) located inside the sliding mass. Time series from the 4 GPS stations are shown in Figure 2-9. According to Wang (2012) during 2008, 145cm of accumulated precipitation (Figure 2-9a) induced 2m of horizontal accumulated displacement (Figure 2-9b) and about 0.9m of vertical accumulated displacement (Figure 2-9c). Horizontal accumulated displacement and vertical accumulated displacement from

the 4 stations monitored inside the landslide show a rapid slide from September 20 to September 23, 2008 (Wang, 2012). The rapid slide showed a strong correlation with the 50cm of heavy rain that fell during the same period (Wang, 2012). According to Wang (2012) the total landslide movement during the heavy rainfall from September 20 to September 23, 2008 was 1m of the horizontal displacement and 0.5m of the vertical displacement. Before the heavy rainfall, the average displacements rates at the head were 6cm per month for the horizontal displacement and 2.5cm per month for the vertical displacement. After the heavy rainfall during September the average sliding rates reduced to 1cm per month for the horizontal displacement and 0.7cm per month for the vertical displacement (Wang, 2012). During September and October 2008 the head of the landslide descended nearly 2m and the toe was uplifted about 0.5m. Wang (2012) attributes the decrease in the rate of displacement to the resultant reduction of the driving forces at the head and the increase of resistance in the toe caused by the displacement of the landslide mass.

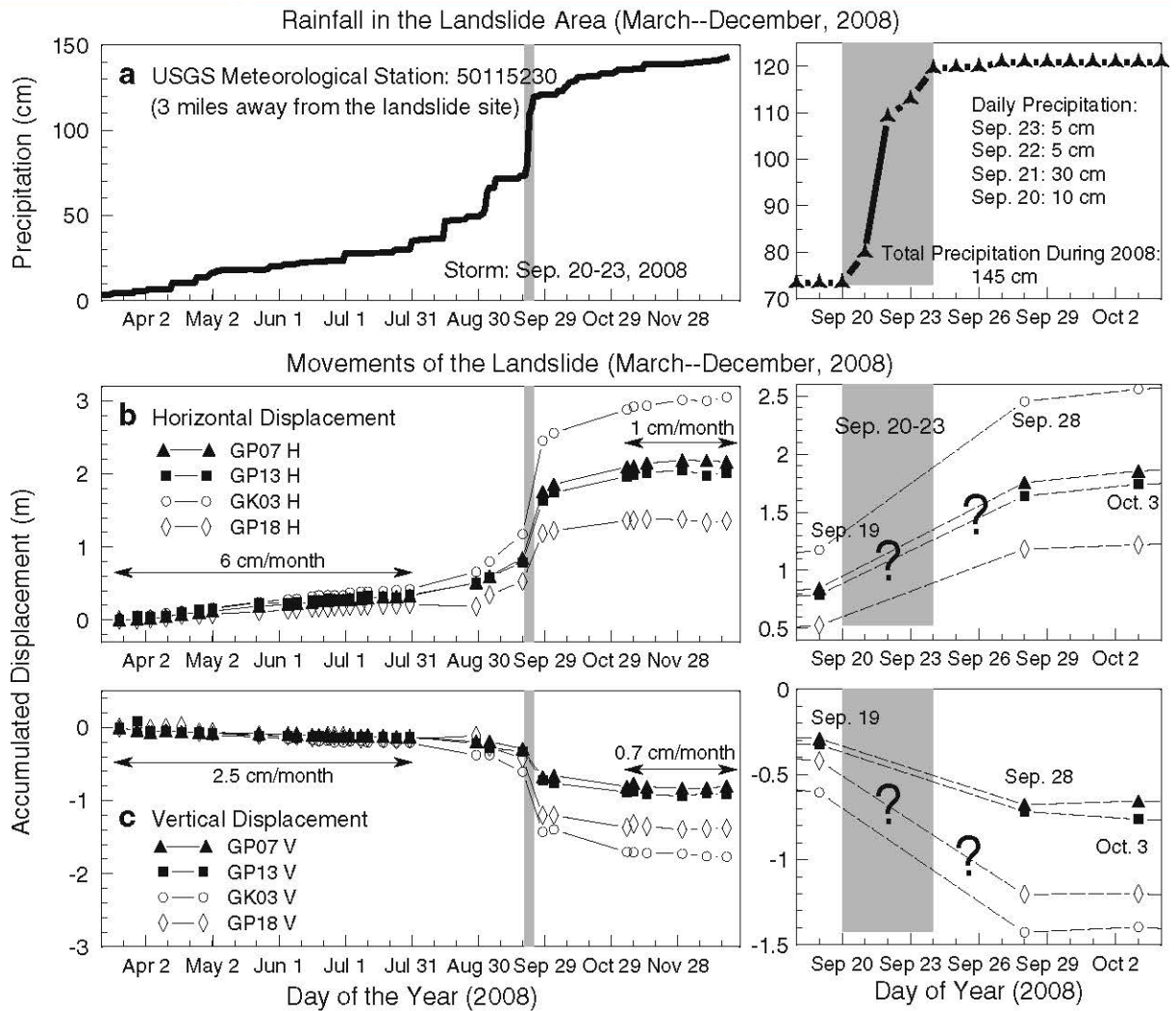


Figure 2-9: GPS measurements performed by Wang (2012) from March to December 2008. At the top precipitation (a), in the middle horizontal displacement (b) and in the bottom vertical displacement (c). Right column is a 15-day window from September 19-October 4, 2008.

In order to closely monitor the landslide, Wang (2012) in 2009, installed a continuous GPS station on the roof of an abandoned house located at the head of the landslide and a rain gauge at the GPS reference location. GPS time series displacement data and local precipitation data collected from June to December 2009 are shown in Figure 2-10. The

total 85cm of accumulated precipitation (Figure 2-10a) induced a total displacement of 6.5cm of the horizontal displacement and 3cm for the vertical displacement (Wang, 2012). According to Wang (2012) from October 30 to November 12, 2009, there were about 25cm of accumulated precipitation that generated 0.8cm of displacement for the north-south (N-S) direction in Figure 2-10b and east-west (E-W) direction in Figure 2-10c and about 0.6cm for the vertical in Figure 2-10d (Wang, 2012a). About three days after the rainfall began in October 30, 2009, the creep displacement of the landslide started to accelerate on November 2, 2009, with about 5cm of precipitation (Wang, 2012). Similar to 2008 another acceleration of the landslide creep occurred from November 7-14, 2009 and was recorded by Wang (2012). Creep of the landslide returned to its previous sliding rate 2 days after the termination of the rain on November 14, 2009 (Wang, 2012). According to Wang (2012), the rapid slide during 2009 did not change the landslide direction (SE), and the slower displacement in comparison to 2008, was due to the less precipitation.

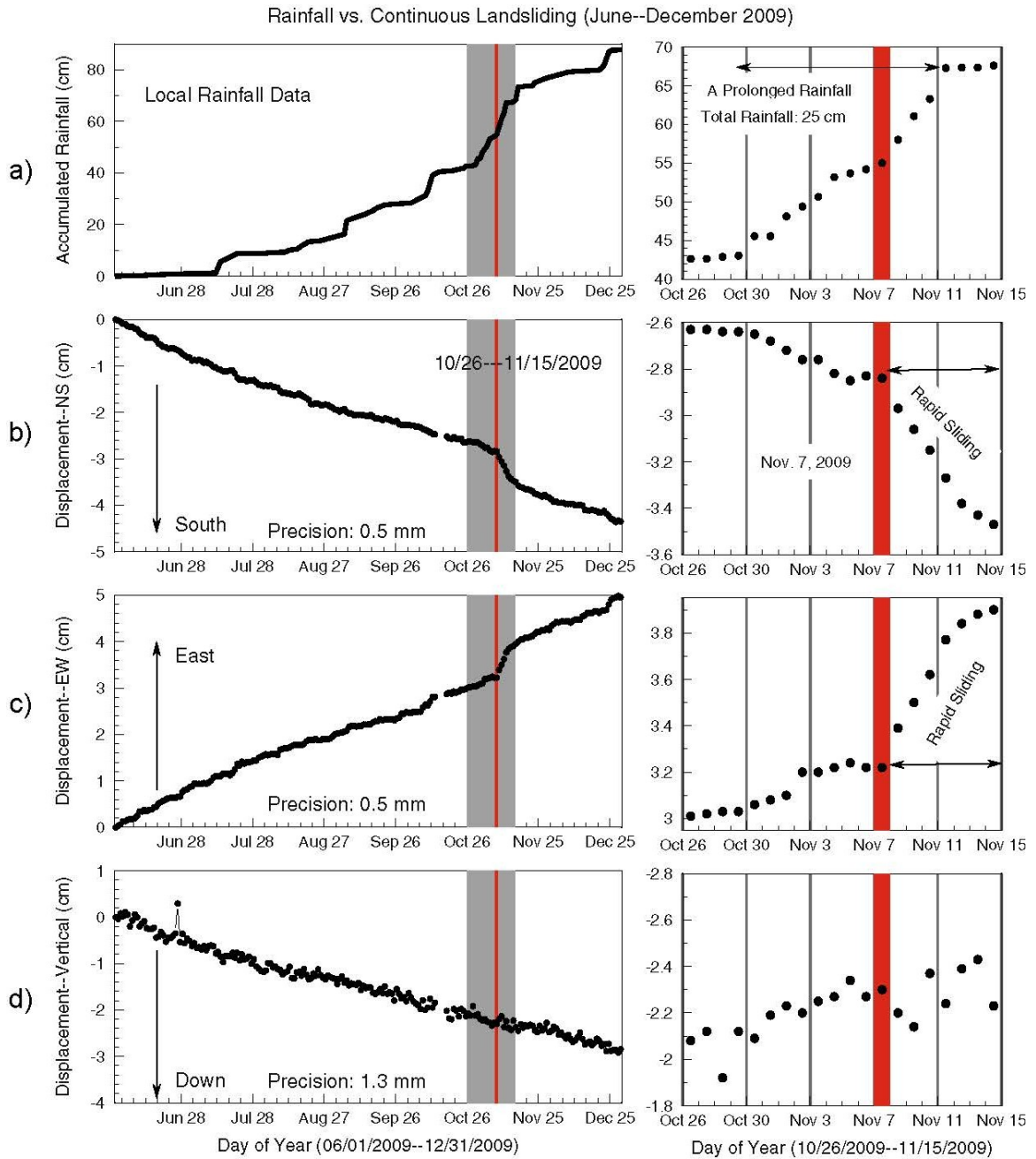


Figure 2-10: GPS measurements performed by Wang (2012) from June to December 2009. At the top local precipitation (a), N-S displacement (b), E-W displacement (c) and vertical displacement (d). Right column is a 2-week window from October 26-November 15, 2009.

3. METHODOLOGY

In order to quantify the geometry, dimensions and evolution of the landslide at The Cerca del Cielo community, a geodetic survey was carried out with stations within and outside the landslide area. In order to assess the kinematics of the landslide, precipitation rates and quantities were compared to its evolution history. Landslide progression is best assessed through monitoring and the most efficient method to understand the behavior is by understanding its kinematics and the triggering conditions. Wang (2012) reported motion of the landslide since 2008 using GPS and Suelos Inc. instrumented the area and studied the landslide using geotechnical methods.

An important development of GPS techniques is the ability to quantify landslide surface displacements at the centimeter level (Gili et al., 2000), dimension, perimeter and even creep rates. Satellites of the GPS constellation have been fully operational for the past decade, which allows more than 4 satellites at a given time both day and night worldwide. The precise position of a geodetic mark could be obtained, either in a reference frame made of a set of sites, or in reference to a base point. A site measured over will indicate a change in its position. This change is the slope of a line or displacement rate, and thus provides the velocity of the, site in a reference frame.

3.1 Geodetic Surveys

This study presents results for 20 static GPS sites (campaign) in the Cerca del Cielo community; 18 sites installed in 2011 specifically for this study, and 2 other sites installed in 2008 used by Wang (2012). Figure 3-1 shows an aerial photograph from

ESRI's ArcMap© that shows all 20 sites used in the study. The GPS monitoring campaign of the Cerca del Cielo landslide for this study consisted of two static stations located within the landslide (Figure 3-1, *CB* and *abeg*).The 18 stations installed outside the landslide boundaries in Figure 3-1were chosen based on the availability of houses and benchmark locations within the community.

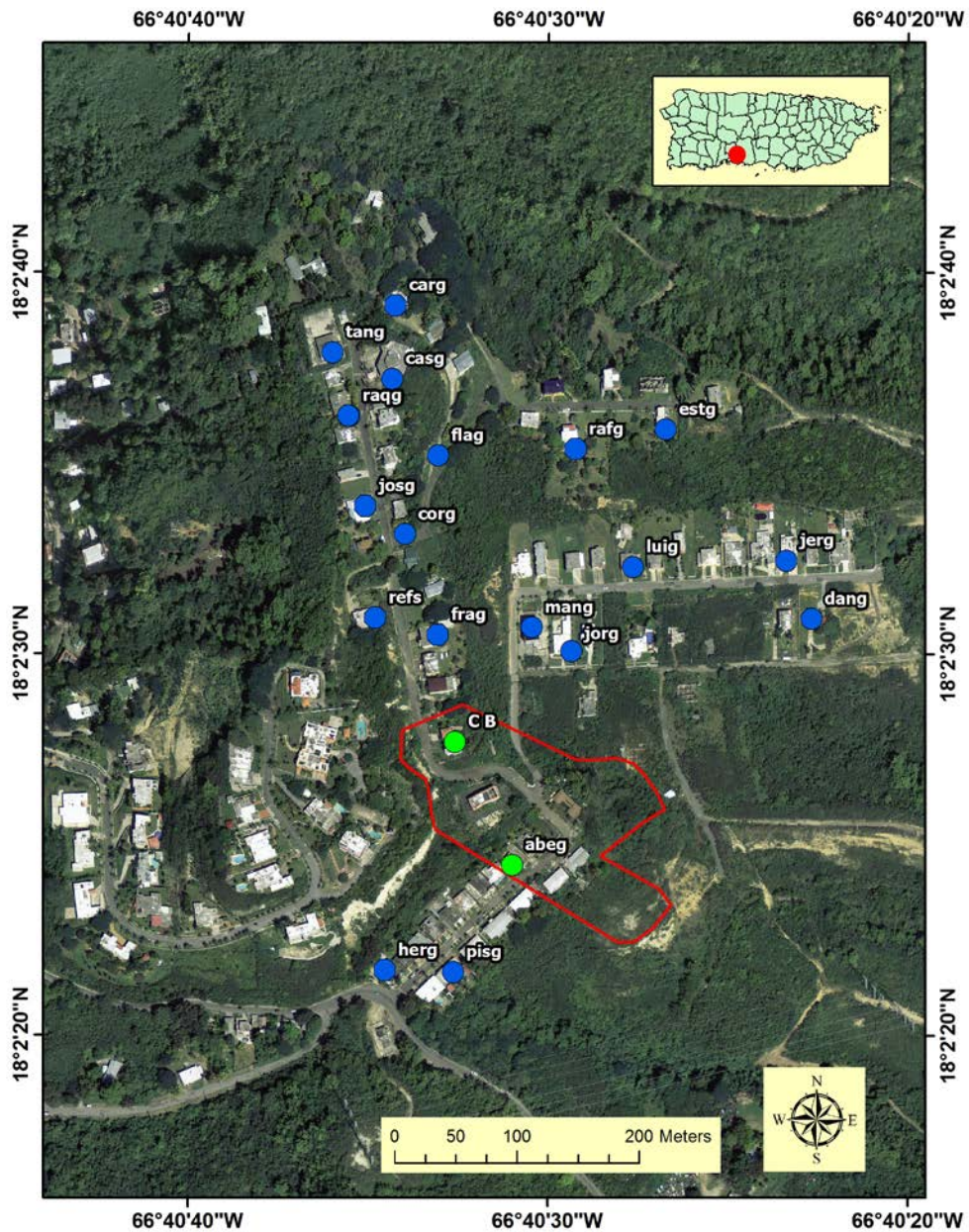


Figure 3-1: Image of the Cerca del Cielo community and the GPS measured points, where the blue markers are stations located outside the boundaries of the landslide (red line) and green markers are stations located inside the landslide (image from 2010 using ESRI ArcMap©).

3.2 Equipment

This study used three GPS receiver models: six Trimble NetR9, one Trimble NetR8 and one Topcon GB-1000. All Trimble receivers were equipped with Trimble Zephyr-Geodetic Model 2 antennae and the Topcon receiver with Topcon PG-A1 antennae. Images of the equipment used for this study are shown in Figure 3-2. The Trimble NetR8 receivers come with 4 gigabytes, the NetR9 with 9 gigabytes and the Topcon receiver comes with 1 gigabyte of internal memory.



Figure 3-2: Equipment used to monitor the Cerca del Cielo community. The left column shows Trimble’s NetR9 receivers (a), Trimble’s NetR8 (www.trimble.com) receivers (b) and Trimble Zephyr-Geodetic Model 2 antennae (c). The right column shows the Topcon’s GB-1000 (www.topconpositioning.com) receiver (c) and Topcon’s PG-A1 (www.unavco.org) antennae (d).

3.3 Data

Data acquisition for the 20 static stations was set at one sample every 15 seconds (0.06Hz). Of the total 20 sites, only two fall within the landslide domain (*CB* and *abeg*). These two sites were established in 2008 by Wang (2012). While *CB* collected data continuously until 2011, *refs* collected data until 2012. For this study we used station *CB* data from January 2010 to July 2011 and data from station *refs* from January 2010 to March 2012. The purpose of sites outside the landslide was to detect further instabilities in the region.

Due to the availability of only six GPS instruments to survey the community, we had to establish a strategy that consisted of rotating the GPS equipment every two weeks. The monitoring periods of all the GPS stations used for this study is shown in Figure 3-3. Notice the continuous collection of data from station *CB* and *refs* that started in 2010. Out of the 18 static GPS stations established in this study, only six stations (*tang*, *casg*, *flag*, *corg*, *abeg* and *pisg*) were established in isolated areas (e.g. without a power source). For the safety of the equipment, these stations were campaign stations monitored for 4 hours every two weeks. GPS station *flag* was co-located with a pre-existing Suelos Inc inclinometer (*Z2_23*). The objective of the co-location was to compare the displacement data registered by GPS and the inclinometer monitoring methods over the same period of time. The monuments of the remaining 12 static sites consisted of a concrete base on the roof of the houses in the community with their own power source provided by the residents. These stations collected data continuously for 24 hours over 2 weeks in 2 week intervals.

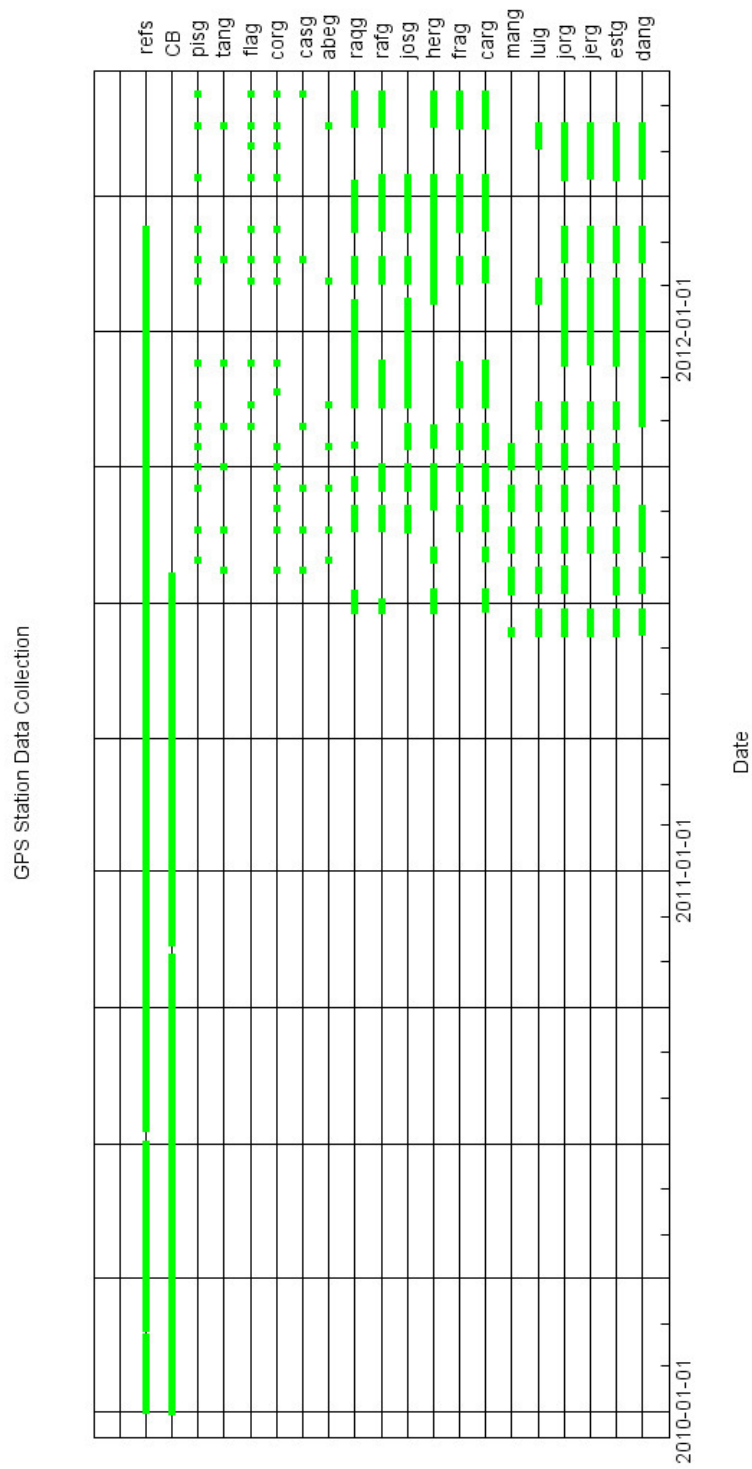


Figure 3-3: GPS stations and the monitored periods from January 2010 to June 2012.

3.3.1 Static GPS method

For this study we applied static GPS surveying to monitor any accumulated displacement (expressed in cm) in each benchmark of the community. Static GPS surveying involves differential GPS or two stationary GPS stations tracking the same satellites to determine their relative position or coordinates. One station is set up as a reference or base station with a known location and the other station is set as a rover station with unknown coordinates. A schematic drawing of the static GPS survey method is shown in Figure 3-4. The method consists on the collection of measurements of the reference and rover simultaneously for a period ranging from 2 hours to 24 hours. To determine the location of a point on Earth, GPS uses the method of resection. Resection is location of one point by its azimuth (orientation) and bearing (angle) between each point. If satellite positions on their orbits are precisely known and if the antenna collects at least four satellites, the receiver can solve by trilateration the three unknown factors defining its position. GPS calculates the position by a set of values called observables also known as the *o-files*. These are derived from electromagnetic waves received from each satellite.

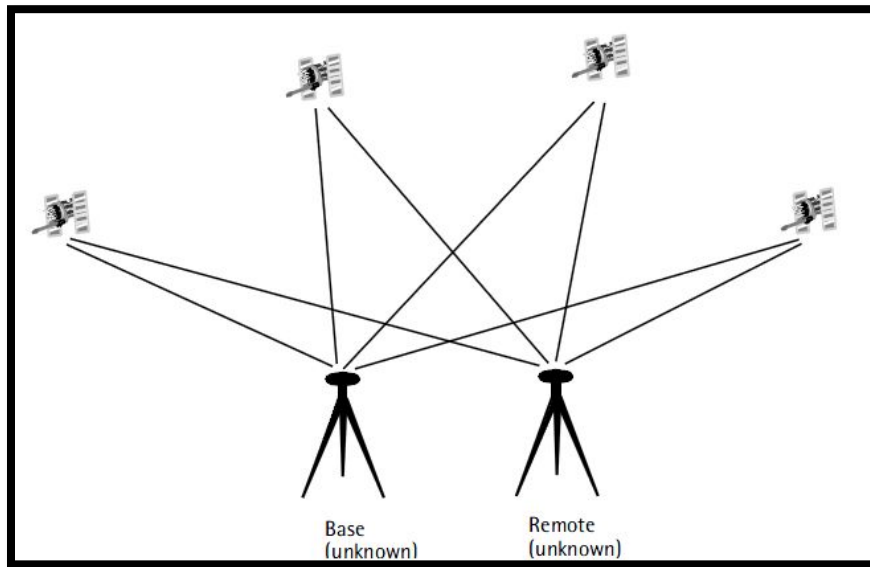


Figure 3-4: Schematic drawing of the static GPS method to determine the position of the rover station using the base station. (El-Rabbany, 2002).

Static GPS is the most accurate positioning technique due to the amount of satellites over the 24-hour observation time span (El-Rabbany, 2002). The GPS accuracy decreases with the reduction of the observation time sessions, errors induced by variation of the satellite constellation, human induced errors (e.g. monumentation or antenna change) and multipath effects (i.e. reflection or diffraction of the desired satellite signal) (El-Rabbany, 2002). The expected accuracy of the static GPS with a 10km baseline is 1cm and 1.5cm for the horizontal and vertical, respectively (Malet et al., 2002). With this accuracy we can detect slow weak displacements and survey temporal change of natural hazards.

3.4 Data Processing

3.4.1 Data pre-processing

Pre-processing refers to the steps involved in converting the raw GPS data into a standardized format to be analyzed (see Figure 3-5). Proprietary binary raw file formats from Trimble (.T00 files) and Topcon (.tps files) receivers need to be converted into the Receivers Independent Exchange (RINEX) format developed by the Astronomical Institute of the University of Berne. The RINEX file consists of three ASCII (American Standard Code for Information and Interchange) files: 1) observable data files (*o-files*), 2) navigation message files (*n-files*) and 3) meteorological data file (*m-file*). The observation file (*o-files*) contains the station name, antenna information, station coordinates, types and number or observation in seconds from the first to last observation. The navigation file (*n-files*) contains information about the satellites: broadcast orbit (ephemerides) and satellite health. The meteorological files (*m-files*) contain the atmosphere data (e.g. temperature, barometric pressure and humidity). These are available only if a meteorological sensor is connected to the GPS receiver.

Trimble's .T00 binary files were converted to .dat files using *runpkr00* (<http://www.unavco.org/software/dataprocessing/preprocessing/preprocessing.html>) program provided by Trimble. The TEQC (Translation, Editing and Quality Checking) (<http://www.unavco.org/software/data-processing/teqc/teqc.html>) program developed by UNAVCO (University NAVSTAR Consortium) was used to convert .dat files from Trimble into RINEX format. Topcon's .tps files were converted to RINEX using

TPS2RIN program (<http://www.topconsupport.com/>) developed by Topcon. For this study we analyzed both Trimble and Topcon observation files.

GPS raw data pre-processing

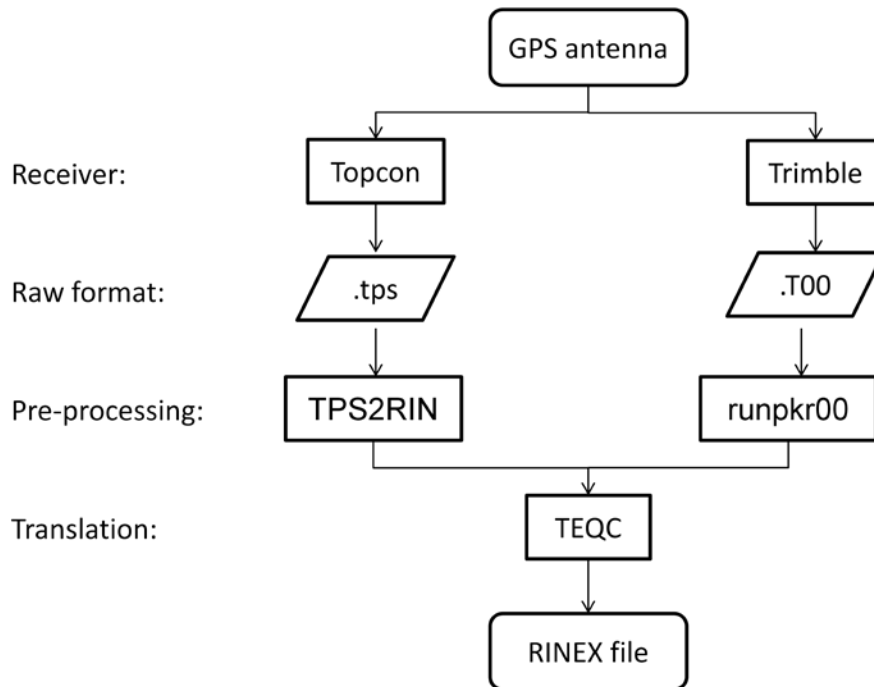


Figure 3-5: GPS raw data pre-processing steps used to obtain the data in RINEX format from their proprietary format (either Trimble or Topcon).

3.4.2 Data processing

Results were processed and analyzed using the Online Positioning User Service (OPUS) online software (<http://www.ngs.noaa.gov/OPUS/>). OPUS, which is a free service provided by the National Geodetic Service (NGS) from NOAA, takes advantage of the Continuously Operating Reference Station (CORS) GPS network from anywhere in the world to calculate the rover coordinates by using differential GPS. The OPUS service

uses the CORS network in the PRVI (Puerto Rico Virgin Island) region and provides a geodetic reference frame for monitoring landslide at the horizontal sub-centimeter accuracy (Wang and Soler, 2012). The OPUS service uses PAGES (Program for Adjustment of GPS Ephemerides) to precisely calculate satellite 3-D satellite position (ephemeris) disseminated by the International GNSS Service (IGS) with accuracies of about 3cm and TEQC to check data quality (Soler et al., 2005). The common procedure we used to calculate each site's position using OPUS was:

1. Upload the observable file (*o-file*) for the desired days from each station.
2. Select the antenna model used
3. Select the antenna height; in our case 0 m was used (solutions are computed using North America Datum (NAD) 83 ellipsoid (2011)). The height of the antenna is the linear distance between the antenna point and the reference ellipsoid.
4. Select the nearest reference stations. Although distance from the rover station to the reference station do not play a major role in position errors (Eckl et al., 2001), for this study the nearest CORS GPS stations with available data in Figure 3-6 (P780, PRMI and PRN4) were used in this thesis. Baseline distance from each of the reference stations to the Cerca del Cielo community were 39km for PRMI, 33km for PRN4 and 11km for P780. The same set of reference stations were used for the entire analysis, this was to restrict any positional error between the reference stations from being introduced in the final solution. During the process, the distance is not of concern because at least 2 hours of tracking sessions are required to produce accuracy of a few centimeters (Schwarz et al., 2008).

5. Enter email to receive the OPUS solution report. The file contains the average position based on the three pre-selected CORS reference baselines
6. Upload static mode (from 2-24 hours of observation)
7. The OPUS solution report is sent by email and shows results of the solution. Figure 3-7 shows an example of the OPUS solution. The northing, easting Universal Transverse Mercator (UTM) coordinates and ellipsoid height solution were extracted from the OPUS solution report for both the International Geodetic Service 2008 (IGS08) and NAD83. For the error or uncertainties, OPUS does not provide the error for the UTM northing and easting coordinates. Instead, the uncertainties from the latitude and longitude in IGS08 and NAD83 (EPOCH 2010.0) were used as uncertainties for the horizontal component. The OPUS report does provide uncertainties for the ellipsoid height in NAD83. The first day of the solution was used as the initial day and the remaining of the period was plotted as the difference between the initial day and the present day. All the solutions were extracted and compiled using Microsoft's Excel© and the open-source scientific graphing program Coplot© was used to plot the accumulated displacement versus measurements dates.

The total horizontal and vertical displacement of each of the stations was estimated using a best-fit linear regression analysis for the 24-hours continuous stations and the difference between the first and last measurements for the 4-hour stations. The best-fit linear regression analysis was also used to estimate the rate of accumulated precipitation.



Figure 3-6: NGS CORS GPS stations (green markers) from the CORS used as reference to monitor the Cerca del Cielo community (red marker) (Google Earth©).

```

FILE: refs3490.11o OP1391013499800

1008 NOTE: Antenna offsets supplied by the user were zero. Coordinates
1008 returned will be for the antenna reference point (ARP).
1008

                        NGS OPUS SOLUTION REPORT
                        =====

All computed coordinate accuracies are listed as peak-to-peak values.
For additional information: http://www.ngs.noaa.gov/OPUS/about.jsp#accuracy

      USER: data.opus@gmail.com          DATE: January 29, 2014
RINEX FILE: refs3490.11o                TIME: 16:41:43 UTC

SOFTWARE: page5 1209.04 master53.pl 072313   START: 2011/12/15 00:00:00
EPHEMERIS: igs16664.eph [precise]           STOP: 2011/12/15 23:59:00
NAV FILE: brdc3490.11n                      OBS USED: 58553 / 59130 : 99%
ANT NAME: TPSPG_A1+GP                       NONE          # FIXED AMB: 145 / 166 : 87%
ARP HEIGHT: 0.0                             OVERALL RMS: 0.020(m)

REF FRAME: NAD_83(2011)(EPOCH:2010.0000)    IGS08 (EPOCH:2011.9548)

      X:      2401933.335(m)  0.013(m)      2401932.637(m)  0.013(m)
      Y:      -5570900.544(m) 0.014(m)      -5570898.744(m) 0.014(m)
      Z:      1962856.989(m)  0.003(m)      1962856.837(m)  0.003(m)

      LAT:    18  2 31.01967      0.008(m)      18  2 31.03441      0.008(m)
      E LON:  293 19 25.07853     0.010(m)      293 19 25.08096     0.010(m)
      W LON:   66 40 34.92147     0.010(m)      66 40 34.91904     0.010(m)
      EL HGT:      184.833(m)  0.016(m)      182.951(m)  0.016(m)
      ORTHO HGT:    224.212(m)  0.027(m)      [ H = h-N (N = GEOID12A HGT)]

                        UTM COORDINATES          STATE PLANE COORDINATES
                        UTM (Zone 19)            SPC (5200 PRVI)
      Northing (Y) [meters] 1996372.154          223106.870
      Easting (X)  [meters] 745982.507           174267.629
      Convergence [degrees] 0.72002533          -0.07604239
      Point Scale           1.00034813          0.99999949
      Combined Factor       1.00031906          0.99997043

US NATIONAL GRID DESIGNATOR: 19QGV4598296372(NAD 83)

                        BASE STATIONS USED
PID   DESIGNATION          LATITUDE  LONGITUDE  DISTANCE(m)
DL6657 PRN4 4N INC CORS ARP  N180442.915 W0662208.704  32784.2
DH9349 PRM1 MAGUEYES ISLAND CORS ARP  N175813.419 W0670243.337  39873.5
DL7773 P780 CERRILLOS_PR2008 CORS ARP  N180430.078 W0663444.887  10925.7

      NEAREST NGS PUBLISHED CONTROL POINT
TV1246  PENUELAS USGS 1934          N180222.211 W0664207.818  2744.9

This position and the above vector components were computed without any
knowledge by the National Geodetic Survey regarding the equipment or
field operating procedures used.

```

Figure 3-7: OPUS Solution report for the 24-hour observations from station *refs* from December 15, 2011. Red boxes show the extracted data for the Northing and Easting in UTM coordinates and the black box shows the errors used from the Latitude and Longitude. Green box shows the extracted Ellipsoid height along with the errors.

The OPUS solution is the mean of three separate single-baseline that yields a peak-to-peak error (Figure 3-8) which provide a more accurate measure of quality to determine

the position (Soler et al., 2005). The peak-to-peak error is the difference between the maximum and minimum values of a coordinate obtained from the three baseline solution (Schwarz et al., 2008).

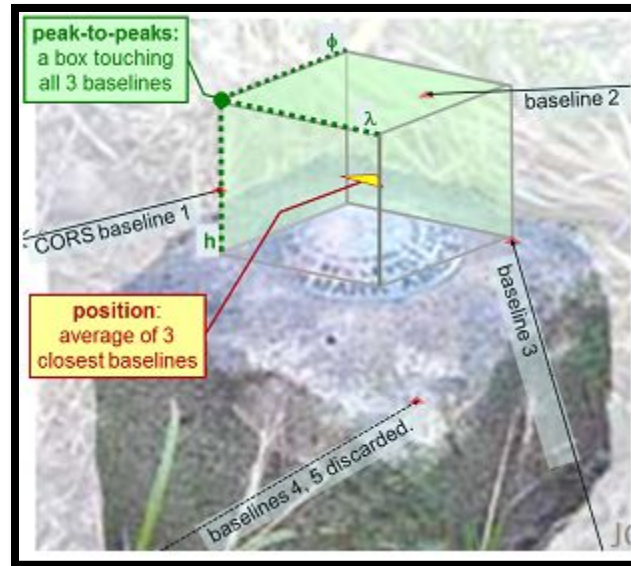


Figure 3-8: Peak-to-peak errors from each baseline (OPUS website).

3.5 Accumulated precipitation

This study seeks to correlate landslide movement with amount of precipitation. Factors such as slope angle, geology of the area and the duration of prolonged precipitation affect slope stability and results in gravitational movement. Puerto Rico is located within the tropics and rainfall is common and frequent. For this study, we used precipitation data from weather station 50115230 located in Portugués River in Ponce approximately 5km NE of the Cerca del Cielo community. Figure 3-9 shows the location of the weather station in relation to the location of the study site. Precipitation data was obtained free of charge from the United States Geological Survey (USGS) website

(<http://waterdata.usgs.gov/pr/nwis>). Daily precipitation data from January 2010 to June 2012 was obtained for the site. The first day of the solution was used as the initial day and the remaining of the period was plotted as the difference between the initial day and the present day. In order to quantify a correlation between rainfall and landslide movement, precipitation values were extracted and compiled using Microsoft's Excel© and Coplot© was used to plot the accumulated precipitation as a function of measurements measurement dates. A best-fit linear regression analysis was used to estimate the rate of accumulation in precipitation.

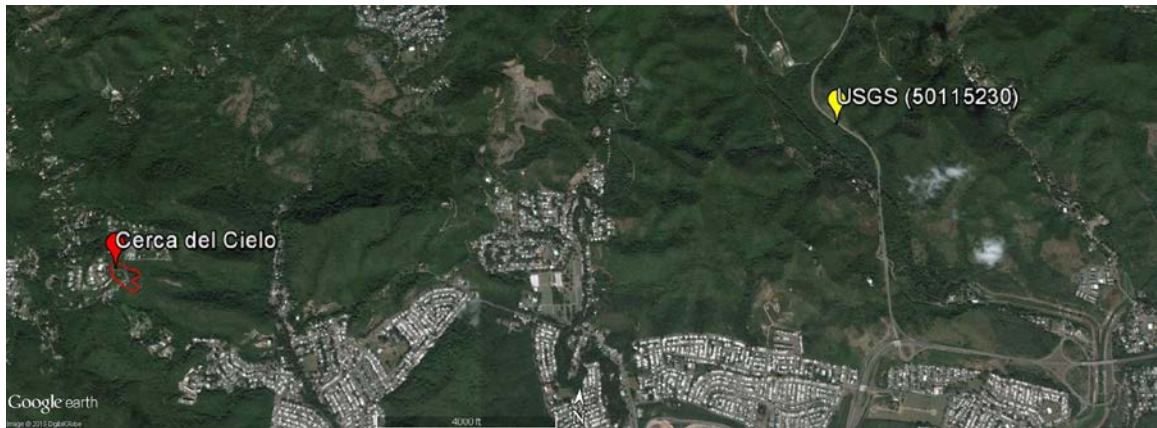


Figure 3-9: Google Earth© image showing the location of the Cerca del Cielo community (red marker), landslide boundaries (red lines) and the USGS weather station 50115230 (yellow marker).

4. RESULTS

This section describes results for stations inside and outside the landslide area with different time spans: continuous and 4-hour data coverage. First, the two sites within the landslide region will be described and followed by the stations outside the landslide area.

4.1 Monitoring stations within the Cerca Del Cielo Landslide

4.1.1 Station *CB*: Continuous

Measuring period

The continuous GPS station *CB* collected data for approximately 19 months from January 2010 to July 2011. The GPS antenna was located on the roof of a house at the head of the landslide just below the head scarp (Figure 3-1, *CB*). This station was located at the same location as the rover station established in 2009 by Wang (2012).

Precipitation

Precipitation data collected at the USGS weather station (station 50115230) over monitoring period were incorporated in the present analysis and are shown on Figure 4-1a. Precipitation data (Figure 4-1a) from USGS weather station recorded 116cm of accumulated precipitation from January 1, 2010 and July 1, 2011. About 40cm of precipitation accumulated during an 8 month period from January 1 and September 1, 2010. The 40cm of precipitation accumulated at a rate of 5cm per month. Around 35cm of precipitation accumulated during a shorter time span of 2 months from September 1 and November 1, 2010. The 35cm of precipitation accumulated at a rate of 18cm per month. After this period, 40cm of precipitation occurred during a 9 month period from

November 1, 2010 and July 1, 2011. The 40cm of precipitation accumulated at a rate of 4.4cm per month.

Displacement

The continuous GPS derived horizontal and vertical displacements that accumulated over the monitoring period are plotted on Figure 4-1b and c, respectively. The total horizontal displacement that accumulated over the monitoring period was 30cm and the total vertical displacement was 14cm. Values of error for individual horizontal data points ranged between -5cm and 19cm and averaged 10cm. Values of error for the vertical data points ranged between -5cm and 12cm and averaged 4cm. The 66% (20cm) of the 30cm total horizontal displacement occurred over a 2 month period between October 1, 2010 and December 1, 2010. The GPS data indicate that the 20cm displacement accumulated at a relatively steady rate of 10cm per month. Prior to the 20cm displacement, only 4cm of displacement accumulated over the 10 month period (rate of 0.4cm per month) between January 1 and October 1, 2010. A similar 4cm total displacement occurred subsequent to the 20cm displacement from December 1, 2010 to July 1, 2011 at a relatively steady rate of 0.5cm per month.

The vertical displacement data show a similar pattern. Figure 4-1c shows continuous accumulated vertical displacement derived from GPS observations for the landslide from January 2010 to July 2011. Vertical observations show a positive displacement in the measurements during September and October, 2010. This positive displacement is an aberration in the observations due to a change of antennas on September 4, 2010. The difference in height of the antenna from the initial point had a positive step in the

observations with relation of the first day of observation; the horizontal was not affected by this disturbance. The 71% (10cm) of the 14cm total displacement occurred after the change of antennas during a 2 month period between October 1, 2010 and December 1, 2010. The GPS data indicate that the 10cm displacement accumulated at a relative rate of 5cm per month. Before the positive step, only 2cm total displacement accumulated over the 10 month period between January 1 and October 1, 2010. The 2cm accumulated at a relative steady rate of 0.2cm per month. A similar 2cm total displacement occurred following to the 10cm displacement from December 1, 2010 to July 1, 2011 at a relative steady rate of 0.2cm per month.

Comparison

The data shows a significant relation exists between landslide displacement and precipitation (Figure 4-1), thus implying that precipitation controls the Cerca del Cielo landslide movement. The total 30cm and 14cm in the horizontal and vertical displacements respectively derived from the GPS data shows an apparent response to the total 116cm of accumulated precipitation. Peak landslide accumulated displacement detected by the GPS occurred during a 2 month period during October 1 and December 1, 2010, not surprisingly, the same time period when the highest precipitation occurred. The 20cm of displacement in the horizontal and the 10cm of displacement in the vertical suggest that the landslide gradually increased the displacement as 30cm of precipitation accumulated during this two month period. Rates of 10cm and 5cm per month of horizontal and vertical displacement respectively are suggested for the two month period.

Prior to October 1, 2010, there was a 9 month period where landslide displacement rates were less than 1cm per month (from January 1, 2010 through October 1, 2010). During this time the landslide recorded low rates of accumulated displacement with rates of 0.4cm per month and 0.2cm per month for the horizontal and the vertical respectively. These low rates of accumulated displacement were during the same period with a low rate of precipitation (5cm per month). The 5 and 2cm of displacement in the horizontal and vertical, respectively occurred during a 7 month period from December 1, 2010 and July 1, 2011, a time in which the rates averaged 0.5cm and 0.2cm per month for the horizontal and vertical components respectively. Precipitation during this 7 month period accumulated 30cm of precipitation at a low rate of accumulated precipitation of 4.4cm per month. Before October 1, 2010 and after December 1, 2010 there was a longer period without continuous precipitation therefore the landslide displacement progressively decreased.

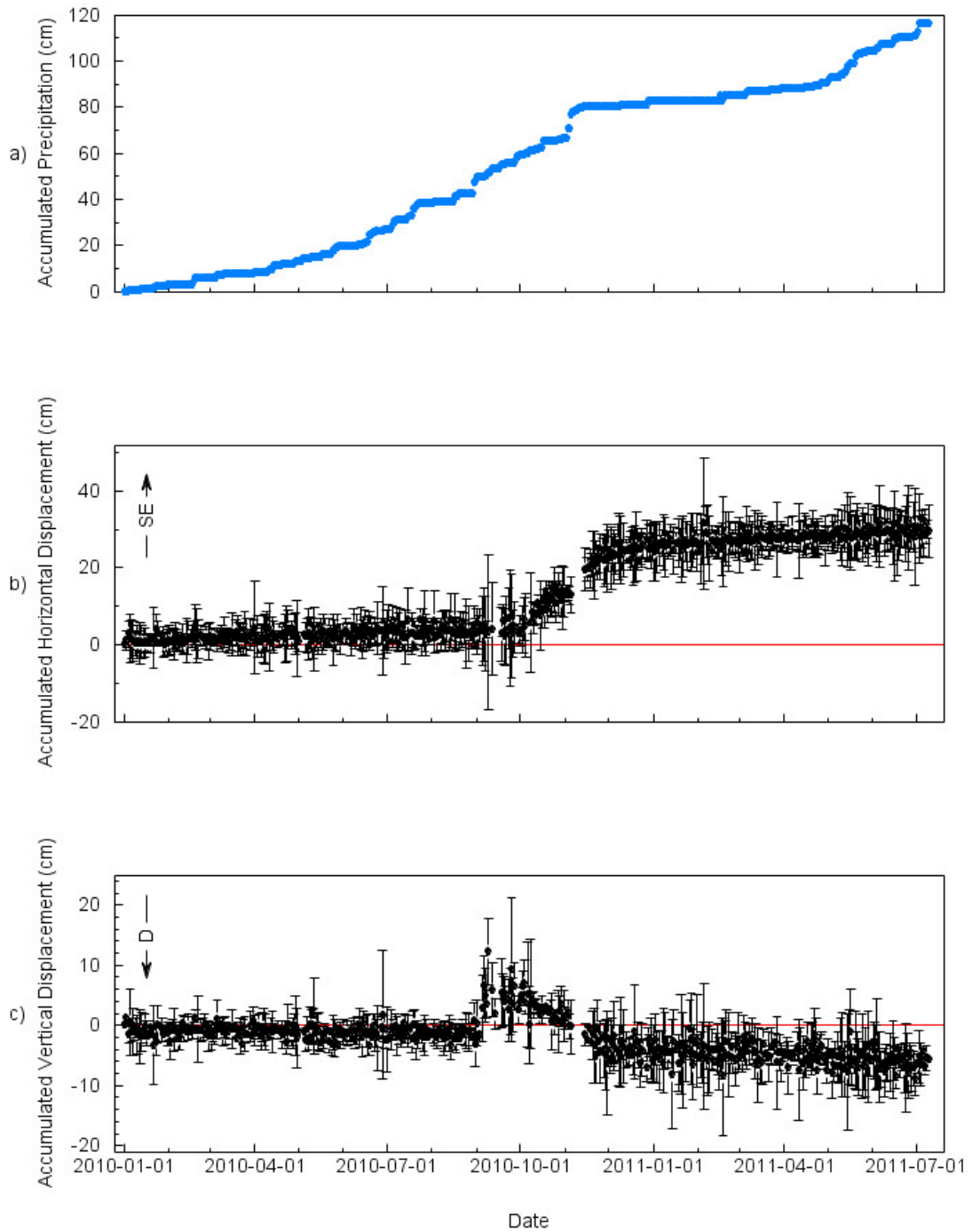


Figure 4-1: GPS time series and precipitation for station *CB*. Starting at the top precipitation (a), in the middle horizontal displacement (b) and in the bottom vertical displacement (c).

4.1.2 Station *abeg*: 4-hour data coverage

Measuring period

The static GPS monitoring station *abeg* was installed inside the right flank, approximately halfway between the head and toe of the landslide (Figure 3-1, *abeg*). The GPS location measurements were collected for 4 hours over a ten-month period from July 2011 to May 2012.

Displacement

Results are plotted in Figure 4-2a for horizontal displacement from the point of origin versus the date of measurement. A total horizontal displacement of 15cm over the monitoring period was estimated using the difference between the first and last data points. The values of error for the horizontal data ranged between -12cm and 22cm for the data and averaged 17cm.

The graph in Figure 4-2b shows the vertical displacements, derived from the static GPS observations that accumulated over the monitoring period. A total vertical displacement of -6cm (downward) over the monitoring period was estimated using the difference between the first and last data points. The values of error for the vertical data ranged between -10cm and 28cm for the data and averaged 12cm.

Comparison

The displacement data from GPS station *abeg* imply that the right flank of the landslide is moving in the same direction and at a similar angle as GPS station *CB* on the left head of the landslide but with 50% less displacement.

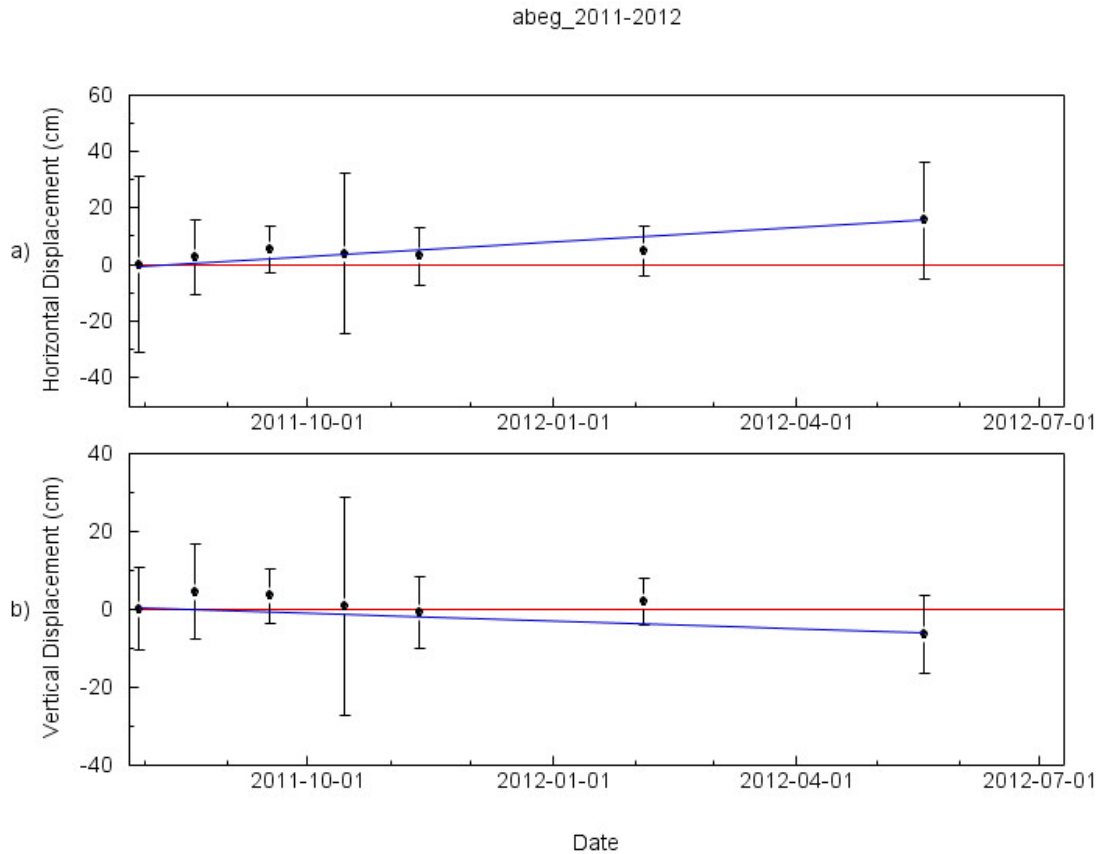


Figure 4-2: GPS time series for station *abeg*. Beginning in the top, the time series show horizontal displacement (a) and in the bottom vertical displacement (b). Blue lines in a and b delineate the first and last observation.

4.2 Monitoring stations outside the Cerca del Cielo landslide

Many of the 24-hour stations exhibited up to 2cm steps in the horizontal and vertical component (green lines in Figure 4-3 to Figure 4-15) in their position data relative to the first observation and/or the previous data. These steps in the data sets are considered to be related to the change of antennas between measurement intervals.

4.2.1 Continuous Stations:

4.2.1.1 raqg

Measuring period

This house displayed a large number of cracks both outside and inside the structure. Static GPS measurements were collected from June 2011 to July 2012.

Precipitation

Accumulated precipitation from the USGS weather station over the same time period are shown on Figure 4-3a. The weather station recorded 171cm of accumulated precipitation over the monitoring period.

Displacement

GPS measurements are plotted as accumulated horizontal and vertical displacements versus the measurement dates on Figure 4-3b and c respectively. Figure 4-3b shows the GPS derived horizontal displacements observations that accumulated over the monitoring period. The data points in each of the measurement intervals form tight horizontal clusters that lie between 0cm and 2cm. Only a few measurements from the first and third intervals lie between 2cm to 3cm. Values of error for individual data points ranged between -2cm and 10cm and averaged 3cm for horizontal data. A best-fit linear regression analysis produced a negative horizontal displacement of 0.94cm over the monitoring period. The tight horizontal clustering of the data indicates no displacement of the house over the measurement period with a detection limit ≤ 1 cm.

Figure 4-3c shows the GPS derived vertical displacements observations that accumulated over the monitored period. The data points in each of the measurement intervals form -

2cm to 4cm thick, horizontal clusters. The data clusters of the first 2 intervals are centered at 1cm, the third at 0cm, the fourth at 2cm and the final interval was centered at 1.5cm. Values of error for the individual data points ranged between -2cm and 10cm and averaged 3cm for the vertical data. The best-fit linear regression analysis estimates a positive vertical displacement of 1.2cm over the monitoring period. The estimate is below the 2cm detection limit established by the steps in the data clusters between measurement intervals.

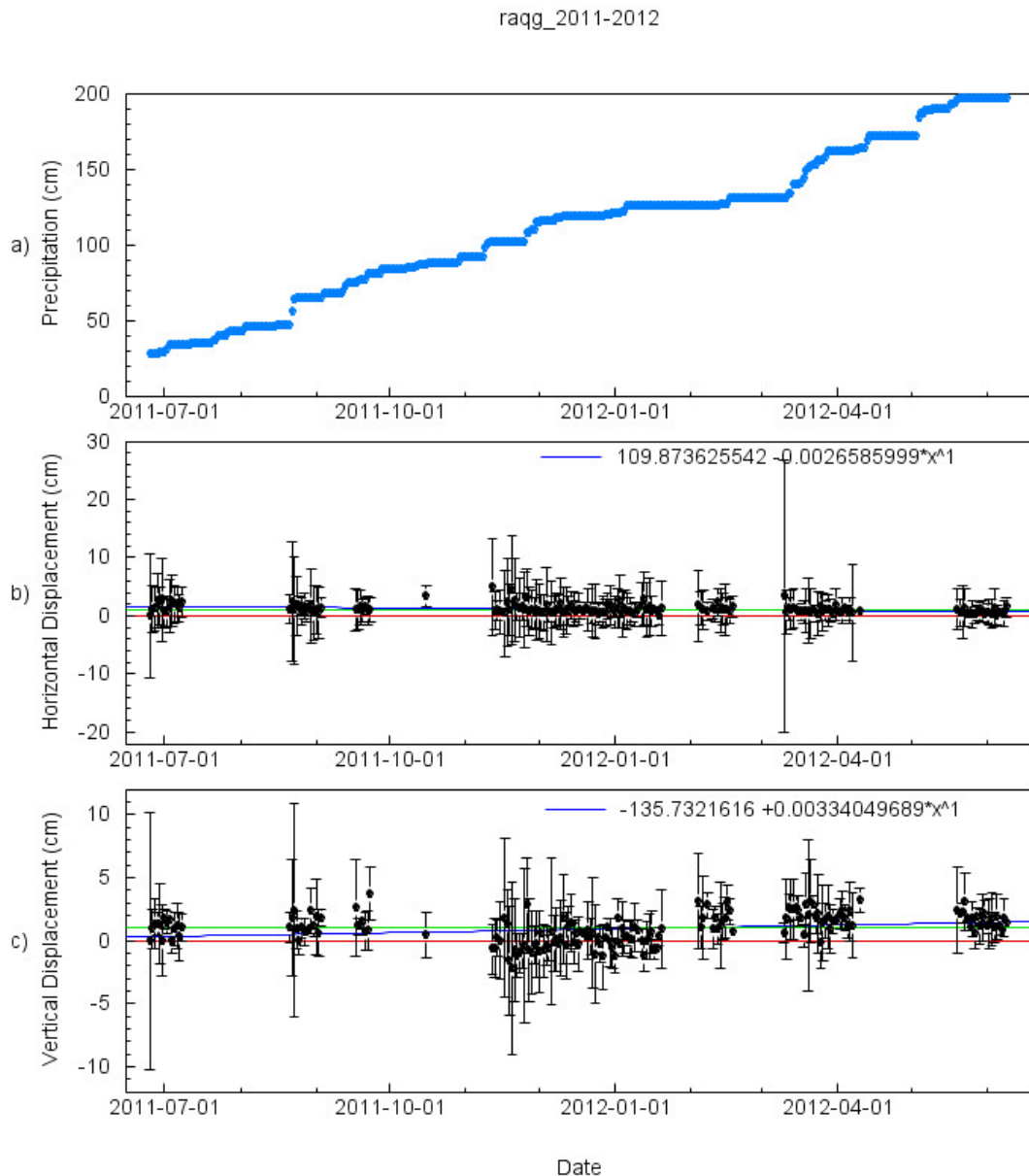


Figure 4-3: GPS time series and precipitation for station *raqq*. Starting at the top precipitation (a), in the middle horizontal displacement (b) and in the bottom vertical displacement (c). Blue lines delineate the best-fit linear regression and green line the 2cm step in figures b and c.

4.2.1.2 mang

Measuring period

Static GPS measurements were collected during a shorter time frame from June 2011 to October 2011.

Precipitation

Accumulated precipitation from the USGS weather station over the same time period are shown on Figure 4-4a. The weather station recorded 62cm of accumulated precipitation over the monitoring period.

Displacement

GPS measurements are plotted as accumulated horizontal and vertical displacements versus the measurement dates on Figure 4-4b and c respectively.

Figure 4-4b shows the GPS derived horizontal displacement observations that accumulated over the monitoring period. The data points in each measurement intervals form a horizontal cluster that lie between 0cm and 2cm. Only the measurements from the last intervals lie between the 2cm and 3cm. Values of error for individual data points ranged between -3cm and 7cm and averaged 3cm for horizontal data. The data points in each of the measurement intervals form 2cm and 3cm thick, horizontal clusters. The tight horizontal clustering of the data indicates no displacement of the house over the measurement period with a detection limit $\leq 2\text{cm}$. A best-fit linear regression analysis estimates a positive horizontal displacement of 1.4cm over the monitoring period. The estimate is below the 2cm detection limit established by the steps in the data clusters between measurement intervals.

Figure 4-4c shows the GPS derived vertical displacements observations that accumulated over the monitoring period. The data points in each of the measurement intervals form 1-2cm thick, horizontal clusters. The data clusters of the first 3 intervals are centered at 1cm, the third and fourth at 2cm. Values of error for the individual data points ranged between -1cm and 7cm and averaged 3cm for the vertical data. The best-fit linear regression analysis estimates a positive vertical displacement of 1.5cm (upward) over the monitoring period. The estimate falls just within the 2cm detection limit established by the steps in the data clusters between measurement intervals.

mang_2011-2012

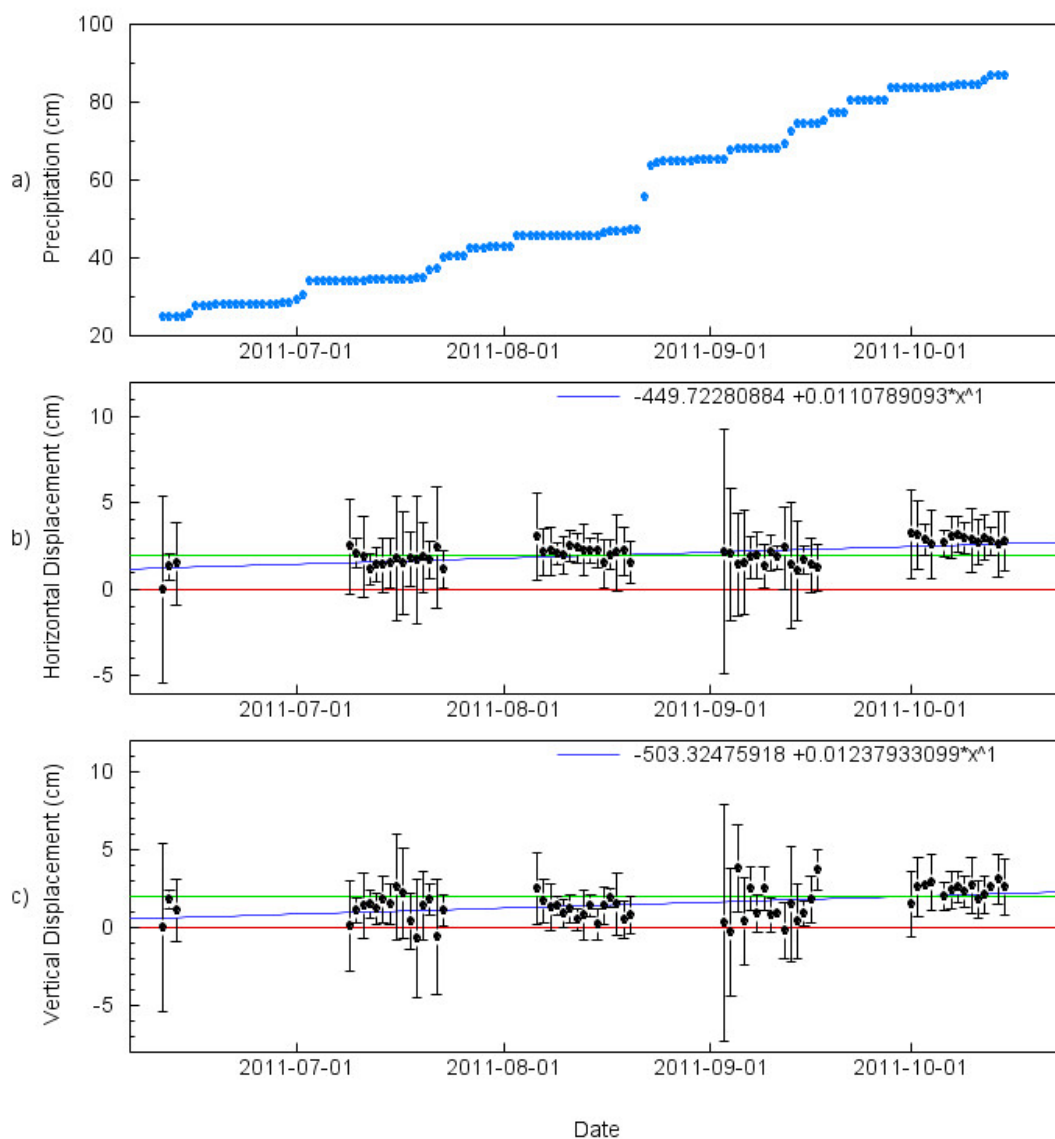


Figure 4-4: GPS time series and precipitation for station *mang*. Starting at the top precipitation (a), in the middle horizontal displacement (b) and in the bottom vertical displacement (c). Blue lines delineate the best-fit linear regression and green line the 2cm step in figures b and c.

4.2.1.3 *josg*

Measuring period

Static GPS measurements were collected from August 2011 to April 2012.

Precipitation

Accumulated precipitation from the USGS weather station over the same time period are shown on Figure 4-5a. The weather station recorded 124cm of accumulated precipitation over the monitoring period.

Displacement

GPS measurements are plotted as accumulated horizontal and vertical displacements versus the measurement dates on Figure 4-5b and c respectively. Figure 4-5b shows the GPS derived horizontal displacements observations that accumulated over the monitoring period. The data points in each of the measurement intervals form tight horizontal clusters that lie between 0cm and 2cm. Only a few measurements from the first and second intervals lie between 0cm and 1cm. The data clusters of the remaining intervals are centered at 2cm. Values of error for individual data points ranged between -2cm and 9cm and averaged 2cm for horizontal data. The tight horizontal clustering of the data indicates no displacement of the house over the measurement period with a detection limit ≤ 1 cm. A best-fit linear regression analysis produced a positive horizontal displacement of 1.3cm between displacement and time. The estimate is below the 2cm detection limit established by the steps in the data clusters between measurement intervals.

Figure 4-5c shows the GPS derived vertical displacements observations that accumulated over the monitoring period. The data points in each of the measurement intervals form 0cm to 2cm thick, horizontal clusters. The data clusters of the first 4 intervals are centered at 1cm and the last interval at 1.5cm. Values of error for the individual data points ranged between -1cm and 8 cm and averaged 2cm for the vertical data. The best-fit linear regression analysis estimates a positive vertical displacement of 0.76cm (upward) over the monitoring period. The estimate is below the 2cm detection limit established by the steps in the data clusters between measurement intervals.

josg_2011-2012

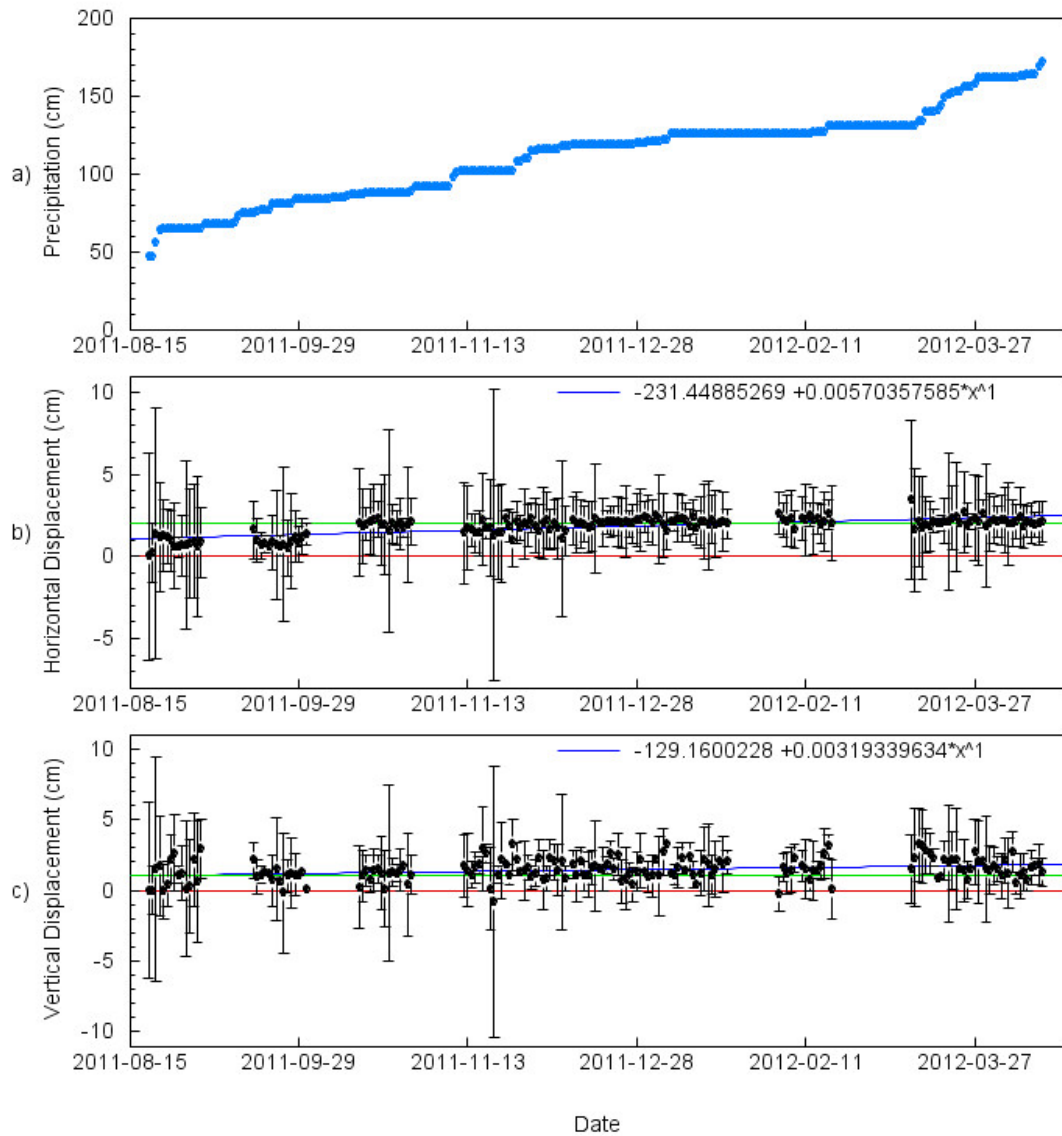


Figure 4-5: GPS time series and precipitation for station *josg*. Starting at the top precipitation (a), in the middle horizontal displacement (b) and in the bottom vertical displacement (c). Blue lines delineate the best-fit linear regression and green line the 2cm step in figures b and c.

4.2.1.4 *carg*

Measuring period

Static GPS collected data from June 2011 to June 2012.

Precipitation

Accumulated precipitation from the USGS weather station over the same time period are shown on Figure 4-6a. The weather station recorded 168cm of accumulated precipitation over the monitoring period.

Displacement

GPS measurements are plotted as accumulated horizontal and vertical displacements versus measurement dates on Figure 4-6b and c respectively. Figure 4-6b shows the GPS derived horizontal displacements observations that accumulated over the monitoring period. The data points in each of the measurement intervals form tight horizontal clusters that lie between 0cm and 2cm. Only a few measurements from the last interval lie between 2cm to 4cm. Values of error for individual data points ranged between -7cm and 13cm and averaged 10cm for horizontal data. The tight horizontal clustering of the data indicates no displacement of the house over the measurement period with a detection limit ≤ 2 cm. The best-fit linear regression analysis estimates a positive horizontal displacement of 0.85cm over the monitoring period. The estimate is below the 2cm detection limit established by the steps in the data clusters between measurement intervals.

Figure 4-6c shows the GPS derived vertical displacements observations that accumulated over the monitoring period. The data points in each of the measurement intervals form 0-

4.5cm thick, horizontal clusters that lie between 0cm and -4.5cm. The data clusters from the first interval are centered at 2cm, the fifth interval at 3cm and the last two intervals are centered at 4cm. Values of error for the individual data points ranged between -2cm and 8cm and averaged -5cm for the vertical data. The best-fit linear regression analysis estimates a vertical displacement of 1.6cm (upward) over the monitoring period. The estimate is below the 2cm detection limit established by the steps in the data clusters between measurement intervals.

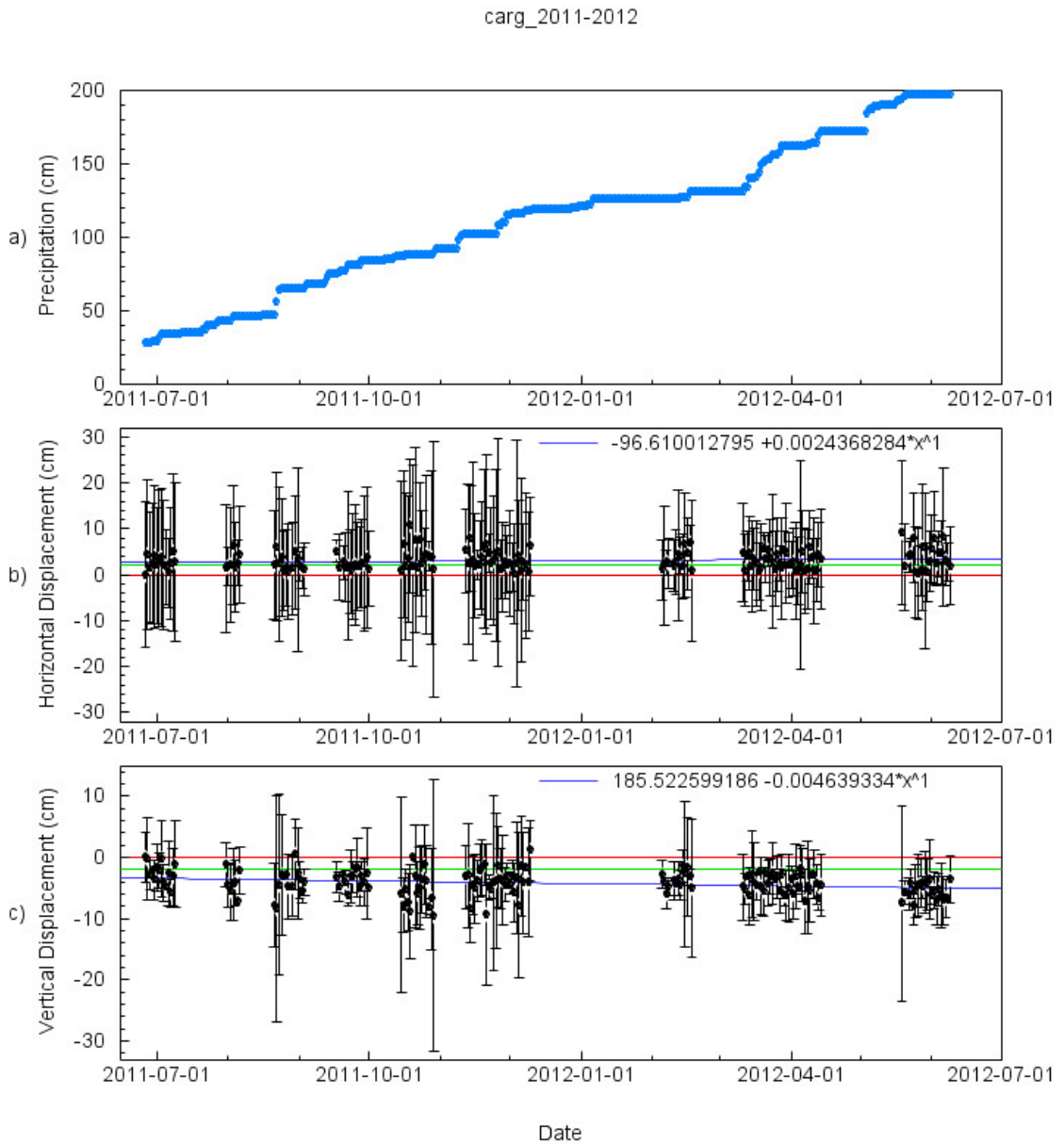


Figure 4-6: GPS time series and precipitation for station *carg*. Starting at the top precipitation (a), in the middle horizontal displacement (b) and in the bottom vertical displacement (c). Blue lines delineate the best-fit linear regression and green line the 2cm step in figures b and c.

4.2.1.5 *herg*

Measuring period

Static GPS collected data from June 2011 to June 2012.

Precipitation

Accumulated precipitation from the USGS weather station over the same time period are shown on Figure 4-7a. The weather station recorded 168cm of accumulated precipitation over the monitoring period.

Displacement

GPS measurements are plotted as accumulated horizontal and vertical displacements versus measurement dates on Figure 4-7b and c respectively. Figure 4-7b shows the GPS derived horizontal displacements observations that accumulated over the monitoring period. The data points in each of the measurement intervals form tight horizontal clusters that lie between 0cm and 2cm. Only a few measurements from the second interval lie between 4cm to 6cm. Values of error for individual data points ranged between -2cm and 16cm and averaged 4cm for horizontal data. The tight horizontal clustering of the data indicates no displacement of the house over the measurement period with a detection limit ≤ 2 cm. The best-fit linear regression analysis estimates a negative horizontal displacement of 0.40cm over the monitoring period. The estimate is below the 2cm detection limit established by the steps in the data clusters between measurement intervals.

Figure 4-7c shows the GPS derived vertical displacements observations that accumulated over the monitoring period. The data points in each of the measurement intervals form 0-

2cm thick, horizontal clusters that lie between 0cm and 2cm. The data clusters from each period are centered at 2cm. Values of error for the individual data points ranged between -2cm and 11cm and averaged 6cm for the vertical data. The best-fit linear regression analysis estimates a negative vertical displacement of 0.58cm over the monitoring period. The estimate is below the 2cm detection limit established by the steps in the data clusters between measurement intervals.

herg_2011-2012

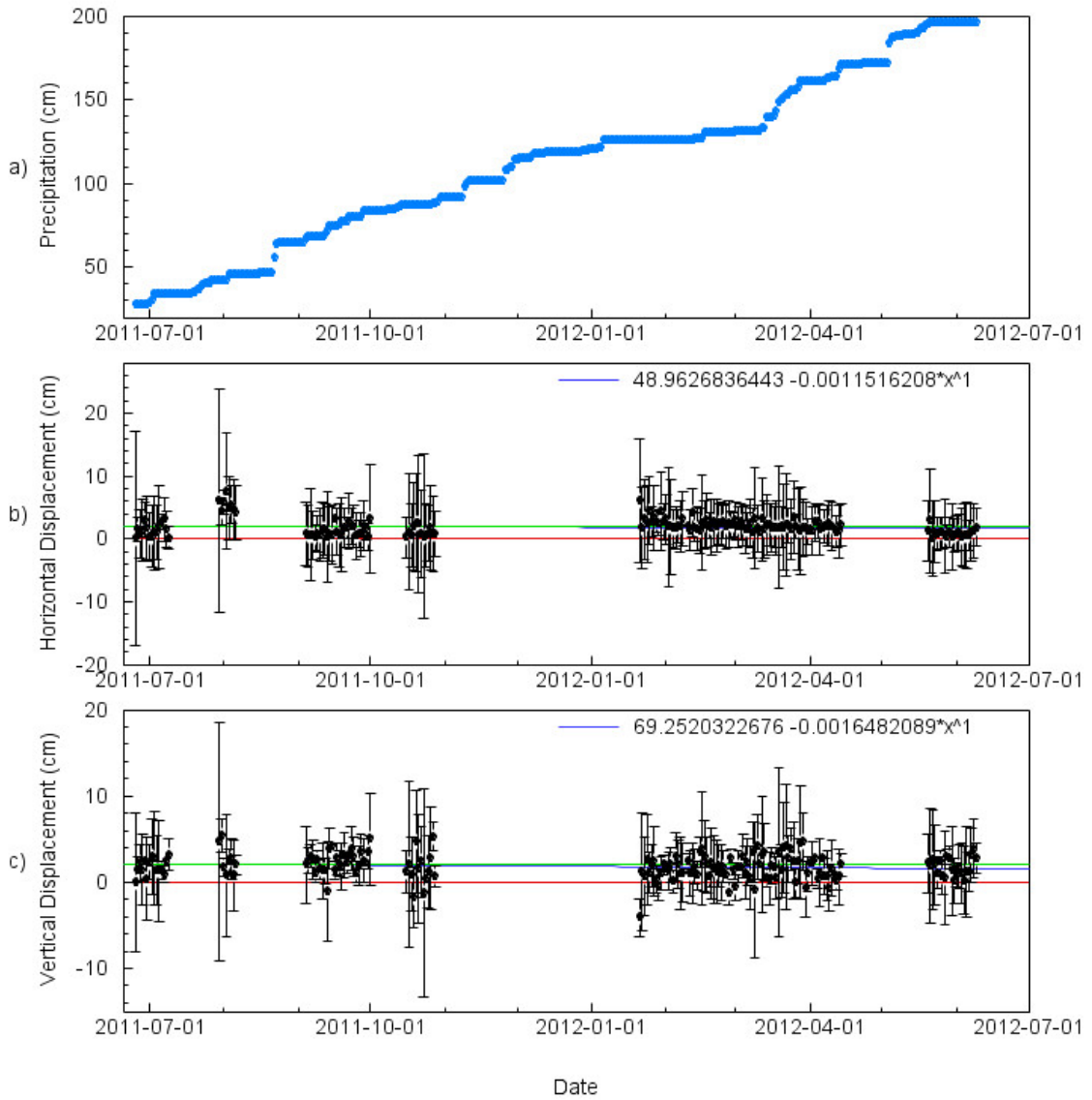


Figure 4-7: GPS time series and precipitation for station *herg*. Starting at the top precipitation (a), in the middle horizontal displacement (b) and in the bottom vertical displacement (c). Blue lines delineate the best-fit linear regression and green line the 2cm step in figures b and c.

4.2.1.6 *estg*

Measuring period

Static GPS collected data from June 2011 to May 2012.

Precipitation

Accumulated precipitation from the USGS weather station over the same time period are shown on Figure 4-8a. The weather station recorded 171cm of accumulated precipitation over the monitoring period.

Displacement

GPS measurements are plotted as accumulated horizontal and vertical displacements versus measurement dates on Figure 4-8b and c respectively. Figure 4-8b shows the GPS derived horizontal displacements observations that accumulated over the monitoring period. The data points in each of the measurement intervals form tight horizontal clusters that lie between 0cm and 2cm. Only a few measurements from the fifth interval lie between 0cm and 1cm. Values of error for individual data points ranged between -1cm and 12cm and averaged 4cm for horizontal data. The tight horizontal clustering of the data indicates no displacement of the house over the measurement period with a detection limit ≤ 1 cm. A best-fit linear regression analysis estimates a negative horizontal displacement of 0.26cm over the monitoring period.

Figure 4-8c shows the GPS derived vertical displacements observations that accumulated over the monitoring period. The data points in each of the measurement intervals form 0cm to -2cm thick, horizontal clusters. The data clusters are centered at -1cm (downward). Values of error for the individual data points ranged between -3cm and 9cm and averaged

-3cm for the vertical data. The best-fit linear regression analysis estimates a negative vertical displacement of 0.05cm over the monitoring period. The estimate is below the 2cm detection limit established by the steps in the data clusters between measurement intervals.

estg_2011-2012

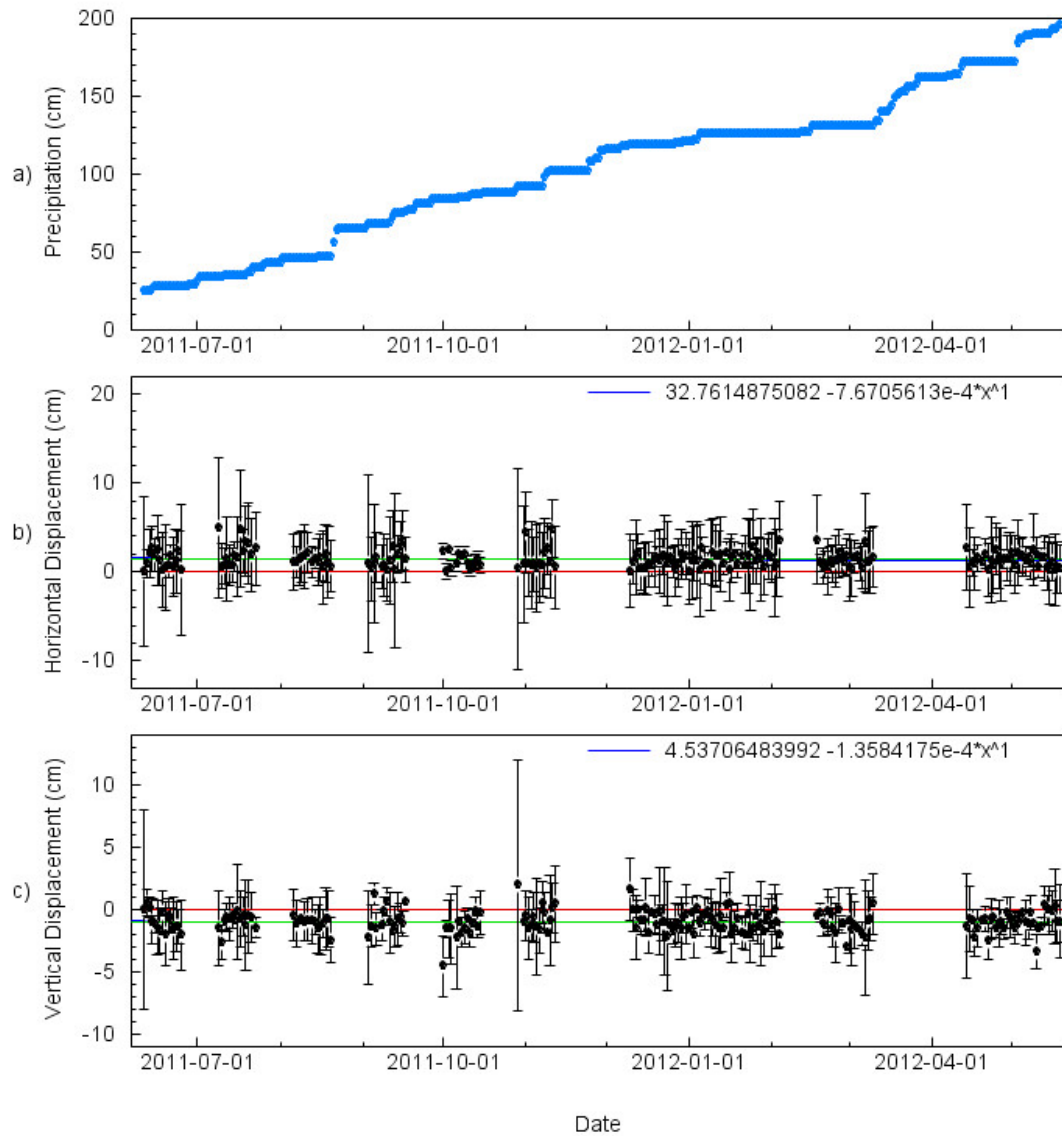


Figure 4-8: GPS time series and precipitation for station *estg*. Starting at the top precipitation (a), in the middle horizontal displacement (b) and in the bottom vertical displacement (c). Blue lines delineate the best-fit linear regression and green line the 2cm step in figures b and c.

4.2.1.7 rafg

Measuring period

Static GPS measurements were collected data from June 2011 to June 2012.

Precipitation

Accumulated precipitation from the USGS weather station over the same time period are shown on Figure 4-9a. The weather station recorded 168cm of accumulated precipitation over the monitoring period.

Displacement

GPS measurements are plotted as accumulated horizontal and vertical displacements versus the measurement dates on Figure 4-9 b and c respectively. Figure 4-9b shows the GPS derived horizontal displacements observations that accumulated from over the monitoring period. The data points in each of the measurement intervals form tight horizontal clusters that lie between 0cm and 1cm. Only a few measurements from the last three intervals lie at 1.5cm. Values of error for individual data points ranged between -2cm and 10cm and averaged 3cm for horizontal data. A best-fit linear regression analysis estimates a positive horizontal displacement of 1cm over the monitoring period. The tight horizontal clustering of the data indicates no displacement of the house over the measurement period with a detection limit ≤ 1 cm.

Figure 4-9c shows the GPS derived vertical displacements observations that accumulated over the monitoring period. The data points in each of the measurement intervals form 0cm to 2cm thick, horizontal clusters. The data clusters from the first to the fifth interval are centered at 1cm and the last two intervals were centered at 1.5cm. Values of error for

the individual data points ranged between -2cm and 8cm and averaged 3cm for the vertical data. The best-fit linear regression analysis estimates a positive vertical displacement of 0.68cm over the monitoring period. The estimate is below the 2cm detection limit established by the steps in the data clusters between measurement intervals.

rafg_2011-2012

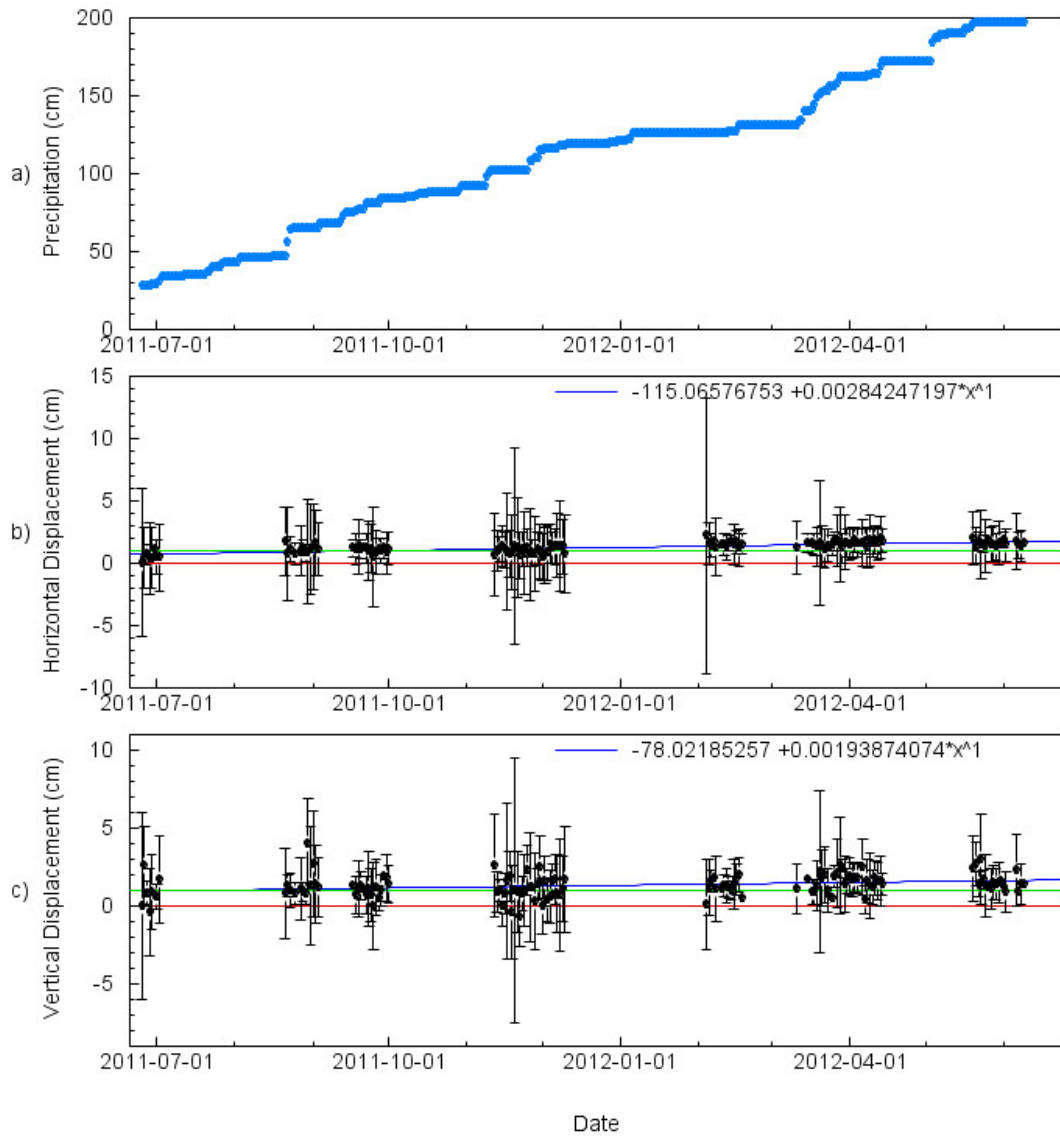


Figure 4-9: GPS time series and precipitation for station *rafg*. Starting at the top precipitation (a), in the middle horizontal displacement (b) and in the bottom vertical displacement (c). Blue lines delineate the best-fit linear regression and green line the 2cm step in figures b and c.

4.2.1.8 jerg

Measuring period

Static GPS measurements collected data from June 2011 to May 2012.

Precipitation

Accumulated precipitation from the USGS weather station over the same time period are shown on Figure 4-10a. The weather station recorded 171cm of accumulated precipitation over the monitoring period.

Displacement

GPS measurements are plotted as accumulated horizontal and vertical displacements versus the measurement dates on Figure 4-10 b and c respectively. Figure 4-10b shows the GPS derived horizontal displacements observations that accumulated over the monitoring period. The data points in each of the measurement intervals form tight horizontal clusters that lie between 0cm and 2cm. Only a few measurements from the fifth interval lie between 3cm to 5cm. Values of error for individual data points ranged between -2cm and 10cm and averaged 4cm for horizontal data. A best-fit linear regression analysis estimates a negative horizontal displacement of 0.06cm over the monitoring period. The tight horizontal clustering of the data indicates no displacement of the house over the measurement period with a detection limit ≤ 1 cm. Figure 4-10c shows the GPS derived vertical displacements observations that accumulated over the monitoring period. The data points in each of the measurement intervals form -1cm to 2cm thick, horizontal clusters. The data clusters of the centered at 1cm, and only fourth interval lies below 1cm. Values of error for the individual data points ranged between -

2cm and 6cm and averaged 3cm for the vertical data. The best-fit linear regression analysis estimates a positive vertical displacement of 0.88cm over the monitoring period. The estimate is below the 2cm detection limit established by the steps in the data clusters between measurement intervals.

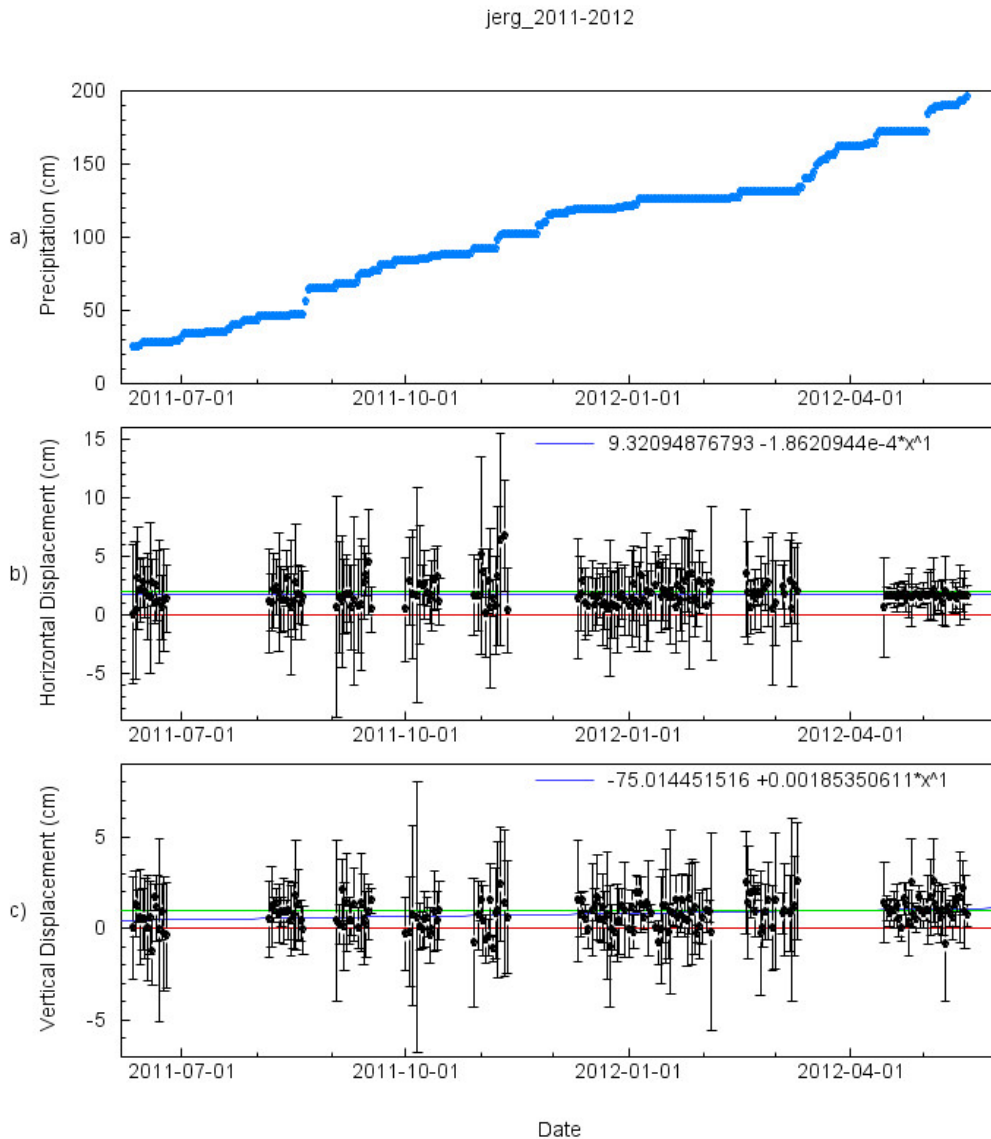


Figure 4-10: GPS time series and precipitation for station *jerg*. Starting at the top precipitation (a), in the middle horizontal displacement (b) and in the bottom vertical displacement (c). Blue lines delineate the best-fit linear regression and green line the 2cm step in figures b and c.

4.2.1.9 *luig*

Measuring period

Static GPS measurements were collected from June 2011 to May 2012.

Precipitation

Accumulated precipitation from the USGS weather station over the same time period are shown on Figure 4-11a. The weather station recorded 171cm of accumulated precipitation over the monitoring period.

Displacement

GPS measurements are plotted as accumulated horizontal and vertical displacements versus the measurement dates on Figure 4-11b and c respectively. Figure 4-11b shows the GPS derived horizontal displacements observations that accumulated over the monitoring period. The data points in each of the measurement intervals form tight horizontal clusters that lie between 0cm and 1cm. Only measurements from the fifth interval lie on 2cm, all the remaining intervals lie on 1cm. Values of error for individual data points ranged between -2cm and 5cm and averaged 3cm for horizontal data. A best-fit linear regression analysis estimates a negative horizontal displacement of 0.20cm over the monitoring period. The tight horizontal clustering of the data indicates no displacement of the house over the measurement period with a detection limit ≤ 1 cm.

Figure 4-11c shows the GPS derived vertical displacements observations that accumulated over the monitoring period. The data points in each of the measurement intervals form 0cm to 1cm thick, horizontal clusters that lie between 0cm and 1cm. The data clusters from each interval are centered at 0cm. Values of error for the individual

data points ranged between -1cm and 11cm and averaged 2cm for the vertical data. The best-fit linear regression analysis estimates a positive vertical displacement of 0.13cm over the monitoring period. The estimate is below the 2cm detection limit established by the steps in the data clusters between measurement intervals.

luig_2011-2012

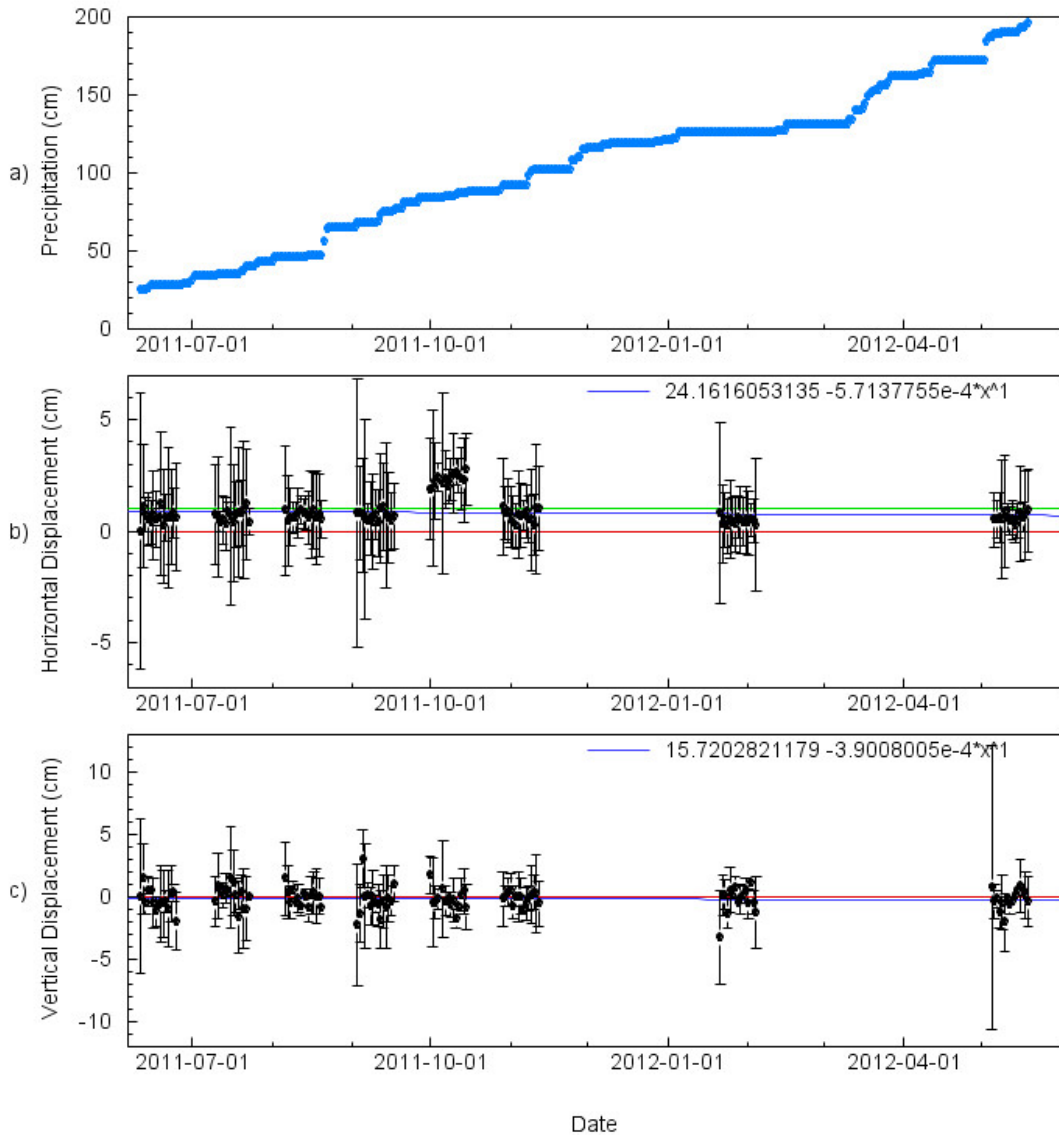


Figure 4-11: GPS time series and precipitation for station *luig*. Starting at the top precipitation (a), in the middle horizontal displacement (b) and in the bottom vertical displacement (c). Blue lines delineate the best-fit linear regression and green line the 2cm step in figures b and c.

4.2.1.10 refs

Measuring period

Static GPS measurements were collected from January 2010 to March 2012.

Precipitation

Accumulated precipitation from the USGS weather station over the same time period are shown on Figure 4-12a. The weather station recorded 213cm of accumulated precipitation over the monitoring period.

Displacement

GPS measurements are plotted as accumulated horizontal and vertical displacements versus the measurement dates on Figure 4-12 b and c respectively. Figure 4-12b shows the GPS derived horizontal displacements observations that accumulated over the monitoring period. The data points in each of the measurement form tight horizontal clusters that lie between 0cm and 1cm. Values of error for individual data points ranged between -2cm and 10cm and averaged 4cm for horizontal data. A best-fit linear regression analysis estimates a negative horizontal displacement of 0.06cm over the monitoring period. The tight horizontal clustering of the data indicates no displacement of the house over the measurement period with a detection limit ≤ 1 cm.

Figure 4-12c shows the GPS derived vertical displacements observations that accumulated over the monitoring period. Vertical observations show a positive displacement in the measurements during September and October, 2010. This positive displacement is an alteration in the observation due to a change of antennas during September 4, 2010. The difference in height of the antenna from the initial point had a

positive offset in the observations with relation of the first day of observation; the horizontal was not affected by this disturbance. The data points in each of the measurement intervals form 0cm to 1cm thick, horizontal clusters. The data clusters from each interval are centered at 0cm. Values of error for the individual data points ranged between -1cm and 11cm and averaged 2cm for the vertical data. The best-fit linear regression analysis estimates a negative vertical displacement of 0.8cm before September 4, 2010 and 0.42cm after September 4, 2010. The estimate is below the 2cm detection limit established by the steps in the data clusters between measurement intervals.

refs_2010-2012

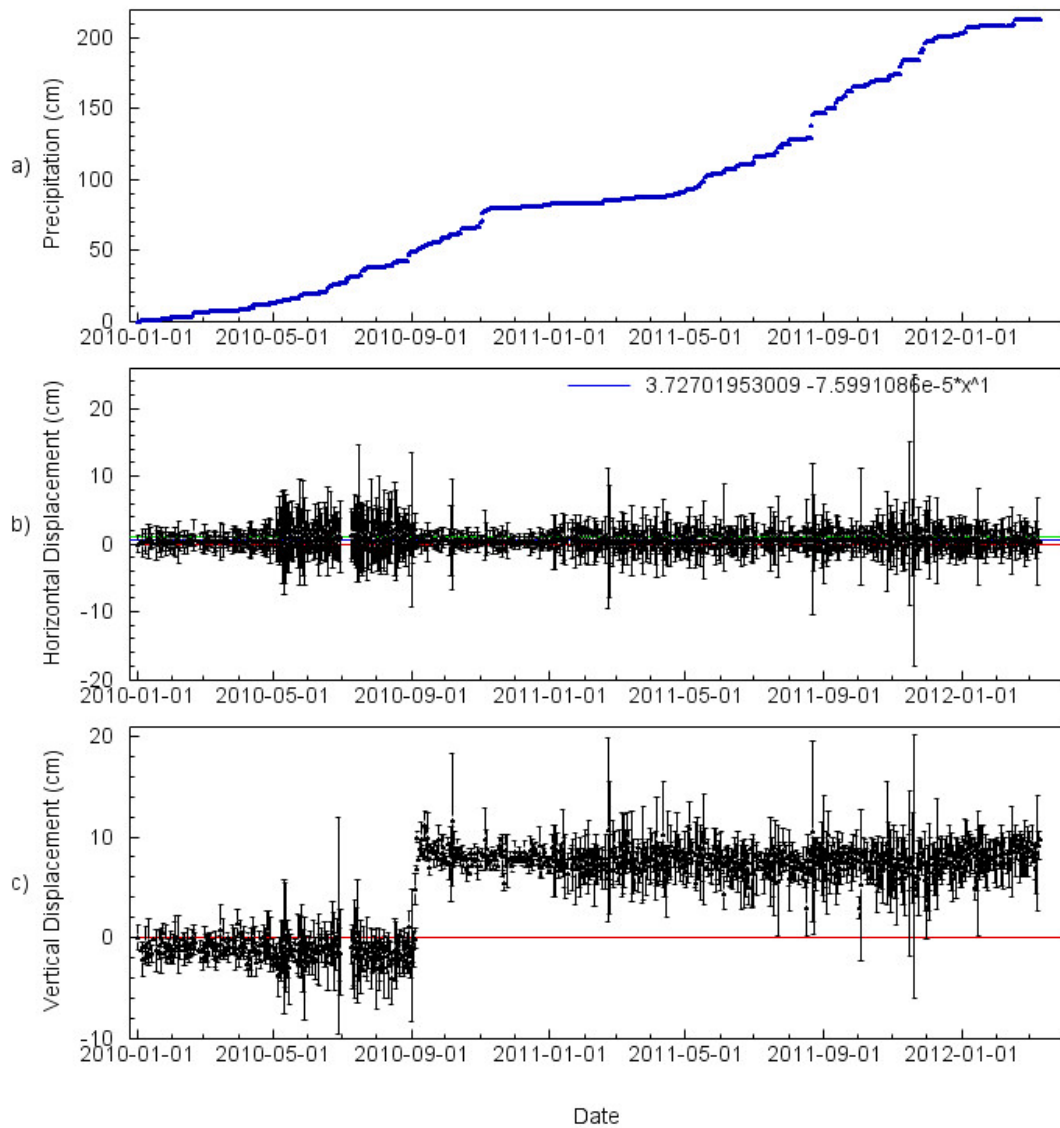


Figure 4-12: GPS time series and precipitation for station *refs*. Starting at the top precipitation (a), in the middle horizontal displacement (b) and in the bottom vertical displacement (c). Blue lines delineate the best-fit linear regression and green line the 2cm step in figures b.

4.2.1.11 dang

Measuring period

Static GPS measurements were collected from June 2011 to May 2012.

Precipitation

Accumulated precipitation from the USGS weather station over the same time period are shown on Figure 4-13a. The weather station recorded 169cm of accumulated precipitation over the monitoring period.

Displacement

GPS measurements are plotted as accumulated horizontal and vertical displacements versus the measurement dates on Figure 4-13b and c respectively. Figure 4-13b shows the GPS derived horizontal displacements observations that accumulated over the monitoring period. The data points in each of the measurement intervals form tight horizontal clusters that lie between 0cm and 1cm. The data clusters from each interval are centered at 2cm. Values of error for individual data points ranged between -2cm and 20cm and averaged 4cm for horizontal data. A best-fit linear regression analysis estimates a positive horizontal displacement of 0.13cm over the monitoring period. The tight horizontal clustering of the data indicates no displacement of the house over the measurement period with a detection limit ≤ 2 cm.

Figure 4-13c shows the GPS derived vertical displacements observations that accumulated over the monitoring period. The data points in each of the measurement intervals form 0cm to -1cm thick, horizontal clusters. The data clusters from each interval are centered at 0cm. Values of error for the individual data points ranged between -2cm

and 20cm and averaged 4cm for the vertical data. The best-fit linear regression analysis estimates a negative vertical displacement of 0.08cm over the monitoring period. The estimate is below the 2cm detection limit established by the steps in the data clusters between measurement intervals.

dang_2011-2012

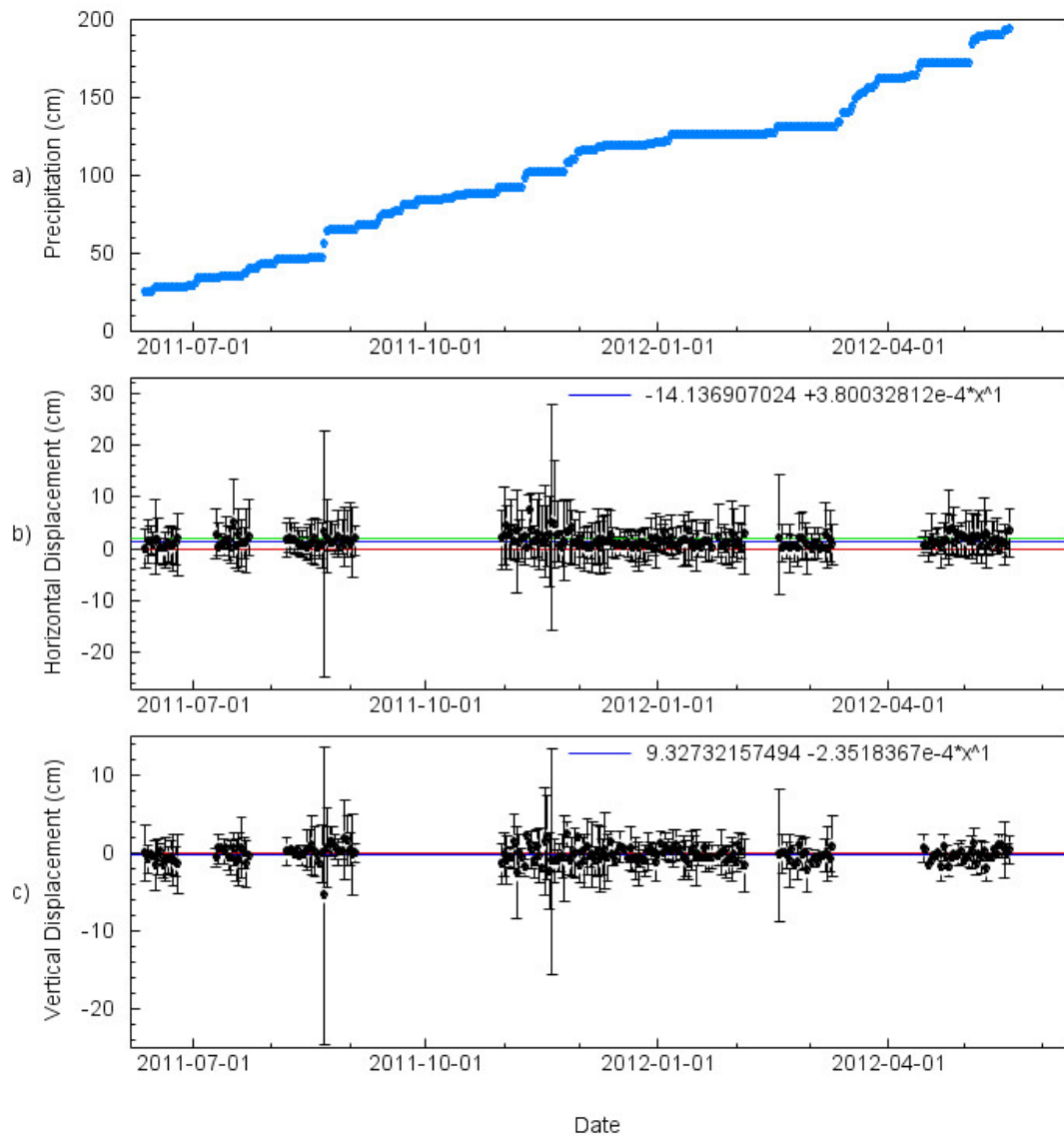


Figure 4-13: GPS time series and precipitation for station *dang*. Starting at the top precipitation (a), in the middle horizontal displacement (b) and in the bottom vertical displacement (c). Blue lines delineate the best-fit linear regression and green line the 2cm step in figures b and c.

4.2.1.12 *jorg*

Measuring period

Static GPS measurements were collected from June 2011 to May 2012.

Precipitation

Accumulated precipitation from the USGS weather station over the same time period are shown on Figure 4-14a. The weather station recorded 179cm of accumulated precipitation over the monitoring period.

Displacement

GPS measurements are plotted as accumulated horizontal and vertical displacements versus the measurement dates on Figure 4-14b and c respectively. Figure 4-14b shows the GPS derived horizontal displacements observations that accumulated over the monitoring period. The data points in each of the measurement intervals form tight horizontal clusters that lie between 0cm and 2cm. The data clusters from each interval are centered at 1cm, only a few measurements from the sixth interval are lie between 4cm to 5cm. Values of error for individual data points ranged between -2cm and 14cm and averaged 4cm for horizontal data. A best-fit linear regression analysis estimates a positive horizontal displacement of 0.6cm over the monitoring period. The tight horizontal clustering of the data indicates no displacement of the house over the measurement period with a detection limit ≤ 1 cm.

Figure 4-14c shows the GPS derived vertical displacements observations that accumulated over the monitoring period. The data points in each of the measurement intervals form 2cm to 2.5cm thick, horizontal clusters. The data clusters from the first

interval are centered at 1.5cm, the eighth and ninth centered at 3cm and the remaining are centered at 2.5cm. Values of error for the individual data points ranged between -2cm and 8cm and averaged 4cm for the vertical data. The best-fit linear regression analysis estimates a positive vertical displacement of 0.8cm over the monitoring period. The estimate is below the 2cm detection limit established by the steps in the data clusters between measurement intervals.

jorg_2011-2012

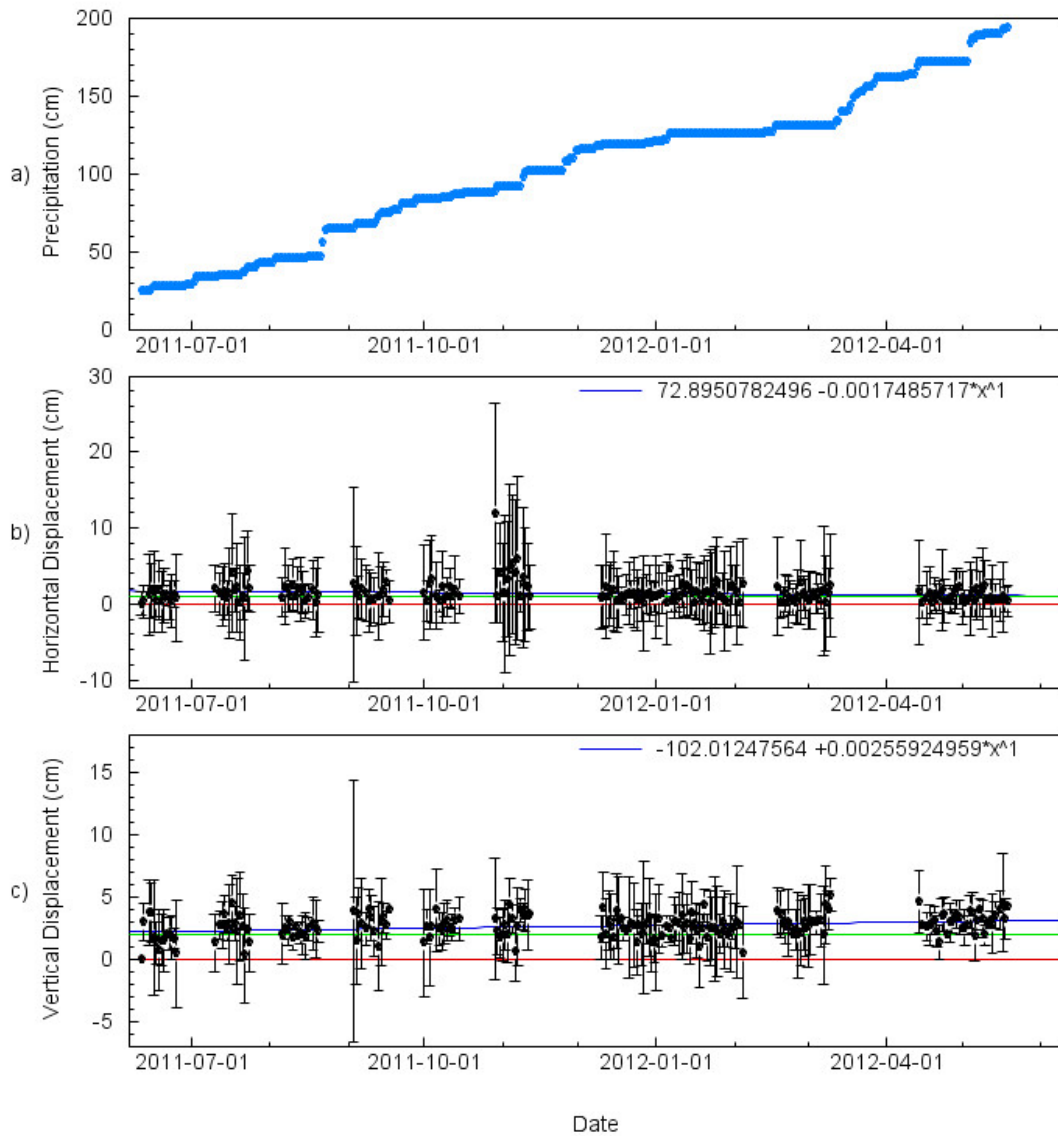


Figure 4-14: GPS time series and precipitation for station *jorg*. Starting at the top precipitation (a), in the middle horizontal displacement (b) and in the bottom vertical displacement (c). Blue lines delineate the best-fit linear regression and green line the 2cm step in figures b and c.

4.2.1.13 frag

Measuring period

Static GPS measurements were collected from August 2011 to June 2012.

Precipitation

Accumulated precipitation from the USGS weather station over the same time period are shown on Figure 4-15a. The weather station recorded 149cm of accumulated precipitation over the monitoring period.

Displacement

GPS measurements are plotted as accumulated horizontal and vertical displacements versus measurement dates on Figure 4-15b and c respectively. Figure 4-15b shows the GPS derived horizontal displacements observations that accumulated over the monitoring period. The data points in each of the measurement intervals form tight horizontal clusters that lie between 0cm and 1cm. The data clusters from each interval are centered at 0.5cm. Values of error for individual data points ranged between -1cm and 10cm and averaged 3cm for horizontal data. A best-fit linear regression analysis estimates a positive horizontal displacement of 0.01cm over the monitoring period. The tight horizontal clustering of the data indicates no displacement of the house over the measurement period with a detection limit ≤ 1 cm.

Figure 4-15c shows the GPS derived vertical displacements observations that accumulated over the monitoring period. The data points in each of the measurement intervals form -0.5cm to 2cm thick, horizontal clusters. Only a few measurements from the third interval lie between 0cm and 0.5cm. Values of error for the individual data

points ranged between -1cm and 7cm and averaged 3cm for the vertical data. The best-fit linear regression analysis estimates a positive vertical displacement of 0.52cm over the monitoring period. The estimate is below the 2cm detection limit established by the steps in the data clusters between measurement intervals.

frag_2011-2012

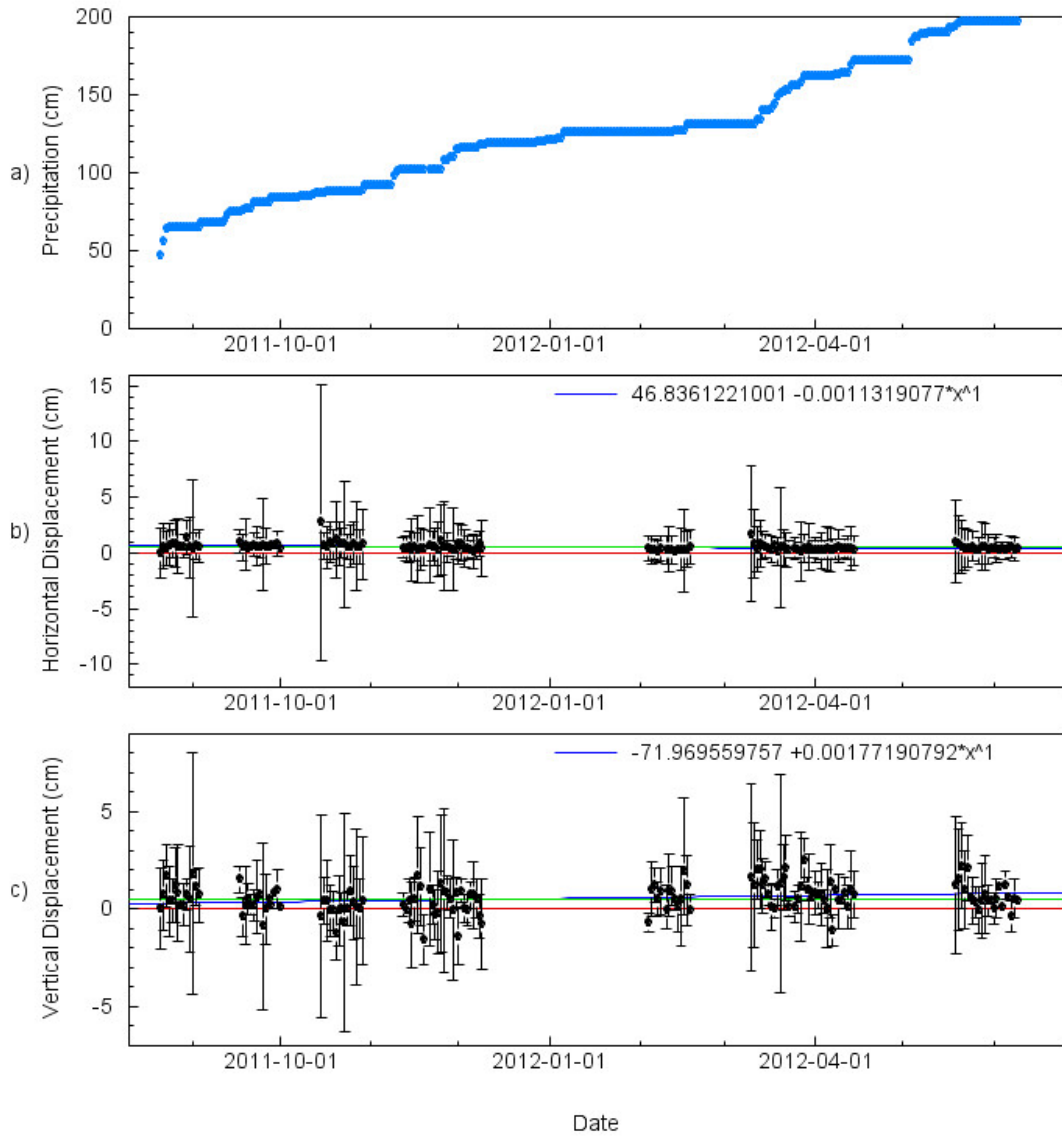


Figure 4-15: GPS time series and precipitation for station *frag*. Starting at the top precipitation (a), in the middle horizontal displacement (b) and in the bottom vertical displacement (c). Blue lines delineate the best-fit linear regression and green line the 2cm step in figures b and c.

4.2.2 Stations with 4-hour data coverage:

4.2.2.1 *flag*

Measuring period

The static GPS data collected data from July 2011 to June 2012.

Displacement

GPS static data are plotted as accumulated horizontal and vertical displacements versus the measurement date on Figure 4-16a and b respectively. Figure 4-16a shows static GPS derived horizontal displacement that accumulated over the monitoring period. The difference between the first and last measurements was used to estimate a total horizontal displacement of 8cm over the monitoring period. Values of error for individual data points ranged between -6cm and 46cm and averaged 30cm for horizontal data.

Figure 4-16b shows static GPS derived vertical displacement that accumulated over the monitoring period. The difference between the first and last measurements was used to estimate a total vertical displacement of 8cm (upward) over the monitoring period. Values of error for individual data points ranged between -5cm and 50cm and averaged 17cm for the vertical data.

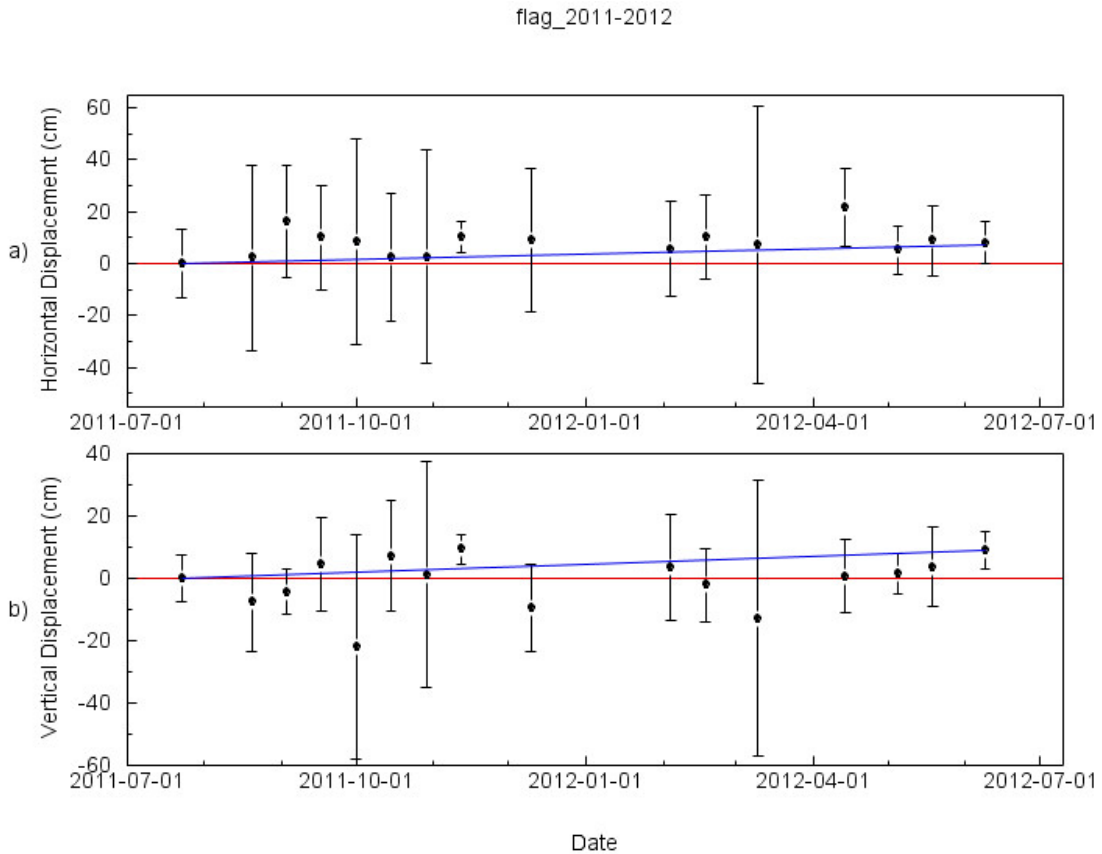


Figure 4-16: GPS time series for station *flag*. Beginning in the top, the time series show horizontal displacement (a) and in the bottom vertical displacement (b). Blue lines in a and b delineate the first and last observation.

4.2.2.1.1 Inclinometer and GPS comparison

GPS derived surface displacements at monitoring station *flag* were compared with the co-located Inclinometer *Z2_23* deflections at depth. The inclinometer deflection data collected from October 2011 through August 2012 are shown on Figure 4-17. The inclinometer registered continuous slow deflection that ranged from 0.3cm (1/8") at depth 12-13m (40-45 ft) to 0.6cm (1/4") near the surface.

GPS and Inclinometer measurements from station *flag* from October 2011 to August 2012 are compared in Table 4-1. A significantly higher horizontal surface displacement of $8\pm 10\text{cm}$ was estimated using the static GPS data collected at station *flag*. The GPS monitoring did show a positive surface displacement trend, but it over estimated displacement by an order of magnitude.

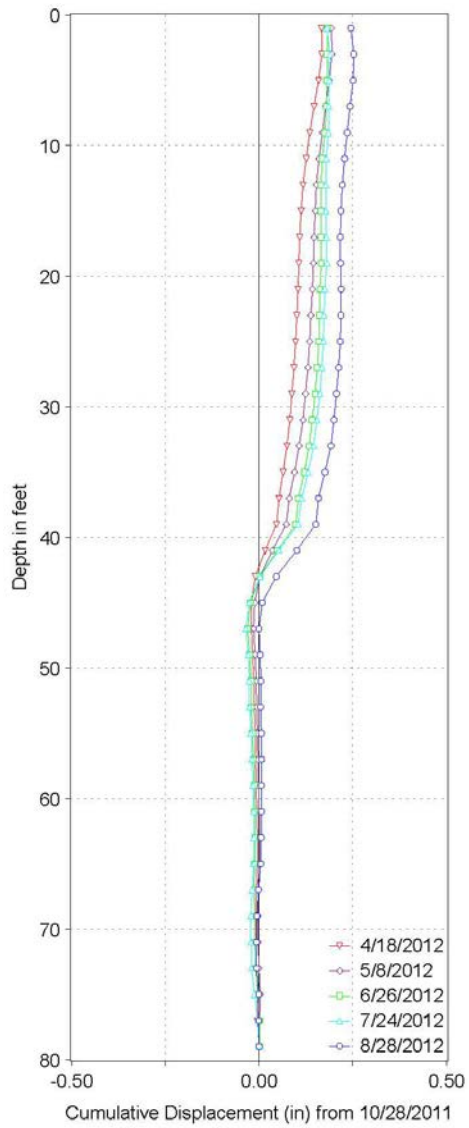


Figure 4-17 : Inclinometer Z2_23 measurements taken from April 18 to August 2012 by Suelos Inc. Each line represents cumulative displacement until April 18, 2012.

Table 4-1: GPS station *flag* and inclinometer *Z2_23* displacement comparison from October 2011 to August 2012.

Name	Equipment	Estimated Cumulative Horizontal Surface Displacement
<i>flag</i>	GPS	8±10cm
<i>Z2_23</i>	Inclinometer	0.6cm

4.2.2.2 *corg*

Measuring period

The static GPS collected data from June 2011 to June 2012.

Displacement

GPS measurements are plotted as accumulated horizontal and vertical displacement versus the measurement date on Figure 4-18a and b respectively. Figure 4-18a shows static GPS derived horizontal displacement that accumulated over the monitoring period. The difference between the first and last observation was used to estimate a total horizontal displacement of 24cm over the monitoring period. Values of error for individual data points ranged between -20cm and 140cm and averaged 37cm for horizontal data.

Figure 4-18b shows static GPS derived vertical displacement that accumulated over the monitoring period. The difference between the first and last measurements was used to estimate a total vertical displacement of 20cm (upward) over the monitoring period. Values of error for individual data points ranged between -5cm and 72cm and averaged 23cm for the vertical data.

corg_2011-2012

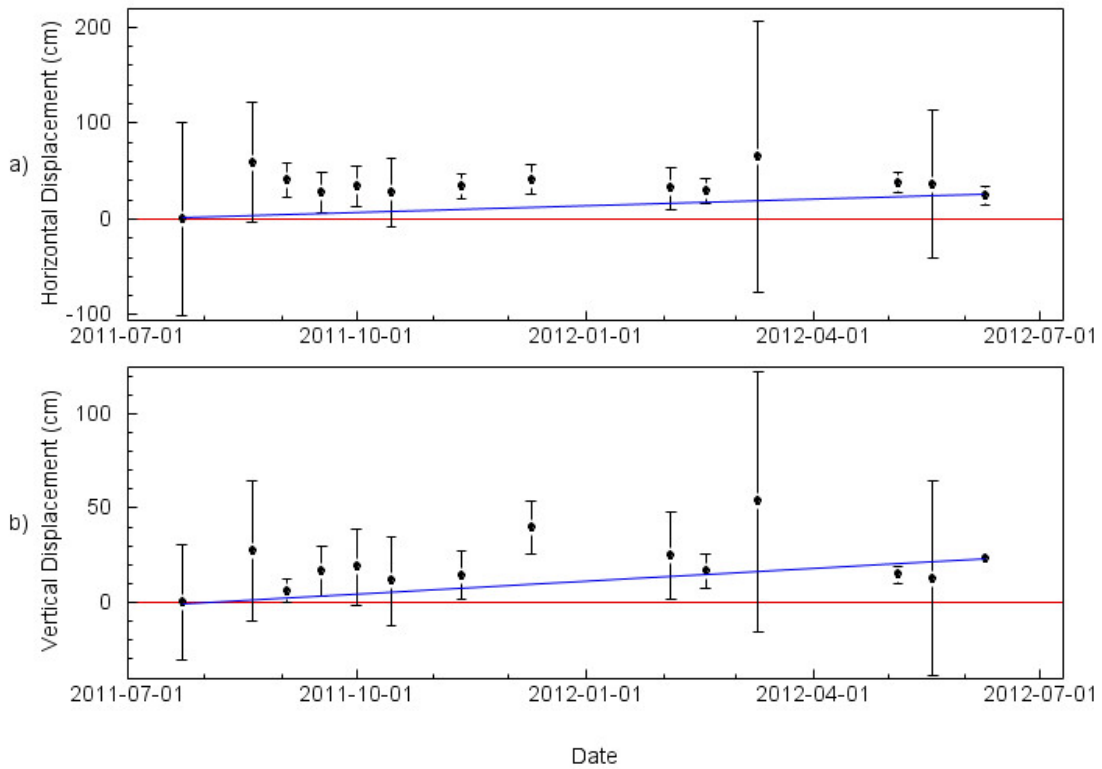


Figure 4-18: GPS time series for station *corg*. Beginning in the top, the time series show horizontal displacement (a) and in the bottom vertical displacement (b). Blue lines in a and b delineate the first and last observation.

4.2.2.3 *tang*

Measuring period

The static GPS data collected data from July 2011 to May 2012.

Displacement

GPS measurements are plotted as accumulated horizontal and vertical displacement versus the measurement date on Figure 4-19a and b respectively. Figure 4-19a shows static GPS derived horizontal displacement that accumulated over the monitoring period.

The difference between first and last measurement was used to estimate a total horizontal displacement of 1.3cm over the monitored period. Values of error for individual data points ranged between -3cm and 8cm and averaged 5cm for horizontal data.

Figure 4-19b shows static GPS derived vertical displacement that accumulated over the monitoring period. The difference between the first and last measurements was used to estimate a total vertical displacement of -1cm (downward) over the monitoring period. Values of error for individual data points ranged between -4cm and 6cm and averaged -5cm for the vertical data.

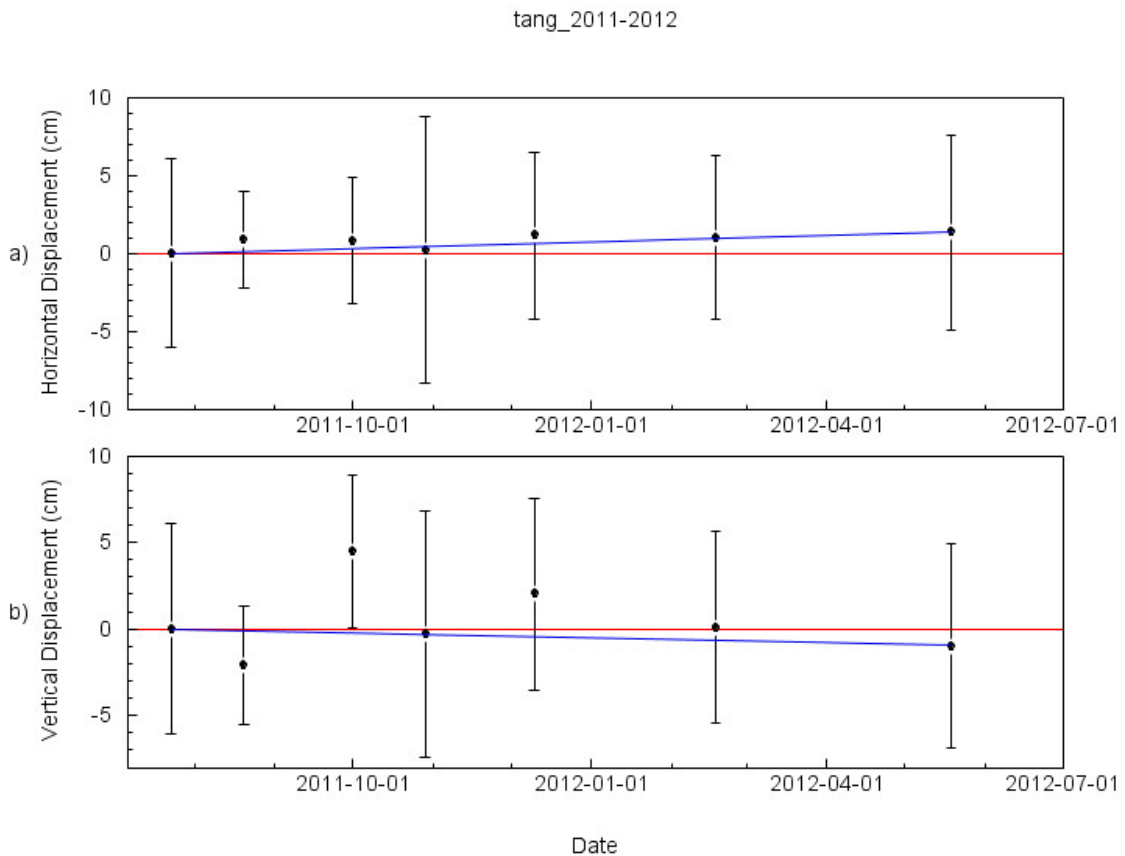


Figure 4-19: GPS time series for station *tang*. Beginning in the top, the time series show horizontal displacement (a) and in the bottom vertical displacement (b). Blue lines in a and b delineate the first and last observation.

4.2.2.4 *pisg*

Measuring period

The GPS measurements were collected from August 2011 to June 2012.

Displacement

GPS measurements are plotted as accumulated horizontal and vertical displacement from the point of origin versus the date of measurement on Figure 4-20a and b respectively.

The graph in Figure 4-20a shows static accumulated horizontal displacement derived from the static GPS observations that accumulated over the monitored period. A total horizontal displacement of 2cm over the monitoring period was estimated using the difference between the first and last points. The values of error for the horizontal data ranged between -10cm and 31cm for the data and averaged 10cm.

The graph in Figure 4-20b shows the vertical displacements derived from the static GPS observations that accumulated over the monitoring period. A total vertical displacement of -0.4cm (downward) over the monitoring period was estimated using the difference between the first and last data points. The values of error for the vertical data ranged between -4cm and 9cm for the data and averaged -6cm.

pisg_2011-2012

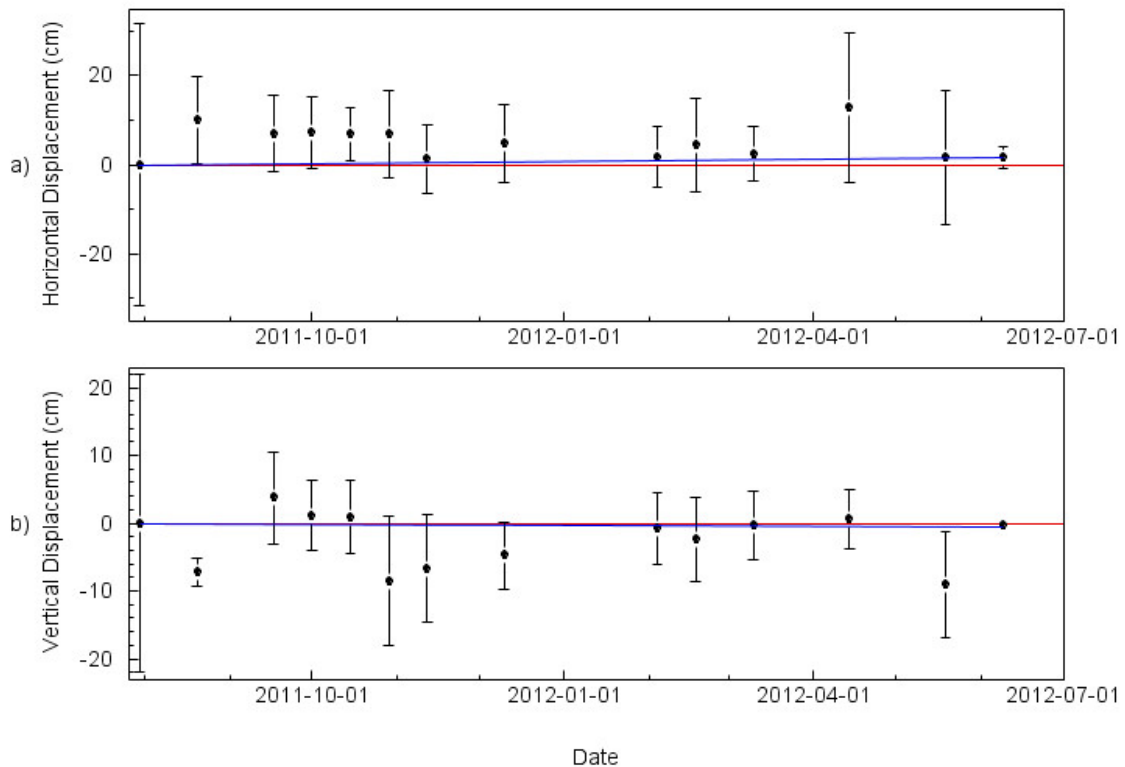


Figure 4-20 : GPS time series for station *pisg*. Beginning in the top, the time series show horizontal displacement (a) and in the bottom vertical displacement (b). Blue lines in a and b delineate the first and last observation.

4.2.2.5 *casg*

Measuring period

The GPS measurements were collected from July 2011 to May 2012.

Displacement

Results are plotted as accumulated horizontal and vertical displacement from the point of origin versus the date of measurement in Figure 4-21a and respectively. The graph in Figure 4-21a shows the horizontal displacement, derived from the static GPS

observations that accumulated over the monitoring period. A total horizontal displacement of 1.4cm over the monitoring period was estimated using the difference between the first and last points. The values of error for the horizontal data ranged between -1cm and 7cm for the data and averaged 4cm.

The graph in Figure 4-21b shows the vertical displacements, derived from the static GPS observations that accumulated over the monitoring period. A total vertical displacement of -3.8cm (downward) over the monitoring period was estimated using the difference between the first and last data points. The values of error for the vertical data ranged between -1cm and 7cm for the data and averaged -4cm.

casg_2011-2012

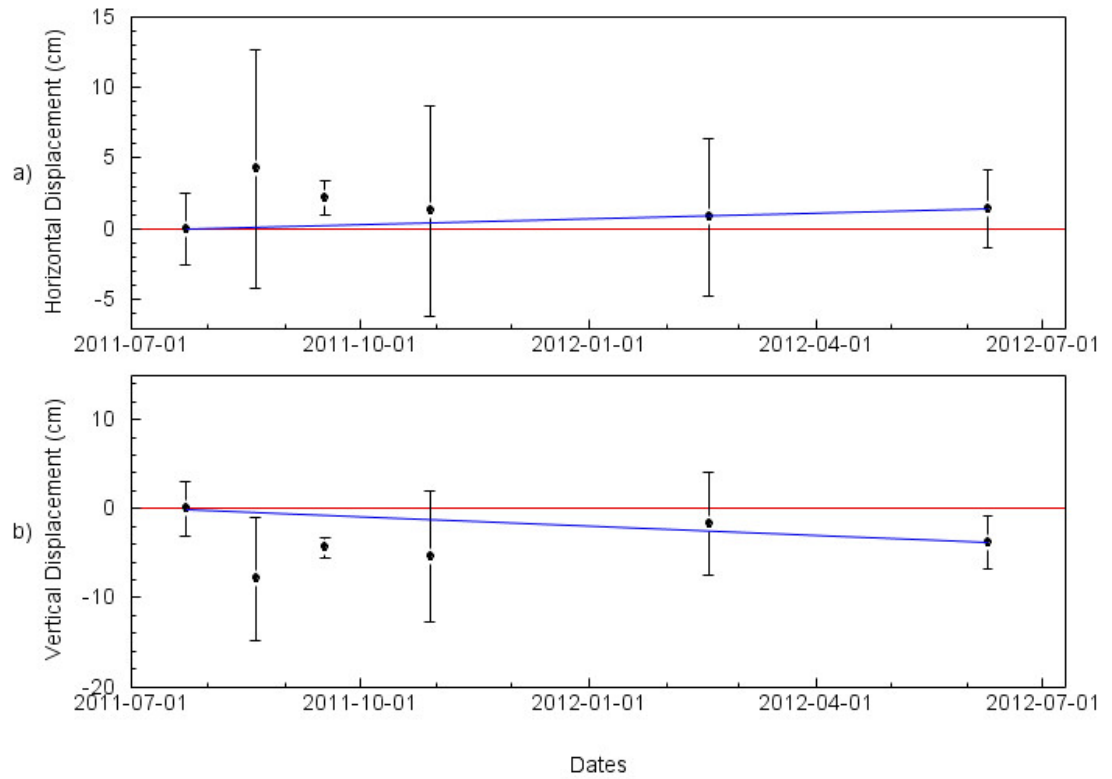


Figure 4-21: GPS time series for station *casg*. Beginning in the top, the time series show horizontal displacement (a) and in the bottom vertical displacement (b). Blue lines in a and b delineate the first and last observation.

5. DISCUSSIONS

Landslide evolution

Results of the continuous GPS data for the Cerca de Cielo landslide enabled us to quantify displacement rate of the landslide. Magnitude variations in velocity demonstrate landslide movement is affected by heavy rain. Landslide velocity is clearly linked to rate induced changes in shear strength of the materials caused by behavior of the clay when shearing.

During 2008 Wang (2012) determined constant displacement creep rate of the landslide during low rainfall periods. The displacement rate of the landslide was increased during heavy rainfall producing the surge event in September 2008. After the surge event the displacement creep rates of the landslide were reduced. The reduction of the displacement creep rates of the landslide was due to the decrease of heavy rainfall.

A steady displacement of the landslide but slower was recorded in 2009, with the exception of the rapid slide in November 2009. Slower displacement during 2009 was related to less precipitation.

Similar results to previous years (2008-2009) occurred during 2010-2011 where the landslide continued at a steady state of creep and was accelerated during prolonged precipitation. A steady state of creep was also recorded before and after the surge event.

Figure 5-1 shows a summary of accumulated displacement and precipitations during the monitored years. Red bars show the accumulated horizontal displacement, green bars show the accumulated vertical displacement and blue bars the accumulated precipitation.

A closer observation in Figure 5-1, the relation between displacements of the landslide

suggests a ratio of 2:1 between horizontal and vertical displacement. Figure 5-1 shows 2008 as the most active year between landslide movement and precipitation. More accumulated displacement and precipitation occurred during shorter periods in 2008. The 4-day period (September 20-24, 2008 in Figure 5-1b) is recorded as the most significantly surge period recorded by the GPS to date.

The following year (2009) monitored for 6-months and had less precipitation in comparison with 2008; as a consequence, less displacement occurred during 2009. Prolonged rainfall from October 26 to November 15, 2009 in Figure 5-1b over a 3-week period accelerated the landslide creep rates but at a lower magnitude. During this period the GPS recorded with precision the quick response between the landslide displacement and precipitation. The slower displacement during 2009 was related to less precipitation (85 cm).

Monitoring for a longer period during 2010 and 2011 suggests a similar pattern to 2008-2009. More precipitation accumulated during 2010-2011 and as a result, more accumulated displacement. The total accumulated precipitation during January 2010 to July 2011 was 20% less than in 2008. The surge period (October 1-December 1, 2010 in Figure 5-1b) that lasted 2 months, also accelerated the creep rates of the landslide similar to previous years.

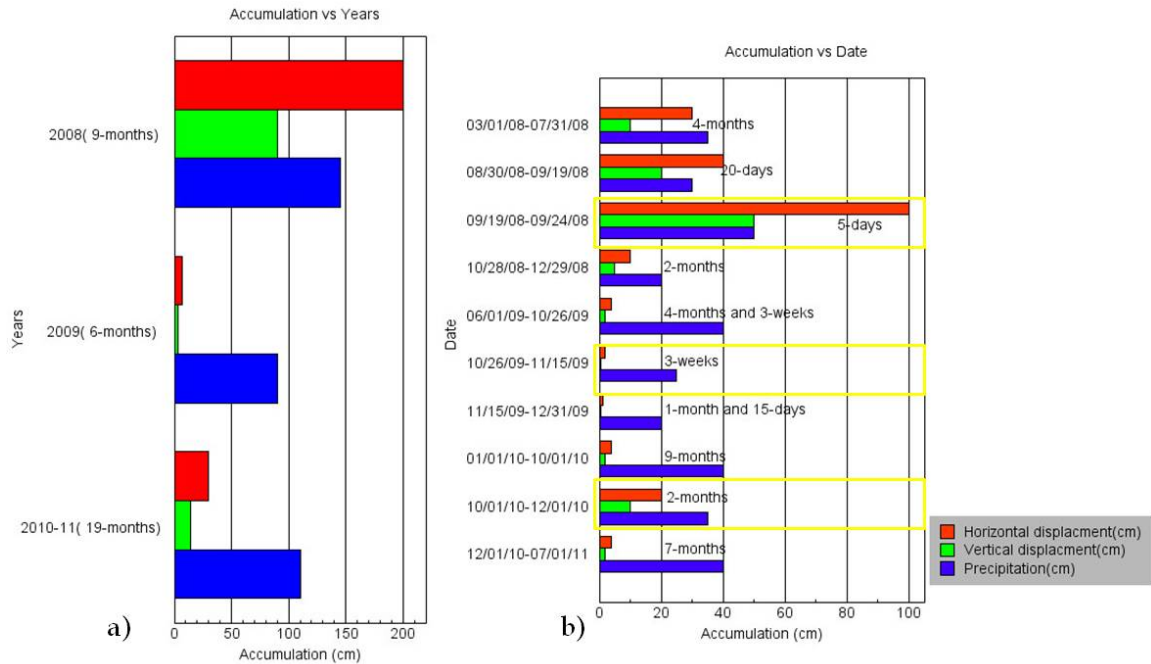


Figure 5-1: Accumulated displacement and precipitation of the landslide during 2008, 2009 and 2010-11. To the left the total accumulated displacement and precipitation during 2008, 2009 and 2010-11 (a). Accumulated displacement and precipitation before, during and after the each of the surge periods (b). Yellow rectangle in (b) delineate the surge periods for each year.

During the monitored periods (2008, 2009 and 2010-2011), three creep and surge events were detected. The creep and surge movement of the landslide within the sharp boundaries was initiated by a positive correlation with the amount of precipitation accumulation during 2008. Landslide displacement after each surge was followed by a decrease in displacement of the landslide due to dry periods. A more in depth discussion between daily rates of accumulated precipitation and daily rates of accumulated landslide displacement is presented in this section. The question remains whether the landslide slowed down significantly since the major surge event in 2008 or just less precipitation. Previous studies of the Cerca del Cielo landslide by Wang (2012) in 2008 were correlated

with recent data presented in this thesis in order to understand if the creep rate of the landslide has slowed down.

5.1 Rate analysis

Figure 5-2 shows the GPS measurement of the landslide of 4 different stations (*GP07*, *GP13*, *GK03* and *GP18*) by Wang (2012) during 2008. Station *GP13* located at the head of the landslide (see Figure 2-8) below the head scarp was analyzed. Displacement time-series in Figure 5-2 show that the longer term creep rate is also controlled by the precipitation accumulation rate.

Each green line in Figure 5-2 represent slopes line draw to data point to estimate displacement rate and precipitation accumulation rate. Six different estimates starting from period 1 (P1) to period 6 (P6) were chosen on having sections of data points defining consistent slopes.

From March to July 2008, Wang (2012) averaged 6 cm per month, but when we divide that period in two different periods we see a change in slope. A slight increase in precipitation and displacement from March to May 2008 is observed during this period (P1). During a late March to early May or P1 in Figure 5-2 the accumulated precipitation was 20cm and the accumulated displacement was 0.2m and 0.1m for the horizontal and the vertical respectively. From late May to late July or P2 in Figure 5-2 the accumulated precipitation was reduced to 10cm and the accumulated displacement also decreased to 0.1m and 0.05m for the horizontal and vertical respectively. Behavior of the landslide during P2 was characterized by long term creep rate controlled by the low precipitation

accumulation. During late August to mid September or P3 in Figure 5-2 the accumulated precipitation is increased to 30cm and the accumulated displacement was also increased to 0.4m and 0.3m for the horizontal and vertical respectively. The acceleration during P3 occurred right before the major surge in late September in P4. During September 19-24 or P4, the landslide was accelerated even further by a major surge with 50cm of accumulated precipitation. The total accumulated displacement was 1m and 0.5m for the horizontal and vertical respectively. An explanation for the major surge is the infiltration of water over 5-days in the clays. During late October to mid November or P5 the accumulated precipitation was reduced to 10cm and the accumulated displacement was reduced to 0.2m and 0.1m for the horizontal and the vertical respectively. From late November to late December the accumulated precipitation was reduced to 5cm and the displacement was also reduced to 0.1m and 0.05m for the horizontal and vertical respectively. Similar to P2, the landslide continues to move at a steady creep rate during P5 and P6. The total 2m accumulated in the horizontal displacement and the 0.9m accumulated vertical displacement of station GP13 over the monitored period suggests a sliding plane of the mass of 27° .

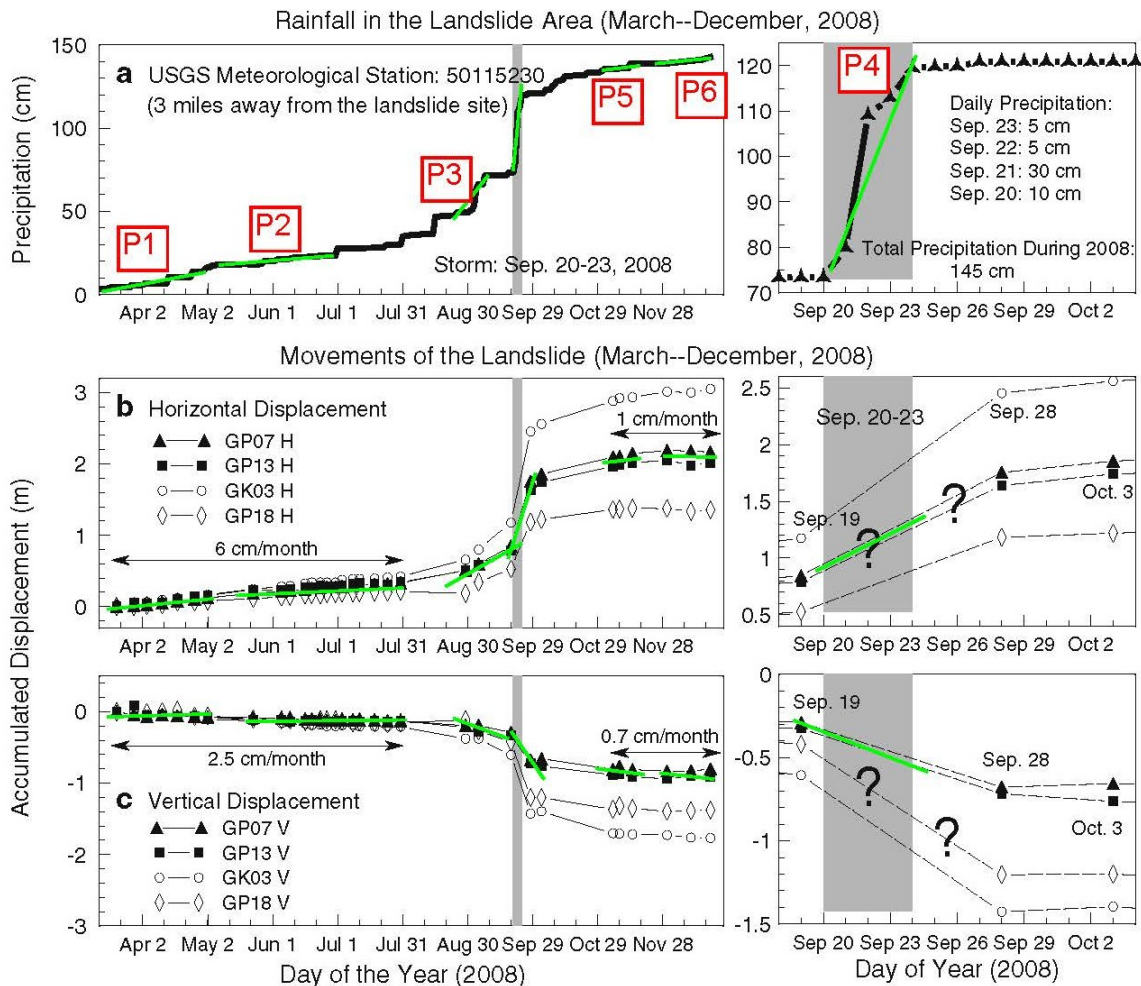


Figure 5-2: Accumulated precipitation and landslide displacement measurements during 2008. Green lines represent the slope lines draw to estimate the rate of displacement and precipitation (modified after Wang, 2012).

A more detailed analysis of the estimated slope lines (green lines in Figure 5-2) for 2008 is presented in Figure 5-3. Blue lines in Figure 5-3 represent the recorded accumulated precipitation rates, the red lines the accumulated horizontal displacement rates and the green lines the accumulated vertical displacement rates. Precipitation and displacement rates during P1 decrease as we move to P2 in Figure 5-3. Rates during P1 for precipitation start at 0.6cm per day and 0.6cm per day and 0.3cm per day for the

horizontal and vertical respectively. A decrease of rates is observed as we move to P2 to 0.3cm per day for precipitation and displacement. Rates for precipitation and displacement start to increase during P3, with 2.2cm per day for the precipitation, 1.3cm per day and 1cm per day for the horizontal and vertical respectively. The major surge event that accumulated approximately 50cm of precipitation from September 19-24, 2008 is shown in P4 on Figure 5-3. During this period, the precipitation accumulated at a rate of 10cm per day. Precipitation intensity rate during this period was the highest accumulated over a 5-day period. Nearly 1m of horizontal accumulated displacement of the 3m total horizontal accumulated displacement and about 0.5m of the 2m total vertical displacement occurred from September 20 to September 23, 2008. The GPS indicate that, during this 5-day period, the 1m of accumulated horizontal displacement for this period accumulated at a rate of 10cm per day, about 5cm per day accumulated for the vertical displacement. Acceleration of the creep rate during the surge event or P4 in Figure 5-3 shows a nearly instantaneous response of the behavior of the landslide as the precipitation is increased.

After the surge during P5, the estimated rates for precipitation are reduced to 0.3cm per day, the displacement is also reduced to 0.03cm per day and 0.02cm per day for the horizontal and vertical respectively. The decrease on rates suggests a decrease in displacement rates over time to a steady state creep rate by the post surge precipitation accumulation. P6 shows more stable rates of accumulation to about 0.5cm per day for the accumulated precipitation, accumulated horizontal displacement and accumulated vertical

displacement. Significant rate changes from P5 to P6 are correlated to a drier period similar to P2 before the surge.

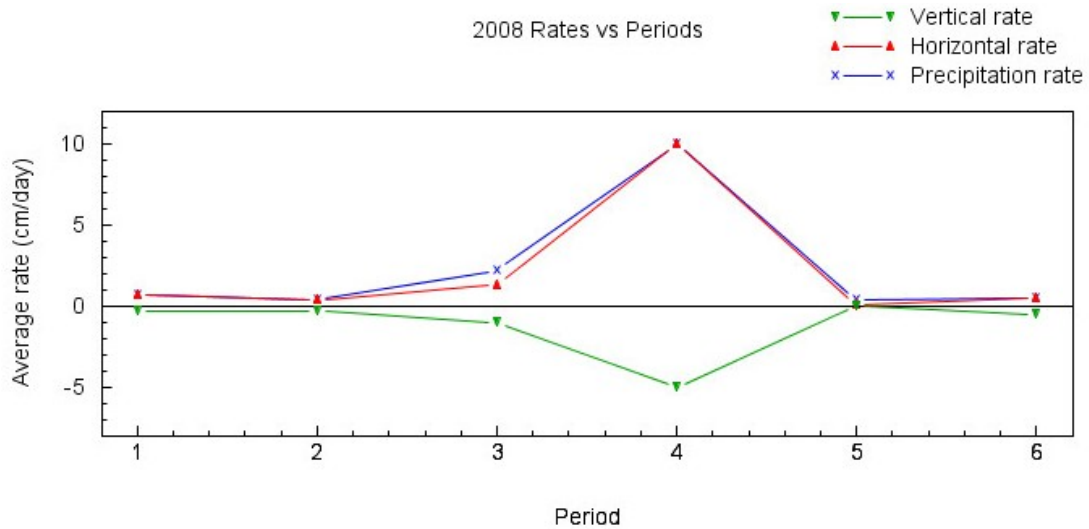


Figure 5-3: Average rates in each period for year 2008. Starting from period 1 (P1) to period 6 (P6).

Figure 5-4 illustrates the continuous GPS measurements by Wang (2012) during 2009. Precipitation was registered by a local rain gauge installed with the GPS over the same time as shown in Figure 5-4a. GPS measurements are plotted as accumulated displacement in the North-South (N-S) direction in Figure 5-4b, accumulated displacement in the East-West (E-W) direction in Figure 5-4c and accumulated vertical displacement in Figure 5-4d versus measurement dates. The resolved total horizontal displacement during this period was 6.5cm for the horizontal displacement and 3cm for the vertical displacement. Green lines in Figure 5-4 delineate slope lines to estimate rates.

Each green line represents eight different slope estimate starting from period 1(P1) to period 8 (P8).

Displacement measurements show a steady creep rate of the landslide from June to early October or from P1 to P4 with a total displacement of 4cm for the accumulated horizontal displacement, and 2cm for the accumulated vertical displacement over this 4-month with 3-weeks period. A total of 40cm of precipitation accumulated over this period. Displacement suggests a continuous steady creep rate of the landslide after the 2008 surge event.

The landslide movement is accelerated due to a surge event in P5 and P6, during 3 weeks from October 26 to November 15, 2009 with nearly 2cm of the 6.5cm total accumulated horizontal displacement. About 0.6cm of the 3cm total accumulated vertical displacement occurred over this period. Precipitation over the 3-week surge period accumulated 25cm of the 90cm total precipitation. An important observation in Figure 5-4 is the quick response or acceleration of the landslide displacement to increasing precipitation during the surge period (P5 and P6). The landslide displacement response to increasing precipitation is most noticeable during November 7, 2009. After the surge event from October 26 to December 31, 2009, during P7 and P8, the landslide displacement returned to a steady creep rate due to the decrease in precipitation.

As stated by Wang (2012), the slower movement in 2009 was due to the decrease in precipitation. GPS measurement shows a continuous slow displacement of the creep movement of the landslide in 2009 with a sliding angle of 27°. The smaller surge during October 26 to November 15, 2009 in comparison with 2008 was about half of the

accumulated precipitation over a longer period that accelerated the landslide displacement creep rate.

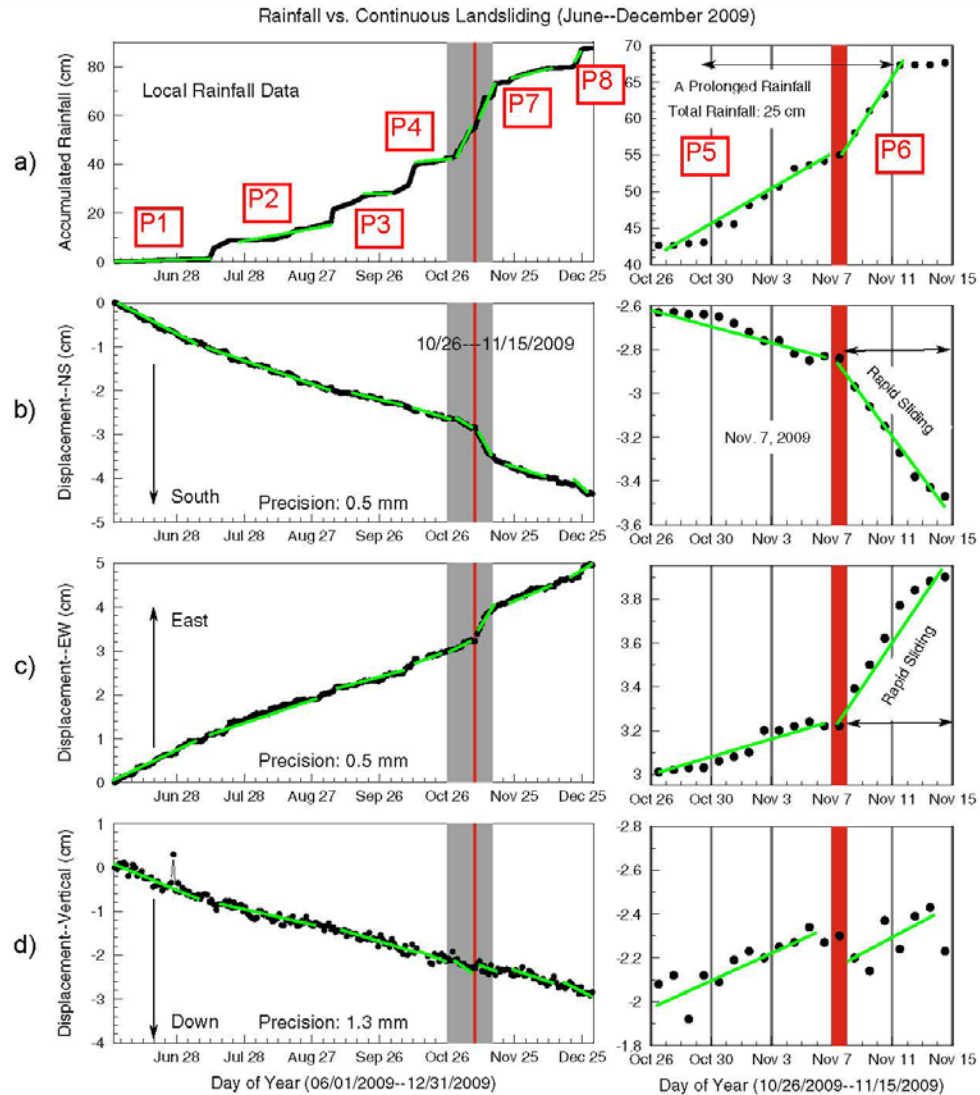


Figure 5-4: Accumulated precipitation and landslide displacement during 2009. Green lines delineate the analyzed periods for this study (modified after Wang, 2012).

Figure 5-5 shows a more detail analysis of estimated rates of accumulations based on the selected slope lines in Figure 5-4 throughout 2009. Blue lines in Figure 5-5 represent the recorded accumulated precipitation rates, the red lines the accumulated horizontal

displacement rates and the green lines the accumulated vertical displacement rates. P1 to P4 show a steady state of creep rates with accumulated displacement less than 1mm per day.

It is not until P5 that rates increase and are more noticeable in the precipitation and horizontal displacement. The increase is due to the beginning of the surge period during October 26 to November 15, 2009 or P5 and P6 in Figure 5-5 where the GPS detected an acceleration of the landslide that accumulated 25cm of precipitation. As mentioned by Wang (2012), the average precipitation was about six times faster during the surge period in comparison with the previous periods. Estimated rates during P5 were 4mm per day for the accumulated precipitation, 1.7mm per day and 0.2mm per day for the horizontal and vertical respectively. The estimated 4mm per day of precipitation was enough to produce an acceleration of the landslide creep rate most distinguished in the accumulated horizontal displacement.

Peak landslide acceleration rates were recorded during P6, where the landslide creep rate was further accelerated. The acceleration was due to the 7.7mm per day of accumulated precipitation that induced an acceleration of 2.7mm per day for the accumulated horizontal displacement and 0.6mm per day for the accumulated vertical displacement.

During P7 and P8, the precipitation is reduced to 1mm per day and, at the same time, displacement rates are reduced below 1mm per day, similar to P1 and P2. As stated by Wang (2012), the slower movement in 2009 was due to the decrease in precipitation. This pattern of displacement acceleration during a surge period (P5 and P6) suggests a continuation of the creep and surge landslide since 2008.

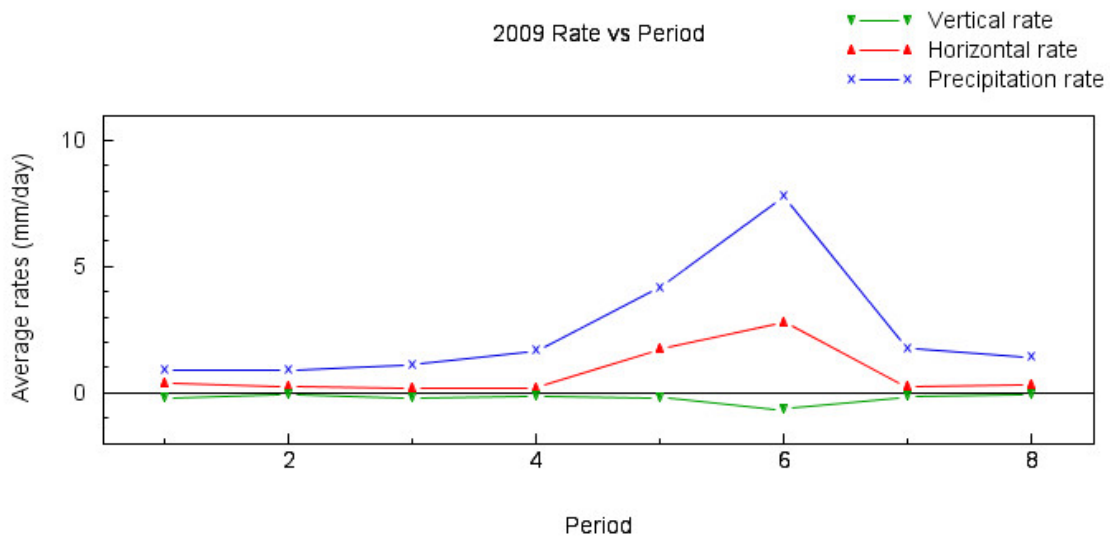


Figure 5-5: Average rates in each period for year 2009. Starting from period 1(P1) to period 8 (P8).

Figure 5-6 shows the most recent continuous GPS measurements from the Cerca del Cielo landslide. Green lines in Figure 5-6 delineate the slope from the best fit linear regression line to estimate rates. Each green line represent an estimate and are divide from period 1 (P1) to period 17 (P17). Slope lines were estimated in precipitation (Figure 5-6a), horizontal displacement (Figure 5-6b) and vertical displacement (Figure 5-6c).

Measurements from January 1, 2010 to September 3, 2010 or from P1 to P10 in Figure 5-6 a and b show a steady creep rate of the landslide. About 5cm for the accumulated horizontal displacement and 2cm for the accumulated vertical displacement were recorder over this period. During this 8 month period, the accumulated precipitation was 40cm of the 110cm total accumulated precipitation.

Measurements during P11 of the landslide showed a 15cm of accumulated horizontal displacement and 6cm of accumulated vertical displacement from a surge event that

accelerated the landslide movement over a 30 day period with about 40cm of accumulated precipitation. Landslide movement is decelerated during P12 as a response to dry period. Accumulated displacement during P12 was reduced to 5cm for the horizontal displacement and 4cm for the vertical displacement. The deceleration of movement during P12 demonstrates the relationship between the mass as it dries due to the reduction of precipitation until it reaches a stable creep rate.

Longer dry periods dominate from P13 to P17. As a consequence the landslide enters a steady creep rate similar to periods prior to the surge. The total 30cm in the accumulated horizontal displacement and 14cm accumulated vertical displacement during the monitoring resolve a basal sliding angle of 27° similar to previous years. The basal slip angle suggests a stable sliding plane for the landslide since 2008. Monitoring of landslide indicates a continuous creep movement during periods with no accumulated precipitation and acceleration during heavy precipitation, but not at the same rate as 2008 reported by Wang (2012).

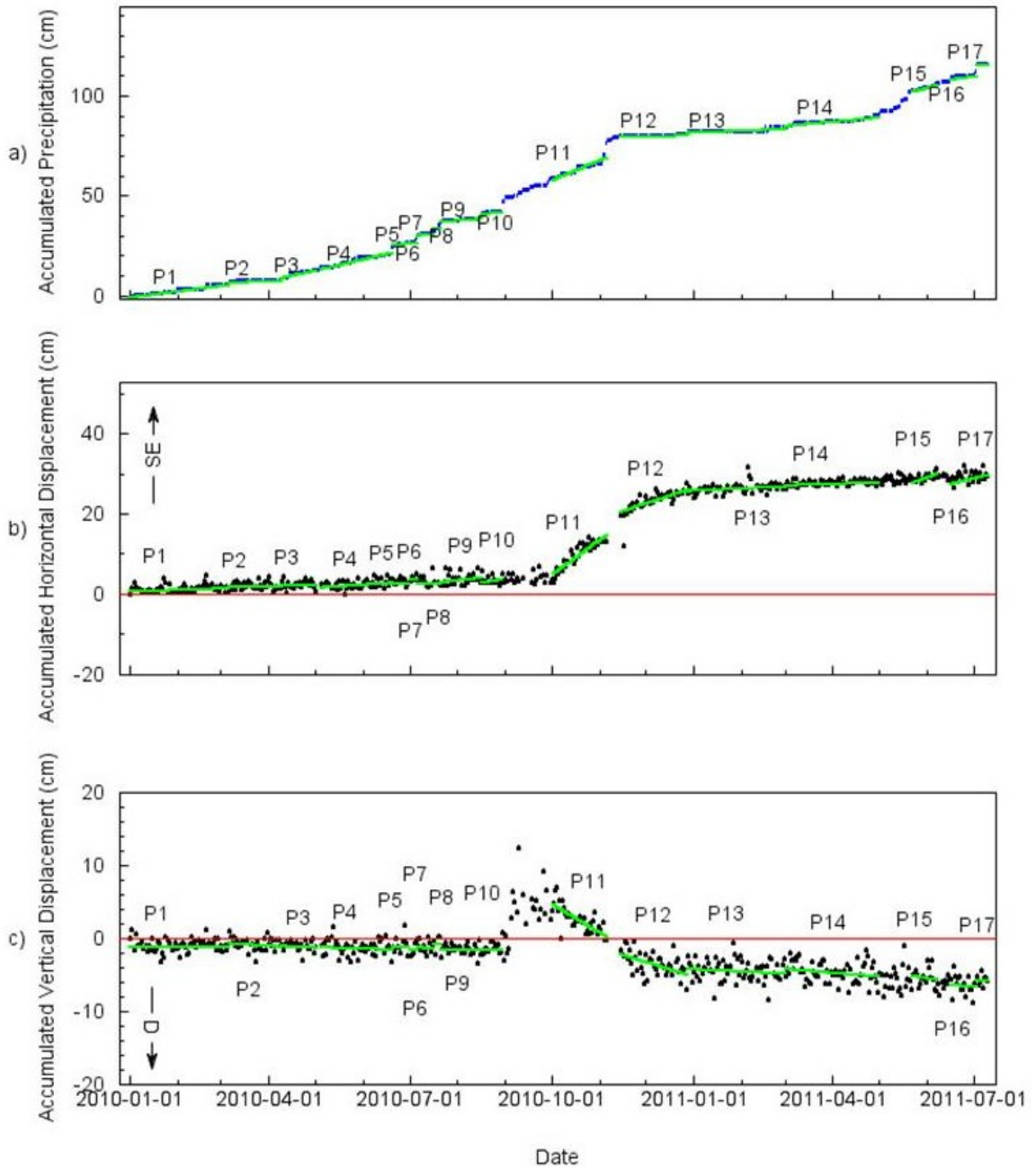


Figure 5-6: Slope lines used to estimate rates for: accumulated precipitation (a), horizontal displacement (b) and vertical displacement (c) of the landslide during 2010 and 2011. The analyzed slope lines marked as green lines.

Figure 5-7 shows a detailed analysis of the estimated rates periods based on Figure 5-6. Blue lines in Figure 5-7 represent the recorded accumulated precipitation rates, the red lines the accumulated horizontal displacement rates and the green lines the accumulated vertical displacement rates. P1 to P8 show a steady state of creep movement with less than 1mm per day as precipitation accumulates at about a similar rate over the 8 month period. During P9, precipitation and accumulated horizontal displacement increase at about 0.5mm per day. P10 shows increment of the rate for the precipitation and accumulated horizontal displacement to 0.7mm per day. No measurable rates over 0.5mm per day were detected for the accumulated vertical displacement during P1 to P10.

Beginning of the surge period of the landslide is distinct in P11. Daily rates of landslide displacement estimated 10cm of accumulated horizontal displacement accelerated at a rate of 3.2mm per day. The estimated 5cm of accumulated vertical displacement for this period accelerated at a rate of 1.4mm per day over a 2 month period. The estimated accumulated precipitation during this period was 21cm with a daily rate of 4.4mm per day. Increase of the rate of precipitation during the surge in P11 produced an acceleration of the constant creep rates similar to previous years.

During P12 in Figure 5-7, there is a decrease in rates to 1.2mm per day for the horizontal displacement and less than 1mm per day for the precipitation and 0.6mm per day for the vertical displacement. In the same way, as the landslide behavior increases the displacement rate during P11 in response to an increase in precipitation, the landslide behavior decreases its displacement during P12 due to drier periods. The low rate of

accumulation in precipitation or dry period slowed down significantly the landslide rates and now the landslide goes through a transition period from unstable to a more stable state of displacement rates. In some cases, slow landslide displacement can continue through both wet and dry periods (Massey et al., 2013).

Rates during P13 and P14 are further reduced for precipitation and displacement, indicative of more stable state of creep of the landslide in response to precipitation. Similar to P11, P15 shows the increment of precipitation to 2mm per day and 1mm per day for the horizontal displacement. Vertical rate over this period was less than 0.5mm per day. Similar to P11, rates during P16 and P17 are gradually decreased to less than 1mm per day.

A look at the precipitation and the landslide displacement before, during and after the highest rate of accumulation, it can be inferred that landslide creep state has been continuous since 2008 and is increased during heavy continuous precipitation season or surge period, while it decreases during dry season. Monitoring of the landslide indicates a steady creep rate during periods with no accumulated precipitation.

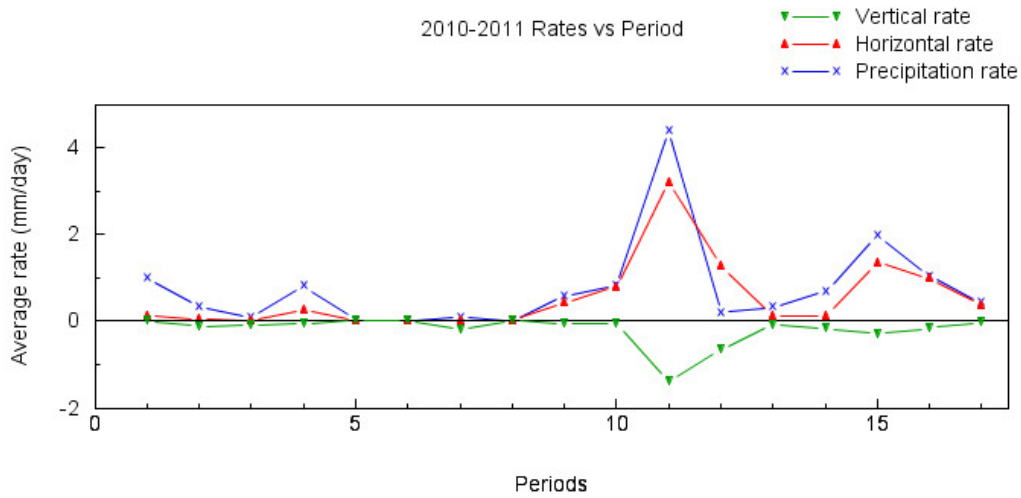


Figure 5-7: Average rates for years 2010 and 2011. Starting from period 1(P1) to period 17 (P17).

5.2 Creep rate and precipitation analysis

A correlation of average precipitation rates and displacement rates in mm per day during the surge events recorded from 2008 to 2011 are shown in Figure 5-8. In Figure 5-8 a best fit linear regression lines with $R^2=0.99$ was used to model the behavior of the landslide in terms of horizontal displacement (red circles), vertical displacement (green circles) and net displacement (blue triangle).

At the Cerca del Cielo landslide, the relationship between increasing displacement and increasing precipitation is linear. Therefore, landslide velocity is expected to increase with induced precipitation. The most noticeable creep event occurred in 2008, with an average rate of 100mm per day of accumulated precipitation that generated up to 100mm per day of horizontal displacement and up to 50mm per day of vertical displacement. The net displacement in Figure 5-8 of the landslide also increases as we increase the

precipitation rate. A 1.10mm per day of net displacement was calculated using the best fit linear regression as a model. The best fit linear regression estimated a rate about 0.98mm per day of average horizontal displacement as we increase the rate of precipitation. The best fit linear regression averaged a rate of 0.49mm per day of vertical displacement as we increase the rate of precipitation.

The increment in the rate of precipitation also increases the rates of displacement. Behavior of the Cerca del Cielo landslide is constrained by the rate of accumulated precipitation. Therefore, in order to have another major creep event there would have to be a surge with a higher or equal rate of 100mm per day of precipitation over a 5-day period or less on the landslide mass to induce more than 2m in the horizontal displacement and 0.9m in the vertical displacement. The resulting rate of accumulation should be higher or equal to 100mm per day of accumulated horizontal displacement and 50mm per day of accumulated vertical displacement.

Displacement Rate vs Precipitation Rate

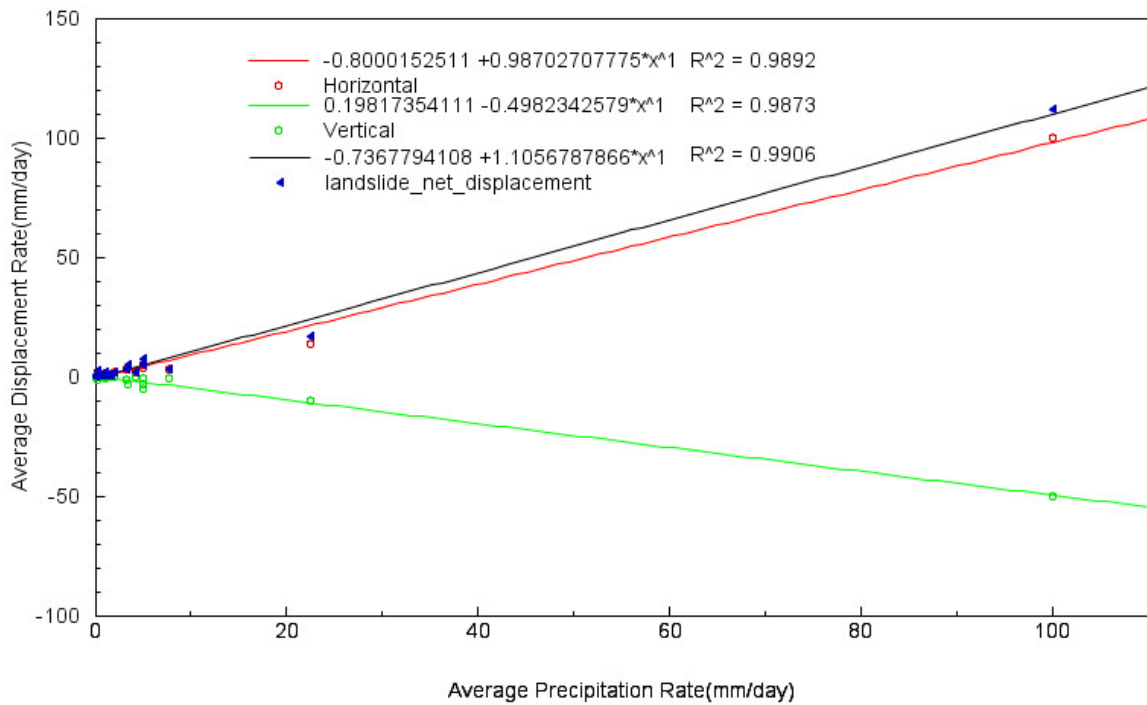


Figure 5-8: Average displacement and precipitation rates comparison

5.3 Rates for 24-hour GPS stations outside the landslide

A summary of the GPS derived displacement data from all of the monitored 24 hour static stations during 2011 and 2012 outside the landslide boundaries is shown in Figure 5-9. Station *refs* (Figure 4-18) was not included in this graphs due to the different time frame, but the station shows the same pattern. Displacement values in Figure 5-9 b,c,e and f of all stations showed constant values within 2cm in both the horizontal accumulated displacement (Figure 5-9b and e) and vertical accumulated displacement (Figure 5-9c and f). Horizontal and vertical measurements in Figure 5-9e and f for station *carg* showed scattered observations higher than 2cm in comparison with other stations.

The scattered measurements for station *carg* are probably due to the dense vegetation surrounding the area and low altitude of the station. Values in the horizontal and vertical component for the remaining stations maintained a constant horizontal line suggesting no accumulation of displacement over the monitored period within the detection limit. No correlation was found with precipitation (Figure 5-9 a and d) during the monitoring period.

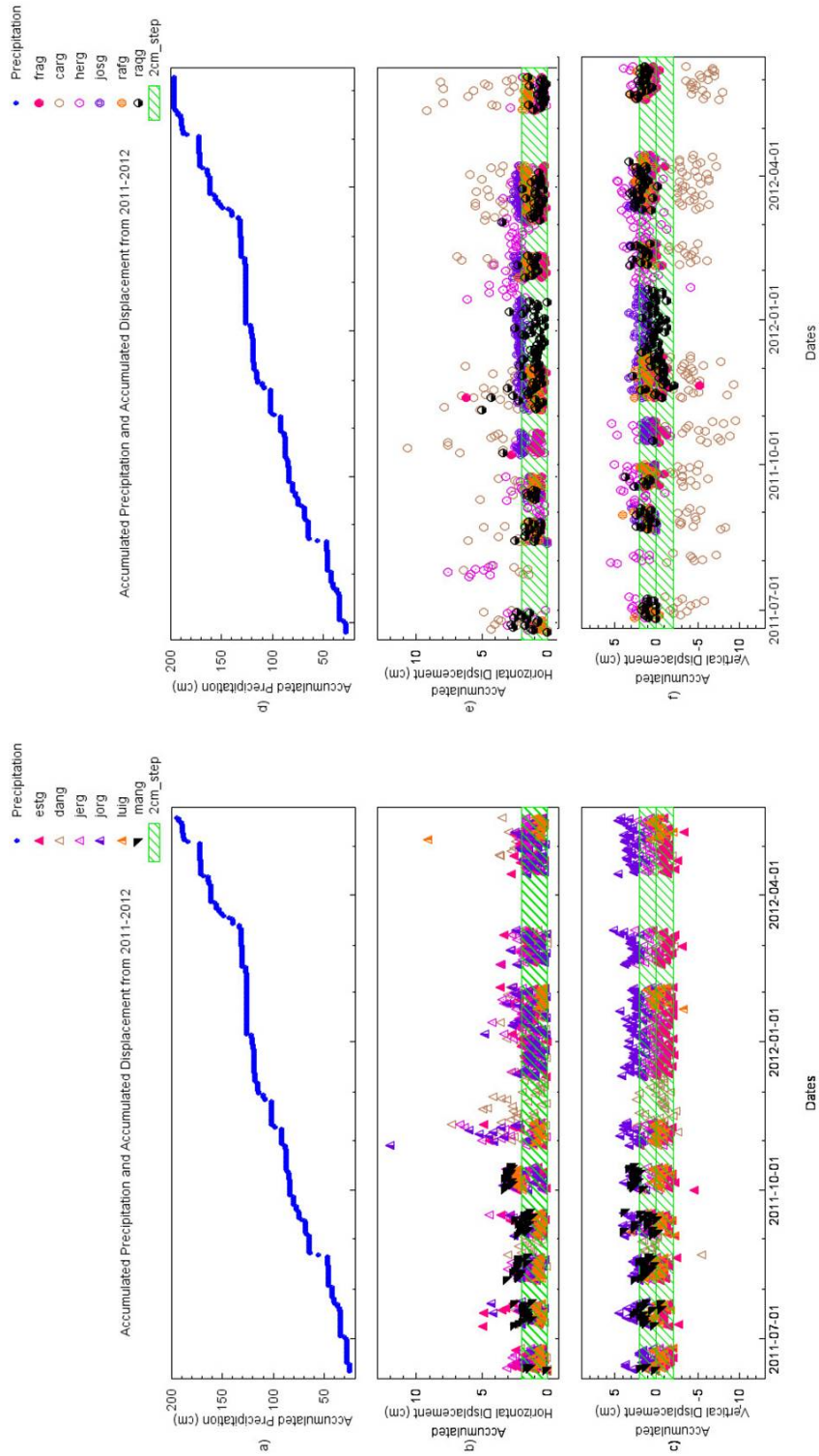


Figure 5-9: Summaries of all 24-hour static stations monitored outside the landslide from June 2011 to June 2012.

5.4 Rates for static 4-hour GPS measurements

Static stations monitored for 4 hours, one day session (Figure 5-10) displayed more scattered measurements when compared to the 24 hour sessions (Figure 5-9).

Only the station *flag* was compared with the inclinometer and measurements did estimate a positive trend but it was greatly overestimated. Station *abeg* located along the flank of the landslide was able to detect landslide displacement at half of the total displacement from GPS station *CB*. General sliding angle for station *abeg* was estimated to be 24° , which is about 3° less than station *CB*.

The station *corg* recorded the highest values of displacement and error mainly because this benchmark was near the main road in the community and may have been disrupted by human activity. The scattered measurements in the 4 hour sessions result from the variation of satellite constellation and multipath effects. High values of error are due to the monitoring of 4 hours and data gaps due to sampling rate of 1-2 measurements per month per station. Another possible explanation for the high values of error in the GPS static stations is that the tropospheric water and moisture is higher in the tropics (Mao et al., 1999). Analysis of the estimated displacement calculated from the initial measurement and last observation of the 4-hour sessions defines the limitation for the GPS with the current resolution to detect displacement at the cm level.

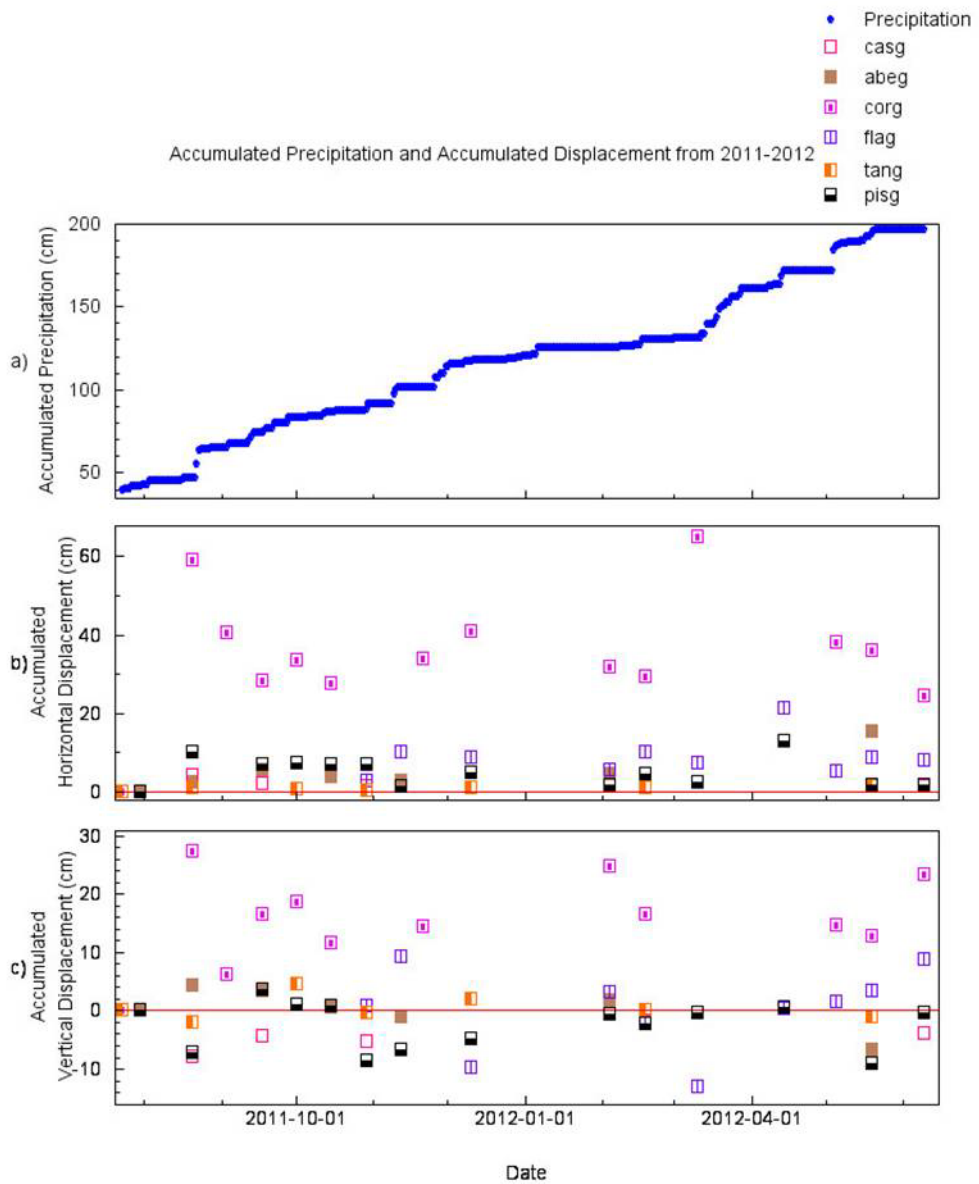


Figure 5-10: Summaries of all 4-hour static stations monitored from June 2011 to June 2012.

Houses and benchmarks monitored outside the landslide did not reveal any apparent accumulated displacement, but did manage to help determine the limitations of the GPS to define stable areas. Antenna changes between each period affect the observations. The

antenna change produced a step in the vertical component during the monitored period of the landslide in Figure 4-1 and also in the vertical component of station *refg* in Figure 4-18. Both time series exhibit a step in the vertical component on September 4, 2010 when the antenna was changed. Wang (2012) studied benchmarks outside the landslide and did not observe any measurable movement. Stations installed during this investigation also followed this trend. Units measured using GPS outside the landslide allowed us to determine the limits of measurements for a stability analysis. Some stations like *tang* and *mang* showed a positive trend of accumulation in the horizontal displacement, but due to the short monitoring period, the detected measurement of the GPS falls within the error limitations. Comparisons between the GPS station *flag* and inclinometer *Z2-23* located at about 10 feet of distance between each other showed different results. The inclinometer observed ¼” of displacement at 40 feet of depth. The GPS was not able to detect any displacement, but we were able to estimate displacement in that area. The estimated displacement was within the detection limits ($\leq 2\text{cm}$) of the GPS equipment.

5.5 Compilation of data and interpretation

Based on data collected in this investigation and previously published data, the Cerca del Cielo landslide could be described as a creep and surge landslide. Steady state creep is not constant over time and it changes during heavy rainfall and dry periods. The creep rate is controlled by the infiltration of water in the highly plastic clays. Surge periods are defined as an acceleration of the landslide creep rate in response to heavy precipitation.

During these periods the highest creep rates were recorded for each of the monitored years suggesting the maximum velocity of the landslide.

Deceleration of the landslide occurs during dry periods and the landslide mass starts to slow down into a steady state of creep. Post surge periods are defined as a steady state creep rate of the landslide that is distinguished by dry periods. The fact that the landslide creep rate accelerates during rainy periods and decelerates during dry periods suggests a change in the behavior of the plastic clays in the landslide. This is supported by the steady state creep rates of the landslide before and after surge events. Cerca del Cielo landslide motion patterns were repetitive, with slow motion punctuated by surges during periods of heavier precipitation. The displacements vary in magnitude and duration.

The 27° sliding plane of the landslide is determined by the 2:1 ratio between horizontal and vertical displacement. Displacement rates show acceleration with the increment of precipitation in agreement with the deceleration of the sliding mass after the significant slide in 2008.

Boundaries of the landslide determined by Suelos Inc have not changed since they were established in 2008. Wang's (2012) investigation from March 2008 to March 2009 did not find any measurable movement outside the landslide area delineated by Suelos Inc. GPS measurements outside the landslide boundaries presented in this study support these findings and Wang (2012).

6. CONCLUSION

Geodetic measurements gathered in the Cerca del Cielo community and previously published data by Wang (2012) and Suelos Inc. (2008) indicate a steady state creep of the landslide during dry periods that is accelerated by surge periods. GPS time-series have revealed patterns of post-failure slow displacement periods of acceleration in creep rates that were triggered by seasonal peaks in precipitation.

The 40cm of precipitation that accumulated during surge event from October-November 2010 increased the displacement from 5cm to 10cm at rates up to 3.2mm per day for the horizontal and from 2cm to 6cm at rates up to 1.4mm per day for the vertical. The acceleration was due to seasonal peaks in precipitation. The deceleration of the landslide after the surge events demonstrates the relationship of the landslide as the clay dries due to the reduction of precipitation. Slow displacement involved the reduction of precipitation and plastic deformation of the clays during dry periods.

Creep rates of the landslide are not constant during dry and surge periods. The driving force of the landslide has not slowed down after the major event in 2008. To date there has not been a similar surge event as that of September 2008 where of 50cm (10cm per day) of precipitation were observed over a 5-day period. In contrast, the subsequent years (2009-2011) were characterized by less precipitation which played a major role in controlling the displacement and creep rate of the landslide.

The 2:1 ratio between horizontal and vertical displacement is controlled by the estimated 27° angle of the sliding plane. The sliding plane has not change since the major surge

event in 2008. An unsaturated sliding mass after the surge events suggest the movement of the sliding mass as it moves from an unstable angle to a more stable one. It is evident from the data that triggering periods of faster displacement after 2008 resulted from long periods of continuous precipitation rather than from large magnitude, short duration precipitation. Geodetic measurements and precipitation data suggest a behavior characterized by a continuous creep and surge periods of the landslide.

The linear relation between the rate of displacement and the rate of precipitation enable us to establish a precise creep rate curve particularly for the Cerca del Cielo landslide, which can predict its displacement in future surge events. Precipitation accumulation equal or greater to 50cm over a 5-day period, similar to the surge event in September 19-24, 2008 should be of concern to the community. It may be expected that such a precipitation rate would result in an acceleration of the landslide within its sharp boundaries. The expected rate of displacement should be 0.98mm per day for the horizontal displacement and 0.49mm per day for the vertical displacement. The net displacement of the landslide during a surge event should be equal or greater to the surge event in September 20-24, 2008 to about 1.10mm per day. The landslide total displacement over the period should be in the order of 3m for the horizontal component and 2m in the vertical component. Any future surge that accelerates the creep should follow the established creep rate curve developed in this study. Long term continuous static GPS monitoring of the landslide has proven to be useful to detect displacement at the cm level and estimate rate changes at the mm level. The evident relationship between rainfall and landslide displacement computed in this study should be useful for

emergency management agencies and the Cerca del Cielo community for planning, decision making and understand how rainfall controls the landslide displacement.

GPS estimated displacement presented in this study for the monitored points outside the landslide highlights the detection limits ($\leq 2\text{cm}$) of the static GPS to detect any neighboring areas behaving similarly. However, the fact that GPS computed displacements of sites outside the landslide showed apparent stability due to the signal being smaller than the noise does not necessarily mean these sites are stable and/or free from potential motion in the future. No displacement of residences outside the landslide was detectable using continuous GPS over 2-week periods. The 4-hour GPS stations were not effective in measuring displacement because of large error values and data variability. In this case continuous monitoring of GPS sites and inclinometer data may be useful to detect any creep at certain depth and should be compared with any apparent surface displacement detected by GPS. Results from the inclinometer and GPS station *flag* should be taken in consideration as a possible area that might show any creep. Any apparent surface motion outside the sharp landslide boundaries appears to be unrelated to fluctuations in the precipitation, because within the limits of detection the rate of displacement was insignificant and did not vary.

7. FUTURE WORK

A real time continuous monitoring of the Cerca del Cielo landslide is suggested. This could be accomplished by reinstalling both the continuous GPS site and the weather station within the boundaries of the landslide. Monitoring in this manner will help collect local precipitation and would allow for a more precise observation of the landslide in response to the accumulation of local precipitation during a surge period. Future acceleration of the landslide displacement should follow the creep rate model established in this study.

Geodetic surveys performed outside the landslide boundaries did not detect any displacement over the established limitation of the GPS, however it would be good practice to keep monitoring the existing sites of this study to quantify its motion. It is recommended that for any future surveys of benchmarks and houses outside the landslide boundaries, antennas should not be changed or removed given that a source of error could be introduced in the observations.

REFERENCES

- Cruden, D.M., and Varnes, D.J., 1996, Landslide types and processes: Landslides: investigation and mitigation (Special Report), p. 36–75.
- Eckl, M.C., Snay, R.A., Soler, T., Cline, M.W., and Mader, G.L., 2001, Accuracy of GPS-derived relative positions as a function of interstation distance and observing-session duration: , p. 633–640.
- El-Rabbany, A., 2002, Introduction to GPS The Global Positioning System.
- Gili, J. A., Corominas, J., and Rius, J., 2000, Using Global Positioning System techniques in landslide monitoring: *Engineering Geology*, v. 55, p. 167–192, doi: 10.1016/S0013-7952(99)00127-1.
- Harp, E.L., Reid, M.E., McKenna, J.P., and Michael, J. a., 2009, Mapping of hazard from rainfall-triggered landslides in developing countries: Examples from Honduras and Micronesia: *Engineering Geology*, v. 104, p. 295–311, doi: 10.1016/j.enggeo.2008.11.010.
- Jibson, R.W., 1989, Debris flows in southern Puerto Rico: *Geological Society of America Special Papers* , v. 236 , p. 29–56, doi: 10.1130/SPE236-p29.
- Jibson, R.W., 1985, Evaluation of landslide hazards resulting from the 5-8 October 1985, storm in Rico Puerto: U.S. Geological Survey Open-File Report, v. FEMA-746-D, p. 86–26.
- Krushensky, R.D., and Monroe H., W., 1978, Geologic map of the Peñuelas and Punta Cuchara quadrangles, Puerto Rico.
- Larsen, M.C., Santiago, M., Jibson, R., and Questell, E., 2004, Map Showing Susceptibility to Rainfall-Triggered Landslides in the Municipality of Ponce, Puerto Rico: North, p. 1.
- Larsen, M.C., and Simon, A., 1993, A Rainfall Intensity-Duration Threshold for Landslides in a Humid-Tropical Environment, Puerto Rico: *Geografiska Annaler. Series A, Physical Geography*, doi: 10.2307/521049.

- Larsen, M.C., and Torres Sanchez, A. J., 1992, Landslides triggered by Hurricane Hugo in eastern Puerto Rico, September 1989: *Caribbean Journal of Science*, v. 28, p. 113–125.
- Larsen, M.C., and Torres-Sanchez, A. J., 1996, Geographic relations of landslide distribution and assessment of landslide hazards in the Blanco, Cibuco, and Coamo river basins, Puerto Rico: U.S. Geological Survey Water Resources Investigations Report, v. 95-4029, p. 56 p.
- Malet, J., Maquaire, O., and Calais, E., 2002, The use of Global Positioning System techniques for the continuous monitoring of landslides : application to the Super-Sauze earthf low (Alpes-de-Haute-Provence , France): v. 43, p. 33–54.
- Mao, A., Harrison, C.G. A., and Dixon, T.H., 1999, Noise in GPS coordinate time series: *Journal of Geophysical Research*, v. 104, p. 2797, doi: 10.1029/1998JB900033.
- Massey, C.I., Petley, D.N., and McSaveney, M.J., 2013, Patterns of movement in reactivated landslides: *Engineering Geology*, v. 159, p. 1–19, doi: 10.1016/j.enggeo.2013.03.011.
- Monroe H, W., 1978, Map Showing Landslide and Areas of Susceptibility to Landsliding in Puerto Rico , p. 1.
- Schwarz, C.R., Snay, R. A., and Soler, T., 2008, Accuracy assessment of the National Geodetic Survey's OPUS-RS utility: *GPS Solutions*, v. 13, p. 119–132, doi: 10.1007/s10291-008-0105-0.
- Soler, T., Michalak, P., Weston, N.D., Snay, R. A., and Foote, R.H., 2005, Accuracy of OPUS solutions for 1 to 4-h observing sessions: *GPS Solutions*, v. 10, p. 45–55, doi: 10.1007/s10291-005-0007-3.
- Suelos Inc. (2008) Geotechnical report on landslide investigation, analyses and remedial measures at Cerca Del Cielo Community Tallaboa Ward, Ponce, Puerto Rico (engineering report).
- Wang, G.Q., 2012, Kinematics of the Cerca del Cielo, Puerto Rico landslide derived from GPS observations: *Landslides*, v. 9, p. 117–130, doi: 10.1007/s10346-011-0277-5.
- Wang, G., and Soler, T., 2012, OPUS for Horizontal Subcentimeter-Accuracy Landslide Monitoring: Case Study in the Puerto Rico and Virgin Islands Region: *Journal of Surveying Engineering*, v. 138, p. 143–153, doi: 10.1061/(ASCE)SU.1943-5428.0000079.

Wieczorek, G.F., 1987, Effect of rainfall intensity and duration on debris flows in central Santa Cruz Mountains: Debris flow/avalanches: process, recognition, and mitigation, v. 7, p. 93–104.